TECHNICAL REPORT SL-90-8

Army Corps Engineers

RED RIVER WATERWAY THERMAL STUDIES

Report 2
THERMAL STRESS ANALYSES

by

Sharon Garner, Michael Hammons, Anthony Bombich

Structures Laboratory

DEPARTMENT OF THE ARMY
Waterways Experiment Station, Corps of Engineers
3909 Halls Ferry Road, Vicksburg, Mississippi 39180-6199

December 1991
Report 2 of a Series

STRUCTURES LABORATORY

Prepared for US Army Engineer District, Vicksburg
Vicksburg, Mississippi 39181-0060

Destroy this report when no longer needed. Do not return it to the originator.

The findings in this report are not to be construed as an official Department of the Army position unless so designated by other authorized documents.

The contents of this report are not to be used for advertising, publication, or promotional purposes. Citation of trade names does not constitute an official endorsement or approval of the use of such commercial products.

REPORT DOCUMENTATION PAGE

Form Approved
OMB No. 0704-0188

1. AGENCY USE ONLY *(Leave blank)*	2. REPORT DATE	3. REPORT TYPE AND DATES COVERED
	December 1991	Report 2 of a series

4. TITLE AND SUBTITLE
Red River Waterway Thermal Studies; Report 2, Thermal Stress Analyses

5. FUNDING NUMBERS
DA Form 2544
No. 4908

6. AUTHOR(S)
Sharon Garner
Michael Hammons
Anthony Bombich

7. PERFORMING ORGANIZATION NAME(S) AND ADDRESS(ES)
USAE Waterways Experiment Station
Structures Laboratory
3909 Halls Ferry Road
Vicksburg, MS 39180-6199

8. PERFORMING ORGANIZATION REPORT NUMBER
Technical Report
SL-90-8

9. SPONSORING/MONITORING AGENCY NAME(S) AND ADDRESS(ES)
US Army Engineer District, Vicksburg
Vicksburg, MS 39181-0060

10. SPONSORING/MONITORING AGENCY REPORT NUMBER

11. SUPPLEMENTARY NOTES
Available from National Technical Information Service, 5285 Port Royal Road, Springfield, VA 22161

12a. DISTRIBUTION/AVAILABILITY STATEMENT
Approved for public release; distribution is unlimited

12b. DISTRIBUTION CODE

13. ABSTRACT *(Maximum 200 words)*

This report is the second of a series documenting the findings of the Red River Waterway Thermal Study. It includes the results of thermal and incremental construction analyses of a typical navigation lock chamber monolith and an upper-gate bay monolith for Locks and Dams 4 and 5, Red River Waterway. Also analyzed was a typical dam weir section. These analyses were conducted using a general-purpose heat transfer and stress analysis finite element program which included a time-dependent cracking material model for concrete. Results of thermal properties tests and climate data were used to describe thermal boundary conditions, forcing functions, and thermal properties for the thermal analyses. Results of mechanical properties tests were used to calibrate and verify the time-dependent material model. Concrete mixtures with up to 50-percent replacement of Type II cement with Class C fly ash were studied. Results of two- and three-dimensional finite-element analyses were used to recommend lift heights, placement temperatures, and insulation requirements for construction.

14. SUBJECT TERMS			15. NUMBER OF PAGES
Concrete construction	Finite-element analyses	Mass concrete	129
Concrete mixtures		Stress and strain	16. PRICE CODE
Dams	Locks		

17. SECURITY CLASSIFICATION OF REPORT	18. SECURITY CLASSIFICATION OF THIS PAGE	19. SECURITY CLASSIFICATION OF ABSTRACT	20. LIMITATION OF ABSTRACT
UNCLASSIFIED	UNCLASSIFIED		

PREFACE

The investigation described in this report was conducted for the US Army Engineer District, Vicksburg. Authorization was given by DA Form 2544, No. 4908, dated 30 Dec 1987 and subsequent revisions.

The investigation was performed at the US Army Engineer Waterways Experiment Station (WES) by members of the staff of the Structures Laboratory (SL), under the general supervision of Messrs. Bryant Mather, Chief, and J. T. Ballard, Assistant Chief. Direct supervision was provided by Mr. K. L. Saucier, Chief, Concrete Technology Division (CTD). Project Management was provided by Mr. Michael I. Hammons, Group Leader, Applied Mechanics Group (AMG), Engineering Mechanics Branch, CTD. This report was prepared by Ms. Sharon Garner, Mr. Hammons, and Mr. Anthony Bombich, AMG. The authors acknowledge Dr. C. Dean Norman, Structural Mechanics Division, Messrs. Don Smith, Dan Wilson, Brent Lamb, James Shirley, and Ms. Linda Mayfield, AMG, for their help during this investigation. The authors also acknowledge the assistance of Messrs. Toy Poole, Sam Wong, Michael Lloyd, Percy Collins, Tom Lee, Julies Mason, and Ken Loyd, CTD, and MAJ Stacey Hirata, US Military Academy. Technical direction for this investigation was provided by the Red River Thermal Study Advisory Panel consisting of Mr. Mather, Mr. Fred Anderson, Headquarters, US Army Corps of Engineers, and Dr. William L. Dolch, Purdue University. Valuable direction was provided by Messrs. Dale Goss and Jewel Carpenter, US Army Engineer District, Vicksburg.

Commander and Director of WES during preparation of this report was COL Larry B. Fulton, EN. Technical Director was Dr. Robert W. Whalin.

CONTENTS

CONVERSION FACTORS, NON-SI TO SI (METRIC) UNITS OF MEASUREMENT

Non-SI units of measurement used in this report can be converted to SI (metric) units as follows:

Multiply	By	To Obtain
Btu (International Table) per pound (mass) • degree Fahrenheit	4,186.8	joules per kilogram Kelvin
Btu (International Table) feet per day • square foot • degree Fahrenheit	5,981.41947	watts per metre Kelvin
Calories per gram	4.186	kilojoules per kilogram
Fahrenheit degrees	5/9	Celsius degrees or kelvins*
feet	0.3048	metres
inches	25.4	millimetres
miles per hour (US Statue)	1.609347	kilometres per hour
pounds (force) per square inch	0.006894757	megapascals
pounds (mass)	0.4535924	kilograms
pounds (mass) per cubic foot	16.01846	kilograms per cubic metre

* To obtain Celsius (C) temperature reading from Fahrenheit (F) readings, use the following formula: C + (5/9)(F - 32). To obtain Kelvin (K) readings, use K = (5/9)(F - 32) + 273.15.

RED RIVER WATERWAY THERMAL STUDIES
REPORT 2: THERMAL STRESS ANALYSES

PART I: INTRODUCTION

Background

1. In 1968, Congress enacted Public Law 90-483 which authorized the construction of the Red River Waterway in Louisiana, Arkansas, Texas, and Oklahoma. As a part of this act, Congress directed that the Red River be made navigable from its juncture with the Mississippi River to Shreveport, Louisiana. This improvement includes developing a 9-ft deep, 200-ft wide navigation channel along approximately 236 miles of river. A system of five locks and dams are required along the channel to furnish a maximum lift of 141 ft. Locks and Dams 1 and 2 were completed in 1984 and 1987, respectively. At the time of this writing, Lock and Dam 3 was under construction, and construction of Locks and Dams 4 and 5 was scheduled to begin in 1992.

2. Both Locks and Dams 1 and 2 experienced significant thermal-related cracking with Lock and Dam 1 requiring remedial grouting. Also, similar cracking has been observed on locks and dams constructed by the Vicksburg District on the Ouachita and Black Rivers in Louisiana and Arkansas. Although this cracking does not pose a threat to structural integrity, it leads to increased maintenance costs and possible shortening of service life. The Vicksburg District and Lower Mississippi Valley Division recognized the need for a careful and deliberate thermal stress analysis to be conducted on Locks and Dams 4 and 5. Consequently, the Concrete Technology Division (CTD) of the Structures Laboratory (SL), USAE Waterways Experiment Station (WES), initiated the Red River Waterway Thermal Studies in January 1988.

3. The thermal and incremental construction analysis procedures used for the study were developed at WES beginning in 1984 to provide a modern, consistent, and effective method of analysis to predict cracking in mass concrete structures. This analysis procedure allows better definition of concrete material properties and construction procedures which lead to safe,

serviceable and cost-effective mass concrete structures. The analysis tool is a two- or three-dimensional finite-element (FE) model for concrete which includes the time-dependence of mechanical properties, creep, shrinkage, and thermal effects. Through the use of this model in a proven general-purpose heat transfer and structural FE code, different concrete mixtures can be accurately simulated in the incremental construction analysis of a structure or critical structural component. From this analysis, the engineer can determine the concrete mixture and construction procedures which will yield the most cost-effective and serviceable structure for the given field conditions and practical construction constraints.

4. This report is the second of two documenting the findings of the Red River Waterway Thermal Study. Report 1 (Hammons, Smith, and Neeley 1990) included the selection and characterization of the concrete materials in support of the thermal and incremental construction analysis. Report 2 includes the results of the thermal stress analyses and specific recommendations to limit thermal-related cracking in Locks and Dams 4 and 5.

Objective

5. The primary objective of this research program was to develop and evaluate materials and construction methods which would yield safe, serviceable, long-lived, and cost-effective structures. All products of the research were carefully scrutinized to determine if they were practical for field application. The results of laboratory tests were used to make specific recommendations intended to limit production of heat during the hydration process and reduce costs by proportioning concrete mixtures incorporating high levels of fly ash in the cementitious materials content. The results of the FE analyses were used to recommend improved construction practices intended to limit thermal stresses and related cracking.

Scope

6. This research effort was divided into two integrated phases: (a) concrete materials selection and characterization and (b) thermal and

incremental construction analyses. Each of these phases is discussed below.

7. Much of the thermal-related cracking in mass concrete initiates during the period when material properties change rapidly with time and temperature. Few data exist to help define those changes. Prior research and field experience have proven that the critical material property parameters affecting cracking in mass concrete are the change in modulus of elasticity and strength with time, creep, shrinkage, heat production, and thermal properties. A preliminary mixture proportioning study was conducted to investigate the feasibility of using increased levels of fly ash to limit heat production during early stages of hydration and reduce the cost of cementitious materials. The results of this study were used to select a few representative candidate mixtures for a full suite of mechanical and thermal property tests. These tests were intended to determine the values of critical material response parameters at early ages.

8. Crack surveys of Lock and Dam 2, Red River Waterway, were studied prior to selecting critical structural features for analysis. These features were discretized to allow incremental construction FE analysis. The material and thermal properties test data were used to calibrate state-of-the-art thermal and mechanical material models. The previously defined critical sections were analyzed using two- and three-dimensional FE models. Variations in placement and ambient temperature, concrete mixtures, and temperature control parameters were analyzed for control of thermal stresses.

PART II: ANALYSIS METHOD

Parameters Influencing Thermal Cracking

8. All concrete elements and structures are subject to volume change (ACI Committee 209, 1989). Cracking in mass concrete is caused by restraint of volume change. These volume changes may be due to heat generation and subsequent cooling, shrinkage, creep or stress relaxation, or other mechanisms. Restraint limits the changes in dimensions and causes corresponding tensile, compressive, or flexural stresses in concrete. Of primary concern in mass concrete structures is restraint that causes tensile stresses, particularly in the first few days after the placement of the concrete when the tensile capacity of the concrete can be quite low.

9. Restraint of volume change may be either external or internal. External restraint is caused by bond or frictional forces between the concrete and the foundation or underlying lifts. The degree of external restraint depends upon the stiffness and strength of the concrete and restraining material and upon the geometry of the section. Internal restraint is caused by temperature gradients within the concrete. The warmer concrete in the interior of the lift provides restraint as the concrete in the periphery of the lift cools due to heat transfer to its surroundings. The degree of internal restraint depends upon the quantity of heat generated, the thermal properties of the concrete, and thermal boundary conditions.

10. A number of parameters may be controlled to limit cracking related to the restraint of volume change. These parameters fall into two categories: material parameters and construction parameters. Among the material parameters are the following:

a. Heat generation of the concrete,

b. Mechanical properties of the concrete including strength, modulus of elasticity, and creep or stress relaxation,

c. Shrinkage of the concrete, and

d. Thermal properties of the concrete including coefficient of thermal expansion, specific heat, and thermal conductivity.

The construction parameters are as follows:

a. Lift height,

b. Time between placement of lifts,

c. Placement temperature,

d. Ambient temperature,

e. Use of insulation,

f. Use of cooling coils, and

g. Monolith geometry including section thickness, monolith length, and location and size of inclusions such as galleries, culverts, etc.

11. To be effective, the method used to analyze thermal-related cracking in mass concrete structures must accurately model these complex phenomena. The heat-transfer model must be capable of handling the internal generation of heat and the complex thermal boundary conditions in the incremental construction problem. Similarly, the stress-analysis model must be capable of predicting the mechanical properties of the concrete as they change with time. It must also have the ability to predict cracking in a computationally efficient manner.

Finite-Element Code

12. The thermal stress analyses in this investigation was performed using ABAQUS, a general-purpose, heat-transfer and structural analysis FE program developed by Hibbit, Karlsson, and Sorenson (1988) in conjunction with a user-defined aging material model developed by WES. The analysis procedure was developed at WES and has been used in several previous projects (Bombich and Norman 1987; Norman, Campbell, and Garner 1988; Hammons, Garner, and Smith 1989). Some of the features of the FE code are discussed below.

13. The theoretical formulation of ABAQUS is based on the FE stiffness method with some hybrid formulations included as necessary. The program includes automatic control of solution-step size but also allows the user to select the step size. This feature is very important in the solution of the incremental construction problem. Input is free-format, key-worded, and makes use of set definitions for easy cross reference. A broad element library is included in ABAQUS, and a combination of elements can be used in the same model. Heat-transfer capabilities and a wide variety of constitutive models are also provided in ABAQUS, and a user-supplied material model (the UMAT

subroutine discussed below) may be incorporated as an external subroutine linked to the ABAQUS library.

14. In order to model the incremental construction, calculations are carried out in time steps. By using the REMOVE/INCLUDE element options in ABAQUS, new elements are added to the model at regular intervals of time (5, 10, or 15 days) to simulate the placement of additional lifts. Thermal boundary conditions such as ambient temperature, wind velocity, and use of insulation are allowed to vary with time to simulate field conditions. The placement temperature of the concrete is also varied to model conditions typical of any season of the year.

15. A two- or three-dimensional transient heat-transfer analysis can be performed using heat-transfer elements from the ABAQUS library of elements. The adiabatic temperature rise of the concrete mixture is used as the non-uniform heat flux for the analysis and is supplied by the user in an external subroutine (DFLUX) linked to ABAQUS. Boundary conditions for the heat-transfer analysis can be easily varied. External conditions (wind speed, forms, insulation) are modeled using film coefficients applied to external element faces, and ambient and placement temperatures are specified in the data file. The results of the heat-transfer analysis are temperatures at each node for each time step.

16. The temperature-time history obtained in the heat-transfer analysis is used as the loading in a stress analysis. This analysis can be conducted using plane stress, plane strain, or three-dimensional elements from the ABAQUS element library. Significant changes in material characteristics (strength, elastic modulus, creep, and shrinkage) as well as cracking are incorporated into the calculations using the user-supplied material model (UMAT). The output from the stress analyses includes nodal displacements and stresses and strains at user-selected locations throughout the structure as well as user-selected displacement plots and stress or strain contour plots.

Time-Dependent Material Model

17. The user-supplied constitutive model (UMAT) used in this investigation was developed by WES and includes features to model the effects

of time-dependency and temperature on modulus, strength, and creep compliance along with an interactive cracking criteria for concrete. The model is described at length by Norman, Campbell, and Garner (1988) and Garner and Hammons (1991). Some features of the model are discussed below.

18. Cracking is assumed to have occurred when an interactive stress or strain cracking criterion is satisfied. The criterion is strain-driven, but the tensile strain capacity is modified by the state of stress in the element (Norman, Campbell, and Garner 1988). The crack surface normal is in the direction of the maximum principal tensile strain. A smeared crack approach is used to model the cracked regions of the structure. The cracked region is modeled as an anisotropic continuum effectively "smearing" the cracks in a continuous manner throughout the element (Norman and Anderson 1985). When cracking occurs, stress in the tensile direction is allowed to drop to zero while shear transfer due to aggregate interlock can be maintained. Cracks are allowed to open or close as conditions in the model vary. Thus, the overall structural response can be adequately modeled without regard to completely realistic crack patterns and local stresses (Chen 1982).

19. Key response functions in the model are change in strength with time, change in elastic modulus with time, creep compliance, and shrinkage. Elastic modulus and shrinkage are input through algebraic time-domain functions. Elastic modulus is calculated at a temperature of 70 °F and modified for current temperature. Creep compliance is input through a specific creep function which is mapped in the time domain by an aging factor included in the model. This aging factor is the ratio of modulus at time t to the 3-day modulus $(E(t)/E(3))$ and is the means for updating modulus and compressive strength at each calculation point and time increment.

PART III: THERMAL AND TIME-DEPENDENT MATERIAL MODEL CALIBRATION

General

20. In order to model accurately the field construction process, the incremental construction analysis procedure requires that several material-specific parameters be mathematically described in both the heat-transfer analyses and in the stress analyses. These parameters are input either as constants or as algebraic functions of time. This process of mathematically describing the material response features in the model is referred to as the model calibration procedure. In the case of the time-dependent material model, an additional step is required. After calibration, the UMAT subroutine is used in a finite element analysis procedure to model the suite of creep tests performed on the concrete and verify that the response of the material is being reasonably predicted. The calibration and verification procedure for both the heat transfer and time-dependent material model are described below.

Concrete Mixtures

21. The selection of the concrete mixtures used for the incremental construction analyses are described in detail in Report 1 of this series by Hammons, Smith, and Neeley (1990). A matrix of 15 concrete mixtures was developed to cover the range of possible combinations of water-cement ratios (w/c) and fly ash contents for field use. Of these 15 mixtures, 3 were selected for use in the analyses. These were selected based on the following criteria:

a. Bracket the response of the possible concrete mixtures,

b. Compressive strength at ages of 1 to 120 days,

c. Economy, and

d. Thermal characteristics.

The concrete mixtures selected are described below.

22. The three concrete mixtures were chosen for this study are identified in Table 1. Mixture proportions are given in Table 2. The cement used in this study was a Type II, low-alkali, ASTM C 150 cement with a heat of

Table 1

Concrete Mixtures

Mixture	W/C, by mass	Fly Ash/Cement Ratio, by volume
A8	0.60	0.25
A11	0.45	0.40
A13	0.50	0.50

Table 2

Mixture Proportions

Material	Mass per Cubic Yard, lb		
	A8	A11	A13
Type II Portland Cement	250.0	232.0	171.0
Class C Fly Ash	66.9	124.2	137.4
Fine Aggregate	1,293.9	1,200.2	1,285.5
Coarse Aggregate (19.0-mm (3/4-in.) max.)	937.9	990.3	972.4
Coarse Aggregate (37.5-mm (1-1/2-in.) max.)	1,144.4	1,208.2	1,186.5
Air Entraining Admixture	3.5 oz	1.8 oz	1.5 oz
Water-Reducing Admixture	---	---	19.5 oz
Water	200.0	173.2	170.3

hydration at 7 days of 68 cal/g. The fly ash was a Class C fly ash complying with the requirements of ASTM C 618. The fine aggregate was a natural sand composed of blocky, ellipsoidal, and spherical particles. Chert was the primary constituent in sizes larger than 2.36 mm (No. 8) with quartz predominating in the smaller sizes. The 4.75- (No. 4) to 19.0-mm (3/4-in.) aggregate was primarily chert composed of blocky, pyramidal, and tabular particles with rounded edges and corners. The large aggregate was a crushed, coarse grained syenite, an igneous rock with a composition and textural characteristics similar to those of granite.

Thermal Model

23. The heat-transfer capability of ABAQUS uses the finite-element method to numerically solve the governing differential equation for heat

transfer:

$$\nabla^T k \nabla \theta + Q = \rho c_p \frac{\partial \theta}{\partial t}$$

where

$\theta(x,y,z,t)$ = temperature at a point described by the coordinates (x,y,z) at time t,

k = thermal conductivity

$Q(t)$ = applied heat flux

ρ = mass density

c_p = specific heat

The necessary material parameters, therefore, are the density, thermal conductivity, and specific heat of the material, and a mathematical description of the applied heat flux. Each of these is described below.

Adiabatic temperature rise

24. For the incremental construction problem, the applied heat flux is given by the adiabatic temperature rise curve of the material. The adiabatic curve represents the temperature rise as a function of time of a specimen of concrete in which no heat gain or loss to the surroundings is permitted. Adiabatic tests were performed under contract to WES for mixtures A8 and A13 (Hammons, Smith, and Neeley 1989). These adiabatic curves were input into ABAQUS through the subroutine DFLUX as a set of temperature-time data arrays. The adiabatic curves used in the heat-transfer analyses in the DFLUX subroutine are shown in Figure 1.

Concrete thermal properties

25. Tests to provide thermal properties of concrete needed for input to ABAQUS were performed at WES for mixtures A8 and A13 (Hammons, Smith, and Neeley 1989). The heat-transfer analysis procedure was based on the assumption that the necessary thermal properties for a given concrete did not vary with age. To verify this assumption for mixtures A8 and A13, the tests to yield specific heat, thermal conductivity, and density were performed at two ages: 3 and 28 days. Results showed that the changes with age were negligible and that the thermal properties of mixtures A8 and A13 differed by less than three percent. Because of the small differences, data were averaged over

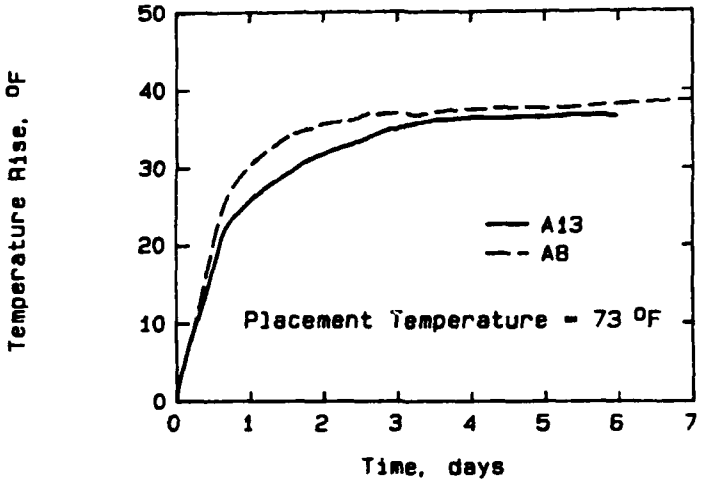

Figure 1. Adiabatic temperature curves

age and mixtures to yield single values for each thermal property. The results used as input to ABAQUS are shown in Table 3.

Table 3

Concrete and Soil Thermal Properties used with ABAQUS

Material	Parameter	Value
Concrete		
	Thermal Conductivity, k, Btu/day-°F-in.	2.3
	Specific Heat, c, Btu/lb-°F	0.21
	Density, ρ, pci	0.0865
Soil		
	Thermal Conductivity, k, Btu/day-°F-in.	2.2
	Specific Heat, c, Btu/lb-°F	0.263
	Density, ρ, pci	0.06428

Soil thermal properties

26. Thermal properties of the soil were not available by direct testing. In lieu of test data, thermal properties were calculated using equations developed by Kersten (1949). Kersten's equations allow the computation of thermal conductivity and specific heat as functions of soil texture and physical properties. A description of the physical properties of the soil in the proposed foundation zone was obtained from soil tests for Lock and Dam No. 4. The soil is described as silty sand. Averaging the properties of 12 samples that fell within the foundation zone yielded the following properties:

Property	Value
Dry Density (ρ_{dry})	103.7 lb per cu ft (pcf) or 0.06001 lb per cu in. (pci)
Moisture Content	11.85 percent of dry soil mass
Saturation	50.0 percent
Void Ratio	0.605

27. Values of dry specific heat (c_{dry}) were given as c = 0.16 Btu/lb-°F at 0 °F and c = 0.19 Btu/lb-°F at 140 °F. Dry specific heat at an average soil temperature of 80 °F (70 °F soil temperature + 10 °F average incremental temperature rise due to heat from concrete) was determined by linear interpolation between theses values to be

$$c_{dry} = 0.176 \text{ Btu/lb-°F at } 80 \text{ °F} .$$

28. The in situ specific heat, (c_{wet}) was computed using the following equation:

$$c_{wet} = \frac{(100 \times c_{dry}) + \text{Moisture Content}}{100 + \text{Moisture Content}} = 0.263 \text{ Btu/lb-°F.}$$

Substituting a moisture content of 11.85 percent and a dry density of

103.7 pcf yielded

$$\rho_{wet} = 111.08 \text{ pcf} = 0.06428 \text{ pci} .$$

29. Thermal conductivity was calculated using Kersten's equation for sandy soils with less than 50% silt or clay content. This equation is

$$k_{wet} = [0.7\log(\text{Moisture Content}) + 0.4]10^{0.01\rho_{dry}}$$

where thermal conductivity corrected for moisture content, k_{wet}, is in Btu/ft^2/in./h/°F. This equation is based on an average temperature of 40 °F. To obtain thermal conductivity at an average temperature of 80 °F, the value calculated from the equation above was increased by approximately 5 percent. Converting to units consistent with the ABAQUS input produced

$$k_{wet} = 2.2 \text{ Btu/day-°F-in} .$$

30. The thermal properties of soil used as input to the heat transfer calculations are listed in Table 3.

Material Model

31. The time-dependent creep model (UMAT) used in the analysis was calibrated for each mixture simulated in the analysis. Information required for calibration included 3-day creep compliance, shrinkage, and elastic modulus as a function of age.

32. In ACI 209-R82, shrinkage is defined as the decrease with time of concrete volume. The decrease is due to changes in the moisture content of the concrete and physico-chemical changes, which occur without stress attributable to actions external to the concrete. Drying shrinkage due to moisture loss only occurs at the surface of mass concrete structures and is not simulated in the material model. However, additional volumetric changes occur during hydration of the cement that are not directly attributable to changes in temperature or moisture loss. In this report the term "shrinkage"

is used to refer to these volumetric changes.

33. Creep is defined (ACI 209) as the time-dependent increase of strain in hardened concrete subjected to sustained stress. It is obtained by subtracting from the total measured strain in a loaded specimen, the sum of the initial instantaneous (usually considered elastic) strain due to the sustained stress, the shrinkage, and the eventual thermal strain in an identical load-free specimen which is subjected to the same history of relative humidity and temperature conditions.

34. The above definition assumes that strain in a loaded specimen consists of an initial elastic strain, creep strain, shrinkage, and thermal expansion or contraction. In a mass concrete structure, however, stresses and modulii are constantly changing throughout the structure and construction period, and initial elastic strain has little meaning. Calibration of the material model must be based on time-dependent modulus and creep compliance.

35. Creep-compliance curves and modulus-time curves for mixtures A2, A8, A13, and A11 were calculated from creep tests conducted at WES and reported by Hammons, Smith, and Neeley (1990). Creep compliance is determined from a plot of specific strain (strain per unit stress) versus time from a 3-day creep test and is the difference between the total specific strain and the elastic specific strain. The relationship between total specific strain J(t), creep compliance (C(t)), and elastic specific strain (1/E(t)) is shown in Figure 2. Calibration of the model for creep and elastic strains is a two-part process. The creep compliance (as determined from a 3-day creep test) given by an equation of the form

$$C(t) = A_1[1 - e^{r_1(t-t_o)}] + A_2[(1 - e^{r_2(t-t_o)}] + A_3[(1 - e^{r_3(t-t_o)}]$$

where

t = age of the concrete in days

t_o = age at loading in days

$C(t)$ = in./in. per psi

The parameters A_1, A_2, A_3, r_1, r_2 and r_3 are determined by trial and error fit to test data. The form of the time-dependent elastic modulus equation is

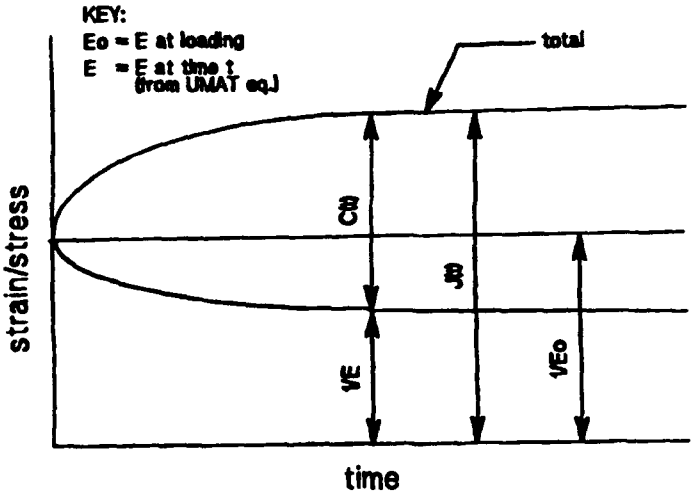

Figure 2. Idealized curve showing relationships between total specific strain, creep compliance, and elastic specific strain

$$E(t) = E_1[1 - e^{x_1(t-1)}] + E_2[1 - e^{x_2(t-1)}] + E_3[1 - e^{x_3(t-1)}] + E(1)$$

where E_1, E_2, E_3, x_1, x_2 and x_3 are constants determined from a trial and error fit to test data, $E(1)$ is the 1-day elastic modulus, t is age of the concrete in days and $E(1)$ and $E(t)$ are in psi.

36. Elastic modulus data from the material properties tests reported by Hammons, Smith, and Neeley (1990) were used to determine the values of the unknown constants in the modulus equation. For Mixture A11, the values were

$$E_1 = 1.801 \times 10^6 \qquad x_1 = -3.135 \times 10^{-2}$$
$$E_2 = 2.145 \times 10^6 \qquad x_2 = -4.076 \times 10^{-1}$$
$$E_3 = -4.375 \times 10^5 \qquad x_3 = -2.649$$
$$E(1) = 2.25 \times 10^6 \text{ psi}$$

For Mixture A8, the values were

$$E_1 = 3.770 \times 10^6 \qquad x_1 = -5.953 \times 10^{-2}$$
$$E_2 = 0. \qquad x_2 = 0.$$
$$E_3 = 4.893 \times 10^5 \qquad x_3 = -2.649$$
$$E(1) = 1.64 \times 10^6 \text{ psi}$$

For Mixture A13, the values were

$E_1 = 3.588 \times 10^6$ $x_1 = -3.251 \times 10^{-2}$

$E_2 = 1.297 \times 10^6$ $x_2 = -4.076 \times 10^{-1}$

$E_3 = 3.328 \times 10^5$ $x_3 = -2.649$

$E(1) = 0.60 \times 10^6$ psi

Plots of the modulus data versus algebraic model for the three mixtures are shown in Figure 3.

37. Constants in the creep compliance function for Mixture A11 were determined using 3-day creep test data. Unfortunately, no 3-day creep test data were available for Mixtures A8 or A13. Therefore, the creep compliance curve for Mixture A8 was determined by trial and error fit to the 7- and 14-day creep test data. For Mixture A8, the values substituted in the creep compliance curve were as follows:

$A_1 = 0.4754 \times 10^{-6}$ $r_1 = -0.05887$

$A_2 = 0.1145 \times 10^{-6}$ $r_2 = -0.1892$

$A_3 = 0.$ $r_3 = 0.$

For Mixture A11, the values were as follows:

$A_1 = 0.1058 \times 10^{-6}$ $r_1 = -0.05887$

$A_2 = 0.1589 \times 10^{-6}$ $r_2 = -0.1892$

$A_3 = 0.1339 \times 10^{-6}$ $r_3 = -1.766$

38. To determine a creep compliance curve for mixture A13, FE predictions were made for the 1-, 7- and 14-day tests using the A13 modulus curve and the A11 creep compliance curve. Elastic strains were then subtracted from total strains in the predicted and test curves, leaving predicted and test creep strains. Predicted and test creep strains were plotted on the same scale for each test to determine a single multiplication factor that could be applied to the A11 curve to simulate A13 creep. A factor of 2.3 was chosen, yielding the following constants.

$A_1 = 0.2433 \times 10^{-6}$ $r_1 = -0.05887$

$A_2 = 0.3655 \times 10^{-6}$ $r_2 = -0.1892$

$A_3 = 0.3080 \times 10^{-6}$ $r_3 = -1.766$

The 3-day creep compliance curves for mixtures A8, A11 and A13 are shown in Figure 4.

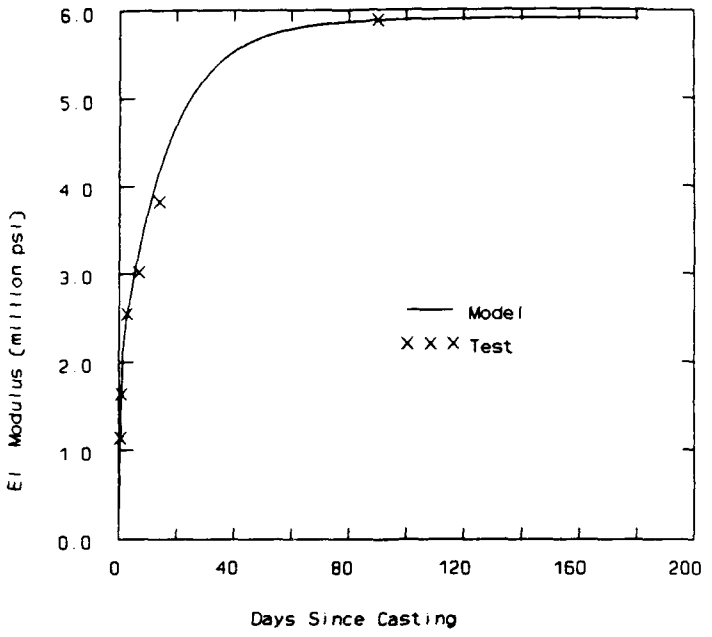

a. Mixture A8

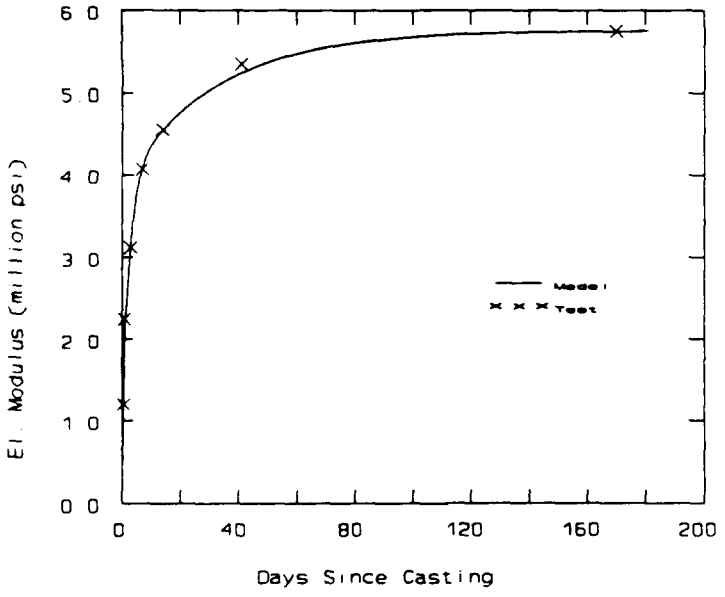

b. Mixture A11

Figure 3. Comparison of elastic modulus-time date with algebraic model (Continued)

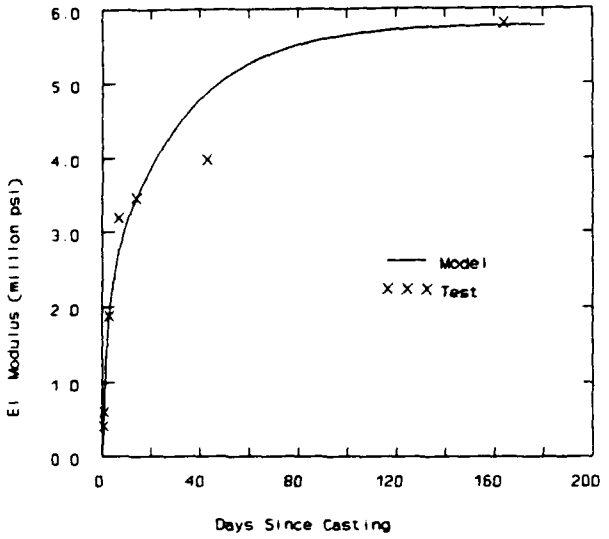

c. Mixture A13

Figure 3. (Concluded)

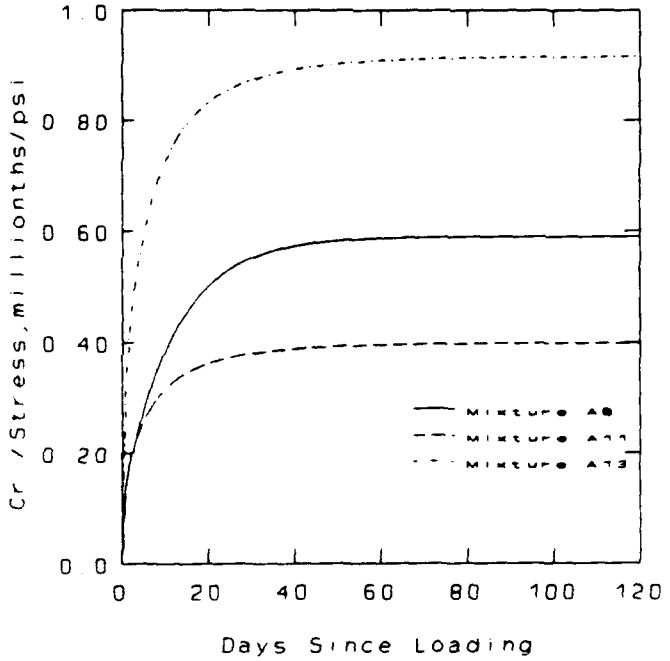

Figure 4. Creep compliance curves in UMAT model

39. To account for the volumetric changes that occur during the curing of concrete the UMAT material model includes an equation of the form

$$\epsilon_{shrinkage} = 204.9 \times 10^6 \left(1 - e^{-0.15t}\right) + 145.1 \times 10^6 \left(1 - e^{-0.02263t}\right)$$

where $\epsilon_{shrinkage}$ has units of in./in. and t is time since casting in days. This relationship was developed from test data on silica-fume concrete (Norman, Campbell, and Garner 1988). The change in strain along the length of a sealed specimen (shrinkage) for each mixture was plotted against the shrinkage curve in the model to determine a scaling factor to be used for each mixture. The scaling factors for the mixtures are given below.

Mixture	Scaling Factor
A8	0.30
A11	0.28
A13	0.32

Plots of these results are shown in Figures 5 through 7.

40. Additional properties data used as input to the material model are shown in Table 4. Concrete parameters (except Poisson's ratio and tensile strain capacity) are based on test results (Hammons, Smith, and Neeley 1990).

Table 4

Other Concrete Parameters Required For Material Model

Parameters	A8	A13	A11
Elastic modulus at 3 days (10^6 psi)	2.55	1.88	3.12
Poisson's ratio	0.15	0.15	0.15
Compressive strength at 3 days (psi)	795.00	600.00	1,100.00
Tensile strain capacity (millionths)	100.00	100.00	100.00

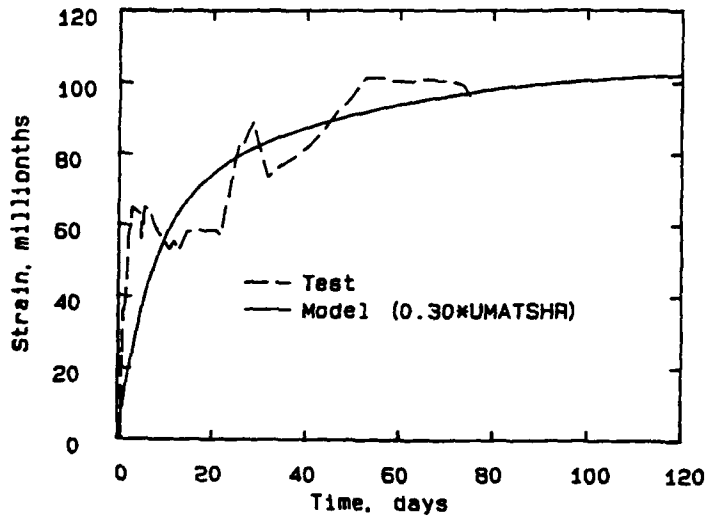

a. Mixture A8

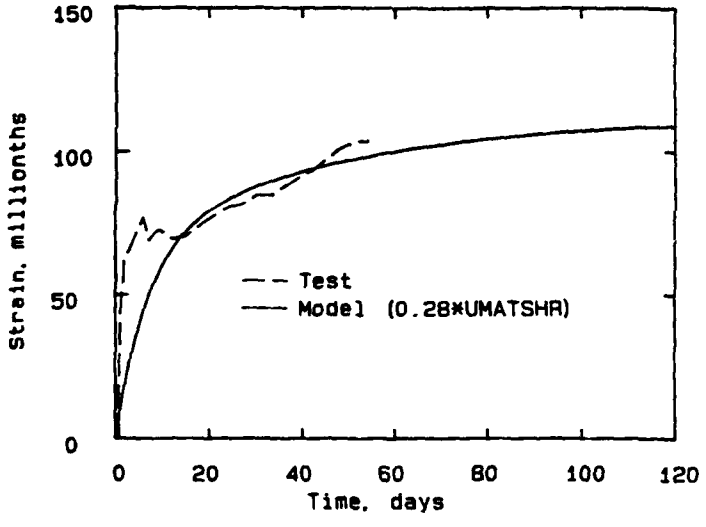

b. Mixture A11

Figure 5. Comparison of shrinkage model with autogenous length change data (Continued)

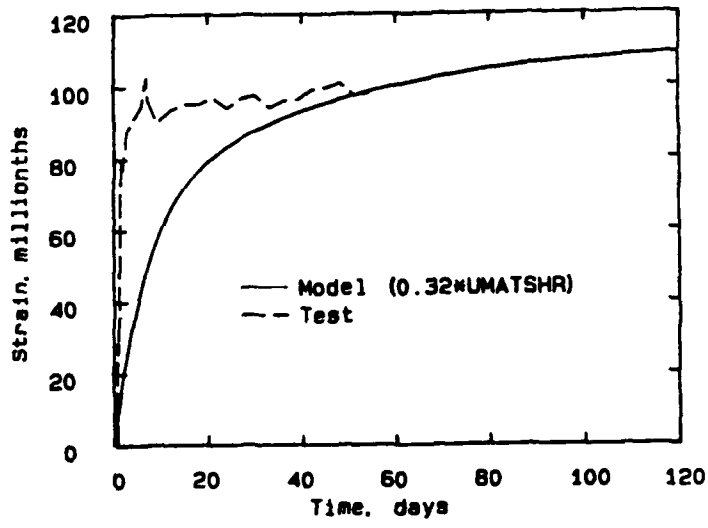

c. Mixture A13

Figure 5. Comparison of shrinkage model with autogenous length change data (Concluded)

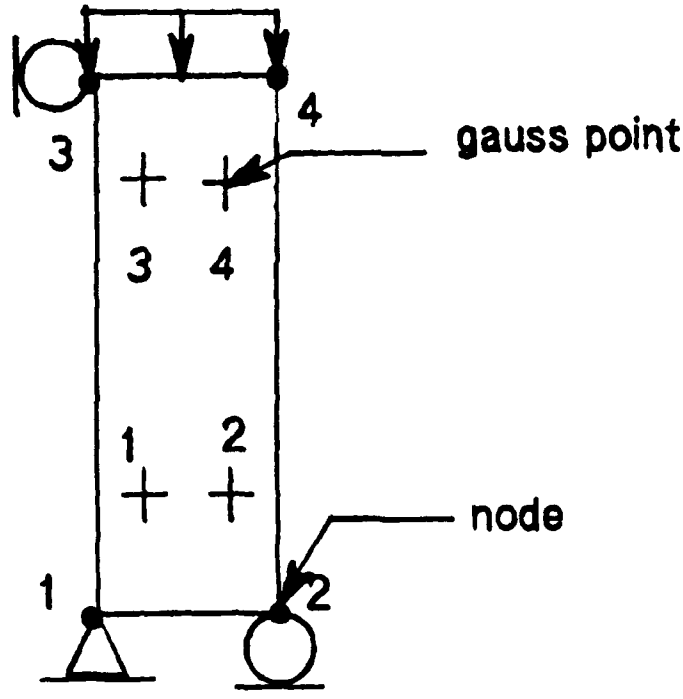

Figure 6. Finite-element model for creep test simulation

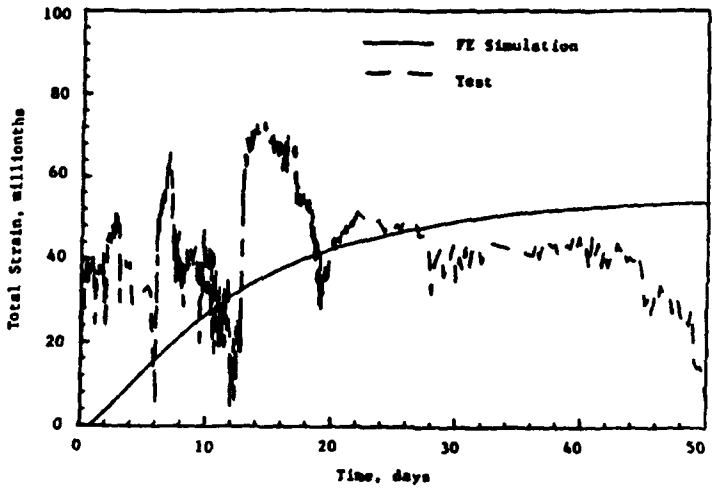

a. Age at loading = 16 h

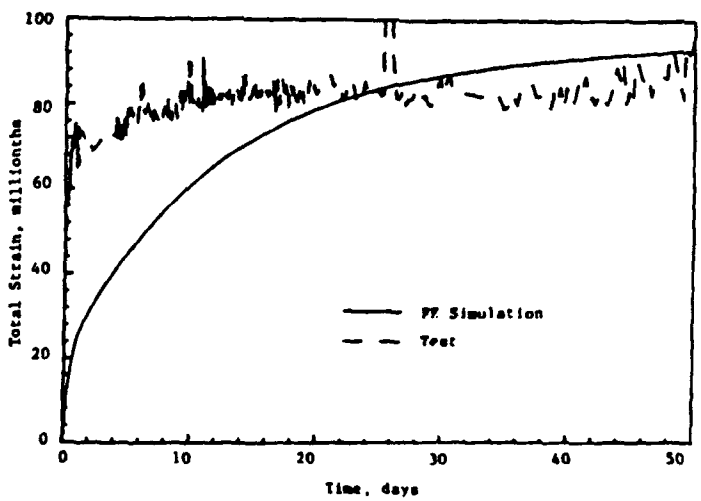

b. Age at loading = 7 d

Figure 7. Comparison of material model with creep test data, Mixture A8 (Continued)

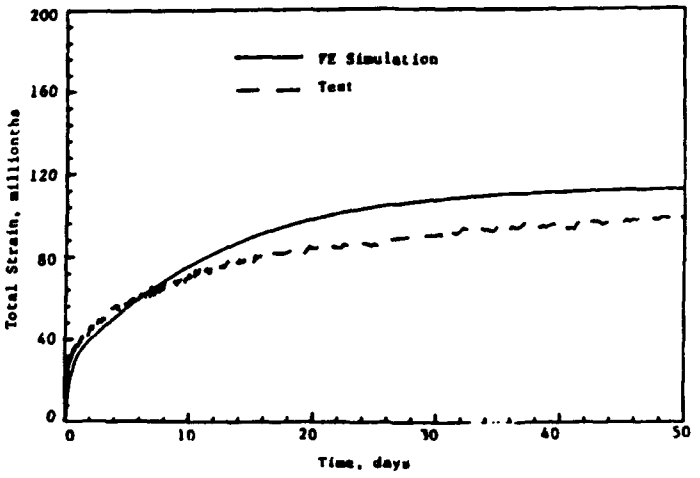

c. Age at Loading = 14 d

Figure 7. (Concluded)

UMAT Verification

41. The model, incorporating these curves, was then used with *ABAQUS* to simulate the entire suite of creep tests for each mixture. Each creep cylinder was modelled using a single axisymmetric element supported on rollers at boundaries and uniformly loaded across the top surface (Figure 6). Loads were varied to simulate loadings recorded by the stress gages (Hammons, Smith, and Neeley 1990). The results of these runs were then plotted against test data for comparison. Results of the verification analyses for mixtures A8, A13, and A11 are shown in Figures 7-9. Due to uncertainties in the elastic strains for Mixture A8, only creep strains are shown in Figure 7. Total elastic and creep strains are shown from Mixtures A11 and A13 in Figures 8 and 9.

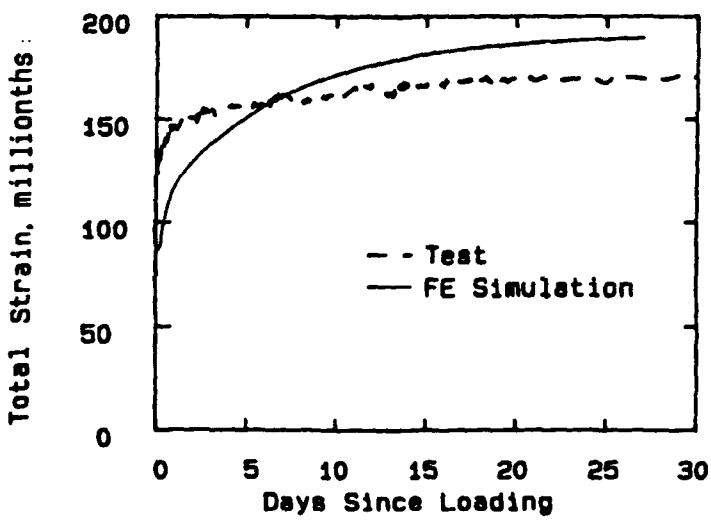

a. Age at Loading = 18h

Figure 8. Comparison of material model with creep test data, mixture All (Sheet 1 of 3)

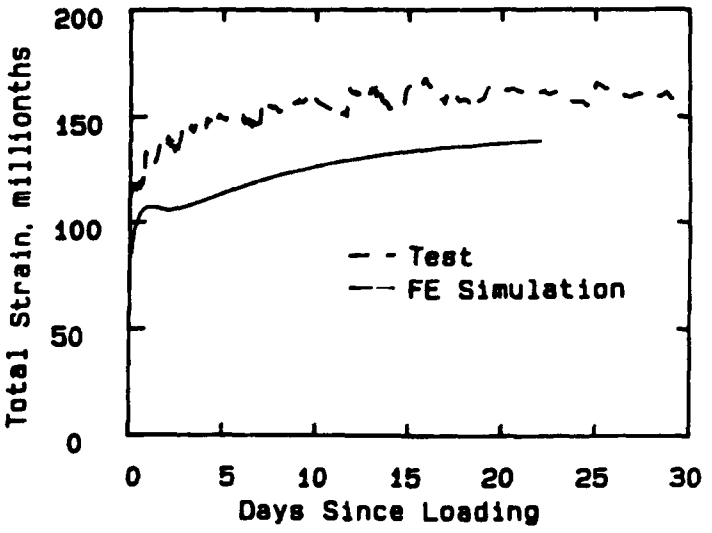

b. Age at loading = 1 d

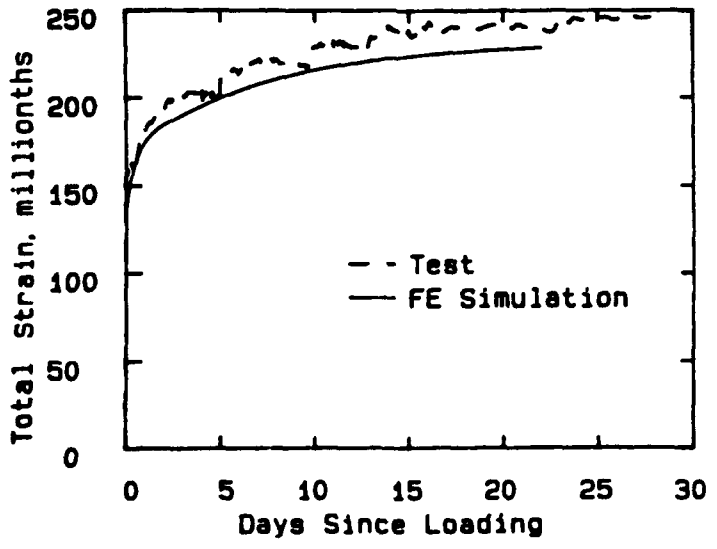

c. Age at loading = 3 d

Figure 8. (Sheet 2 of 3)

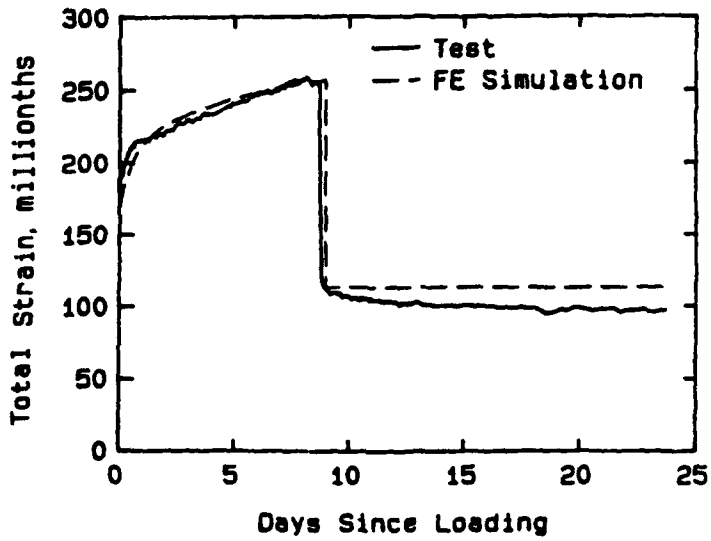

d. Age at loading = 7 d

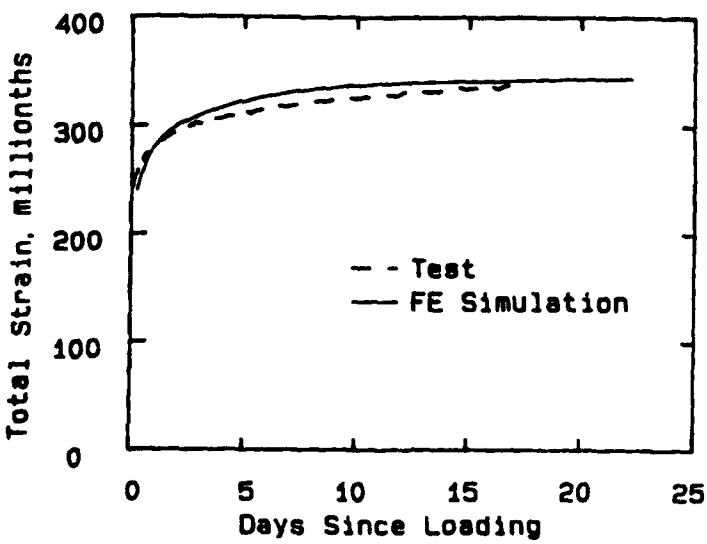

e. Age at loading = 14 d

Figure 8. (Sheet 3 of 3)

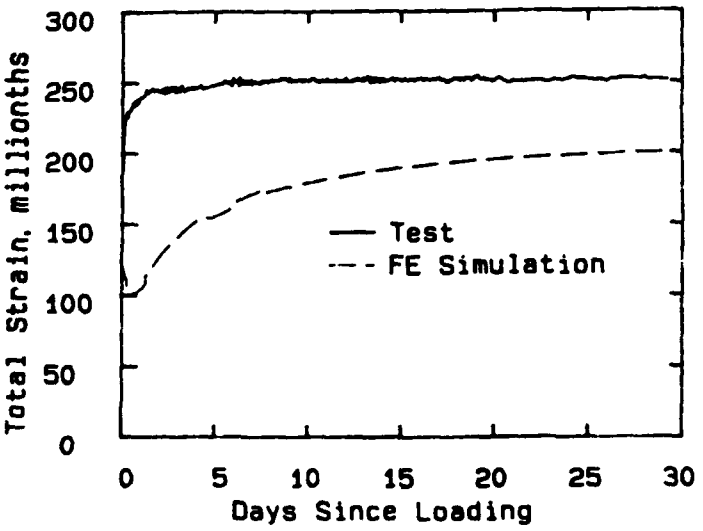

a. Age at loading = 19 h

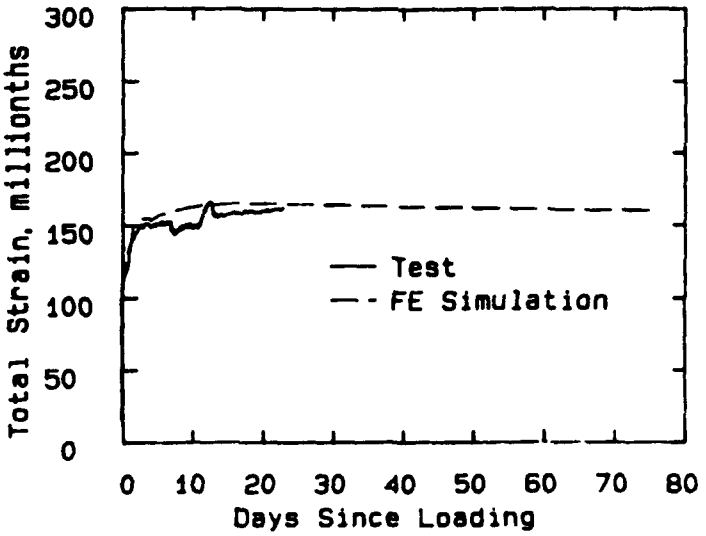

b. Age at loading = 7 d

Figure 9. Comparison of material model with creep test data, Mixture A13 (Continued)

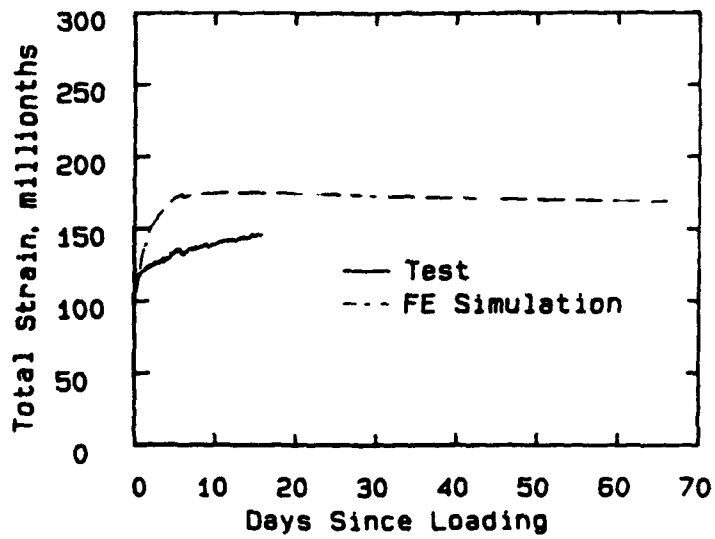

c. Age at loading = 14 d

Figure 9. (Concluded)

PART IV: FINITE-ELEMENT MODEL

Selection of Structural Sections for Analysis

42. The results of a crack survey of Lock and Dam 2, that was conducted for the Vicksburg District, were used to determine the monoliths to be modeled in the two-dimensional study. Cracks were observed running longitudinally along the floor sections of all lock monoliths. Particularly severe cracking occurred in the relatively thick upper-gate-bay monolith floor. Some random vertical cracking was observed in the walls, but most wall cracks occurred near extreme changes in section along the length of the wall (for example, at the miter gates and at the tainter-valve recesses). Whenever a relatively thin wall section was surrounded by more massive upstream and downstream sections, cracking occurred in the thinner section. A two-dimensional analysis cannot be expected to predict this type of cracking in a wall section. Cracking was also observed along the top surface of the dam weir monoliths. Conversations with Vicksburg District personnel confirmed that cracking is common in the thick floor section in the upper-gate-bay monolith and in the high-strength layer that normally tops the dam weir monoliths.

43. Based on this information, three sections were selected for the initial analysis: (1) a typical chamber monolith section, (2) the upper-gate-bay section (slightly downstream of the miter gates), and (3) a typical dam weir section. The two-dimensional grids generated for the chamber monolith and upper-gate-bay sections represent sectional planes transverse to the axis of flow. Lock monoliths were assumed to be symmetrical relative to the axis of flow, and the chamber monolith and upper-gate-bay models represent one-half of the transverse cross section. The dam weir monolith section was parallel to the axis of flow.

FE Grid Generation

44. Two-dimensional analyses were made using 8-node heat transfer, plane-strain, and plane-stress elements from the ABAQUS library of elements. These elements provide nonlinear fields for temperatures and displacements.

Standard 3 x 3 integration (with nine calculation points per element) was used for all heat-transfer analyses, and reduced integration (with four points per element) was used in the stress analyses.

45. Initially, a plane-strain element was selected for stress analyses. In a plane-strain analysis, strains in the out-of-plane direction are assumed to be constant along the length of the structure. This type of analysis is considered to be valid for very long structures. In practice, however, the out-of-plane strain is always zero. This condition corresponds to total restraint of out-of-plane strains, a condition which probably does not exist in mass concrete structures. Since stresses due to this restraint are calculated in the UMAT model, a plane-strain analysis can result in excessive out-of-plane stresses and out-of-plane cracking. In cases where out-of-plane cracking caused convergence problems, plane-stress analyses were used. In a plane-stress analysis, out-of-plane stresses are assumed to be constant (or zero) along the length of the structure. This corresponds to no restraint in the out-of-plane direction. Obviously, neither of these analyses gives a complete picture of stresses in most mass concrete structures. However, they can be used to determine the upper and lower limits of in-plane and out-of-plane stresses.

46. The volume of a mass of concrete increases as the internal temperature rises due to hydration of the cement. Restraint of this increase in volume results in compressive stresses. As the concrete begins to cool, tensile stresses are generated in the horizontal and out-of-plane directions due to restraint of volumetric decreases caused by cooling and shrinkage. A plane-strain analysis can be expected to give a "worst case" for these tensile stresses. Stresses in the out-of-plane direction are maximized and the Poisson's effect of these stresses is added to in-plane tensile stresses. A plane-stress analysis should result in slightly lower in-plane tensile stresses.

47. In the FE heat-transfer analyses, openings in the concrete at equipment rooms or culverts were modeled using 8-node elements and properties of air. For the stress analyses, no elements were generated at the voids.

48. In each of the heat-transfer analyses, soil was included for a depth of 10 ft from the base of the concrete and extending 10 ft beyond the outermost concrete element. From work done on the Lock and Dam 26R analyses (Truman, Petruska, and Fehri 1989), 10 ft has been found to be the critical depth for modeling the effects of the soil on concrete temperatures. Based on soil borings at the Lock and Dam 3 site, soil temperature at that depth was assumed to be a uniform 70 °F.

49. The element size for the finite-element grids was based upon two constraints. The first constraint resulted from the type of integration procedure used in the transient heat-transfer algorithm in the finite element code. A relationship exists between the minimum usable time step and the distance between nodes (ABAQUS Users Manual 1988). A maximum time step of 0.25 day is required in order to reproduce accurately changes in temperature during the first two days after placement. The approximate maximum distance between nodes corresponding to a time step of 0.25 day is 14 in. This yields an element length (for 8-node elements) of 28 in. However, from past experience at WES, it has been established that this limit is critical only in the direction of heat flow. Thus, in a lock monolith floor slab, where heat loss occurs in the vertical direction only except near the outer edges, longer elements can be used. With a few exceptions, a maximum element size of 30 in. was maintained in the direction of heat flow. The second constraint on element size is based upon anticipated lift heights. A minimum of two elements is required to capture the stress distribution across a section. This limitation also dictated 30-in. element heights, because 5-ft lifts were used in the initial analysis.

50. The upper-gate-bay grid used in the heat-transfer analysis and the grid used in the corresponding stress analysis are shown in Figures 10 and 11, respectively. The grids used in the stress analysis of the chamber and dam weir monoliths are shown in Figures 12 and 13, respectively.

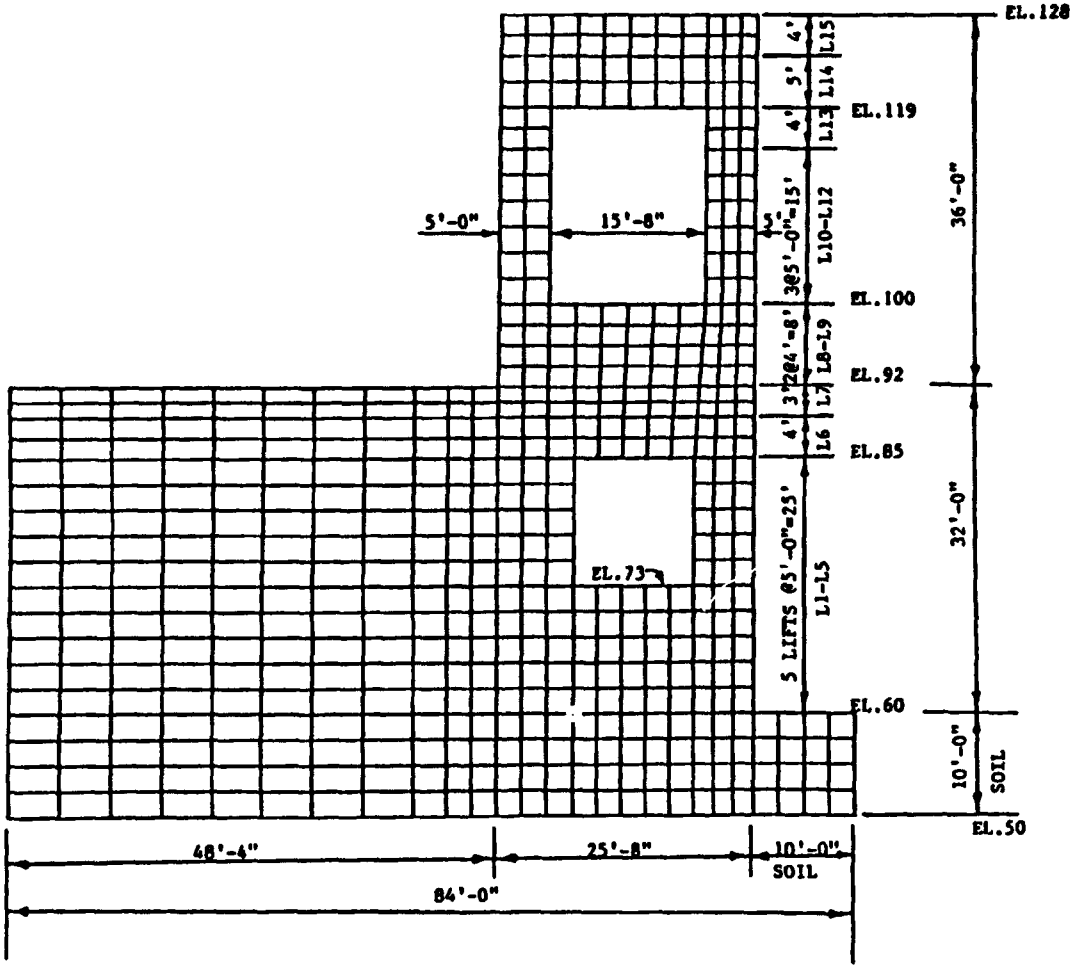

Figure 10. FE grid of upper-gate-bay monolith for heat transfer analyses

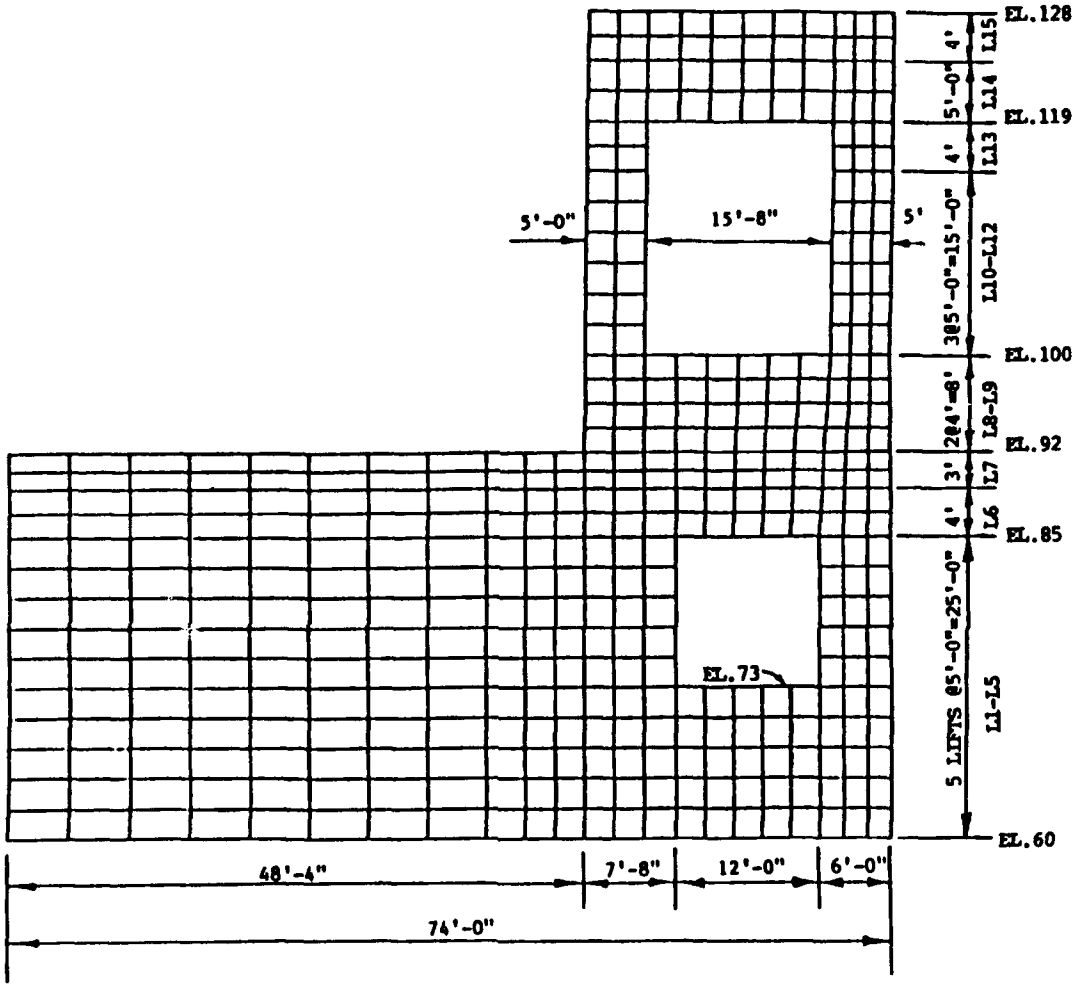

Figure 11. FE grid of upper-gate-bay monolith for stress analyses

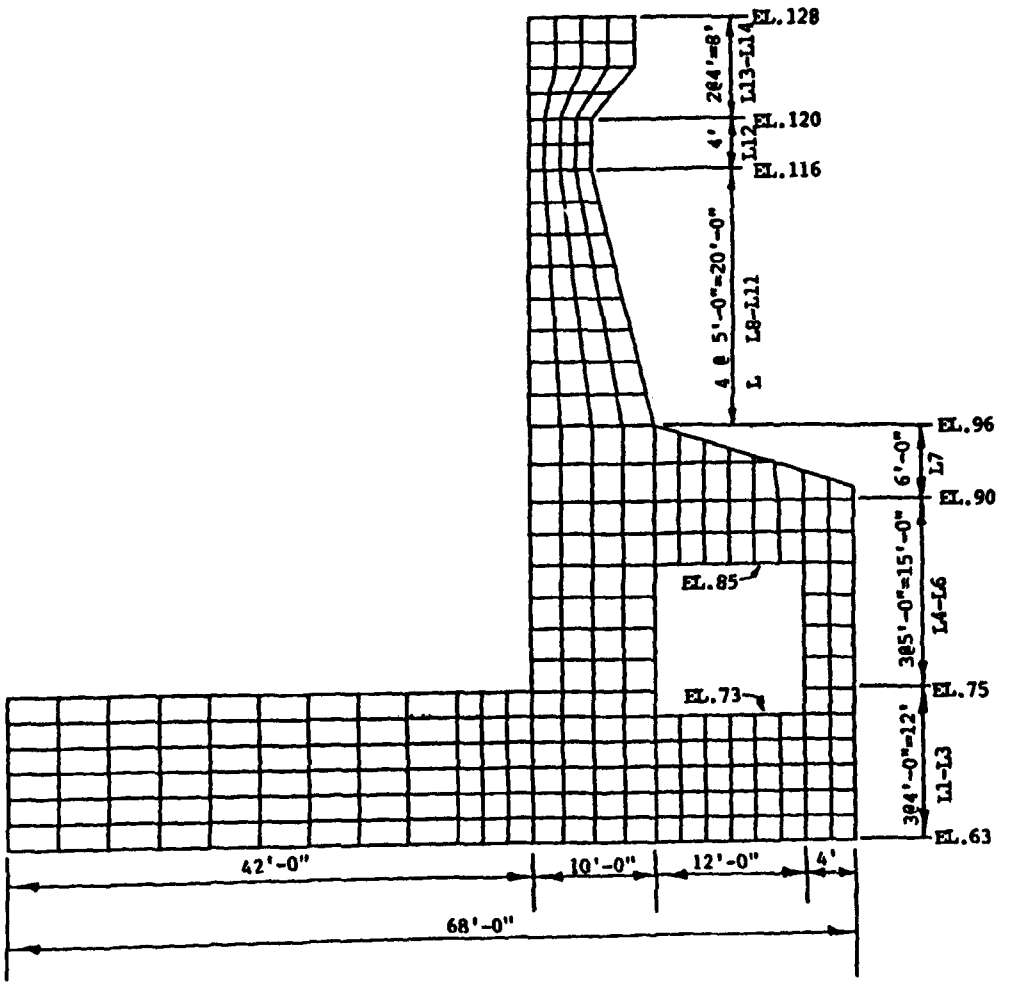

Figure 12. FE grid of lock chamber monolith for stress analyses

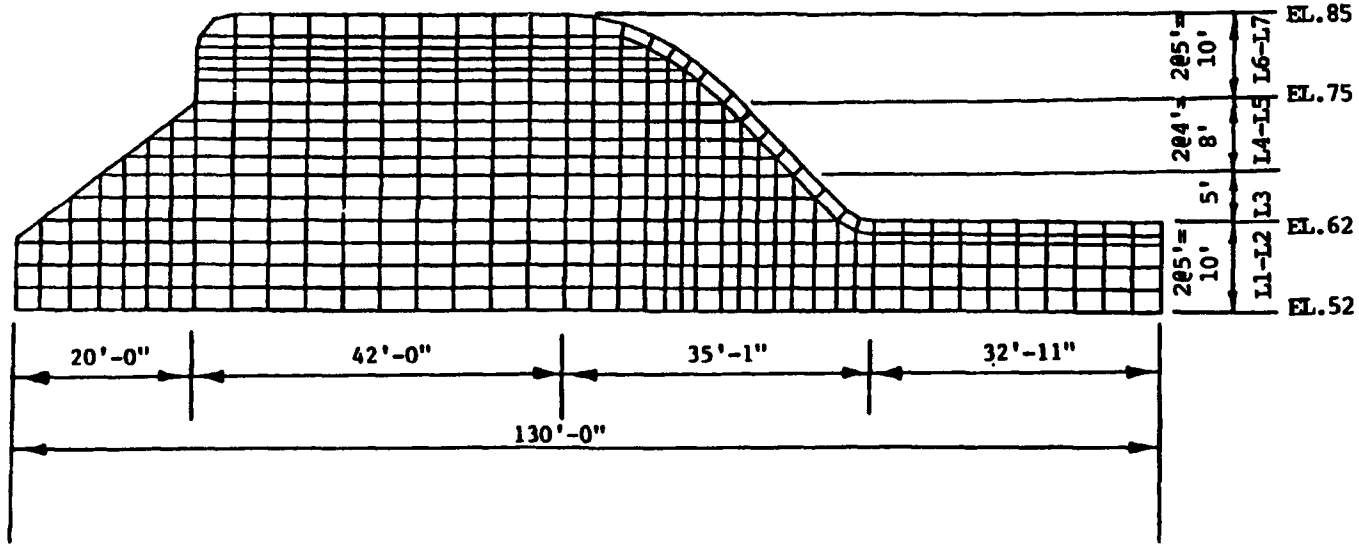

Figure 13. FE grid of dam weir monolith for stress analyses

Construction Parameters and Boundary Conditions

Construction parameters

51. Lift heights used in the FE models were based on discussions with Vicksburg District personnel. An initial lift height of 5 ft was selected, with lift heights of up to 10 ft to be used in later analyses in the walls. Because of anticipated concrete batch plant limitations, larger lifts were not considered for the dam weir section or the lock monolith floors. Lift locations are shown in Figures 10 through 13.

52. The concrete placement rate and concrete form removal times were selected based on actual field practices as determined from a review of the records from Overton Lock and Dam and from discussions with field engineers. Although lift placement intervals of as little as 5 days were used in the lock walls at Overton Dam, placement intervals in the lock floors varied from about 10 days to over a month. Accordingly, a placement interval of 10 days between lifts was used in the dam weir section and in lock monolith floors, while a 5-day interval was used for walls.

53. Placement temperatures and air temperatures at Overton Lock and Dam for a complete calendar year were studied to determine placement temperatures for input into the thermal analyses. The year 1985 was chosen because a complete set of placement temperature data and air temperature data was readily available. Placement temperature data were obtained from the Vicksburg District. Actual mean daily temperatures and expected mean daily temperatures were obtained from the National Weather Service for Alexandria, Louisiana, and Shreveport, Louisiana, respectively. Figure 14 shows a plot of these data. From the plot, it is observed that the weather in 1985 was characterized by an unusually cold winter (the first 50 or so days of the year), a warmer than normal spring and fall, and a near-normal summer. A 28-day moving average of the concrete placement temperature, actual mean daily temperature, and expected mean daily temperature were calculated to smooth the daily fluctuations. In reality, the concrete placement temperature on a given day is strongly dependent upon the temperature history in the previous weeks because of a time-lag effect in which the temperature of the materials lags

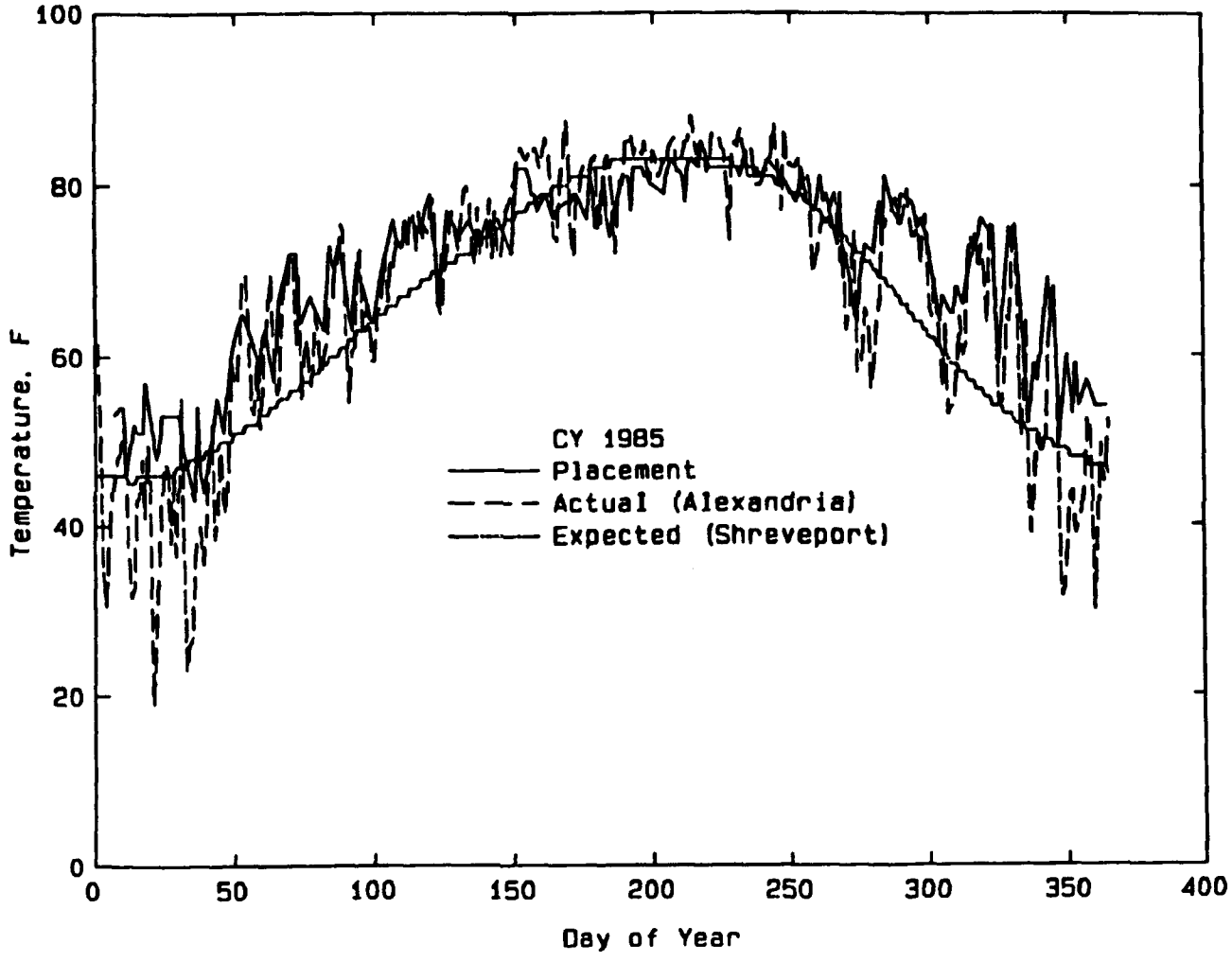

Figure 14. Daily temperatures for calendar year 1985, Lock and Dam 2

behind the short-term air temperature trends. Plots of the 28-day moving averages are shown in Figures 15 and 16.

54. Because it is not possible to forecast actual mean daily temperatures during construction, the air temperature was assumed to follow the expected mean daily temperature in the thermal calculations. From Figure 16, it is apparent that even though 1985 was a year of temperature extremes, the 28-day moving average of placement temperature shows some relationship to the expected mean daily temperature. During the winter, spring, and late fall months, the placement temperatures ran approximately 5 °F above the expected mean daily temperatures. During the early summer, the placement temperatures ran a few degrees below the expected mean daily temperatures. However, during the late summer and early fall, the placement temperatures are almost equal to the expected temperatures.

55. With the above considerations in mind, placement temperatures in the thermal calculations were chosen to be 5 °F above the expected mean daily temperature with an assumed ceiling of 85 °F as was specified for Lock and Dam 3. This represented a worst case for analysis.

56. Form removal was simulated in the heat-transfer analyses by changing film coefficients to allow more heat loss. In the stress analyses, gravity loads were applied as body forces. The formwork was assumed to prevent lateral strains from developing prior to its removal, hence body forces were not applied to new concrete (but were simulated as pressures on existing concrete) until forms were removed. Form removal times used in the analyses were 2 days for vertical surfaces and 5 days for culvert ceilings and cantilevers. These times corresponded closely with actual field practice and conveniently occurred at new time steps in the analysis.

57. Two methods were possible for modeling the high-strength layer on the surface of the dam weir section (Figure 13). The high-strength concrete could be considered to be placed at a later time than the lower-strength concrete below, or it could be incorporated into appropriate lifts. Placing the high-strength layer at the same time as the underlying concrete should result in less cracking and was the method used in the Overton Dam weir monoliths; therefore, this method was simulated in the analyses.

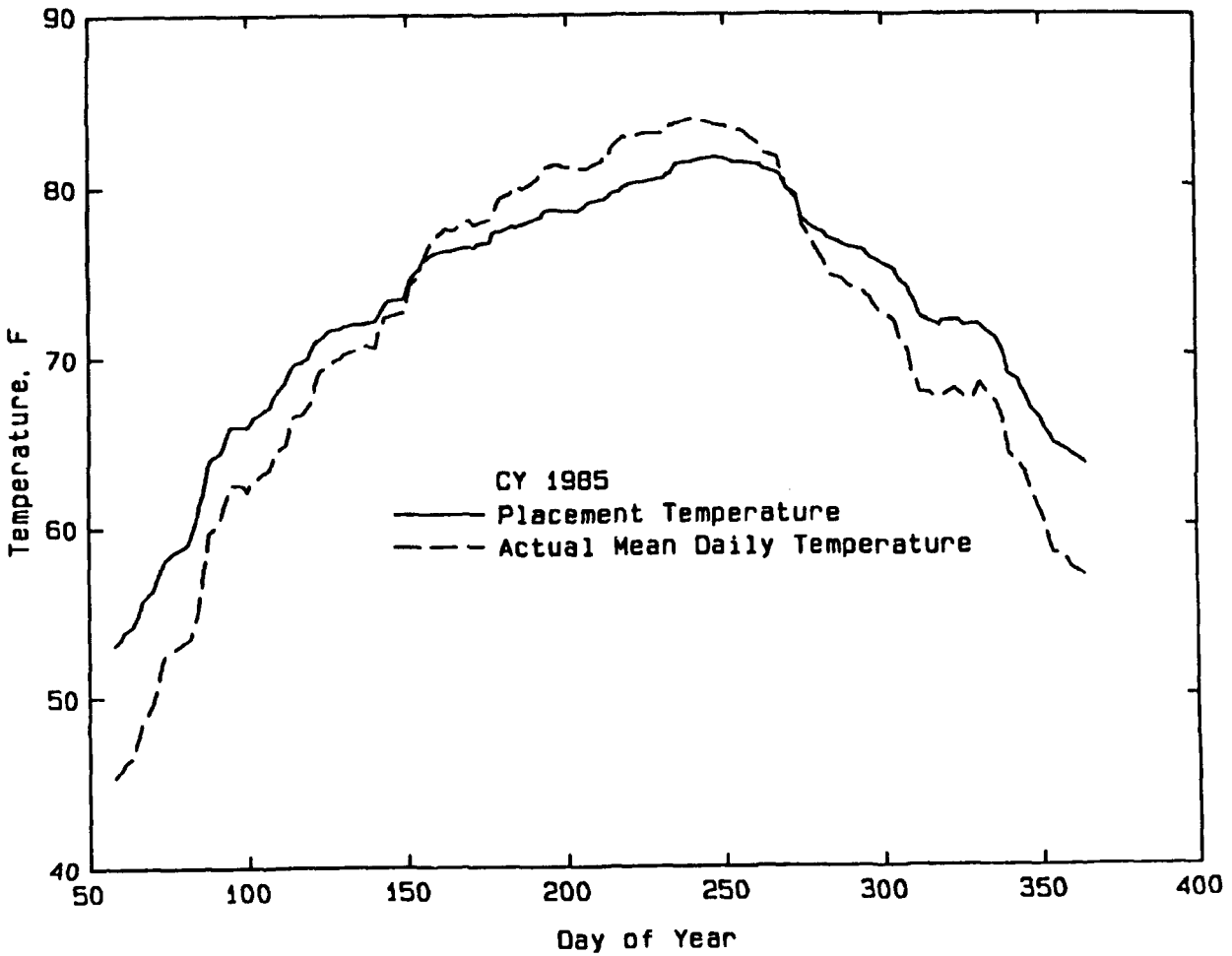

Figure 15. 28-day moving average concrete placement and mean daily air temperatures

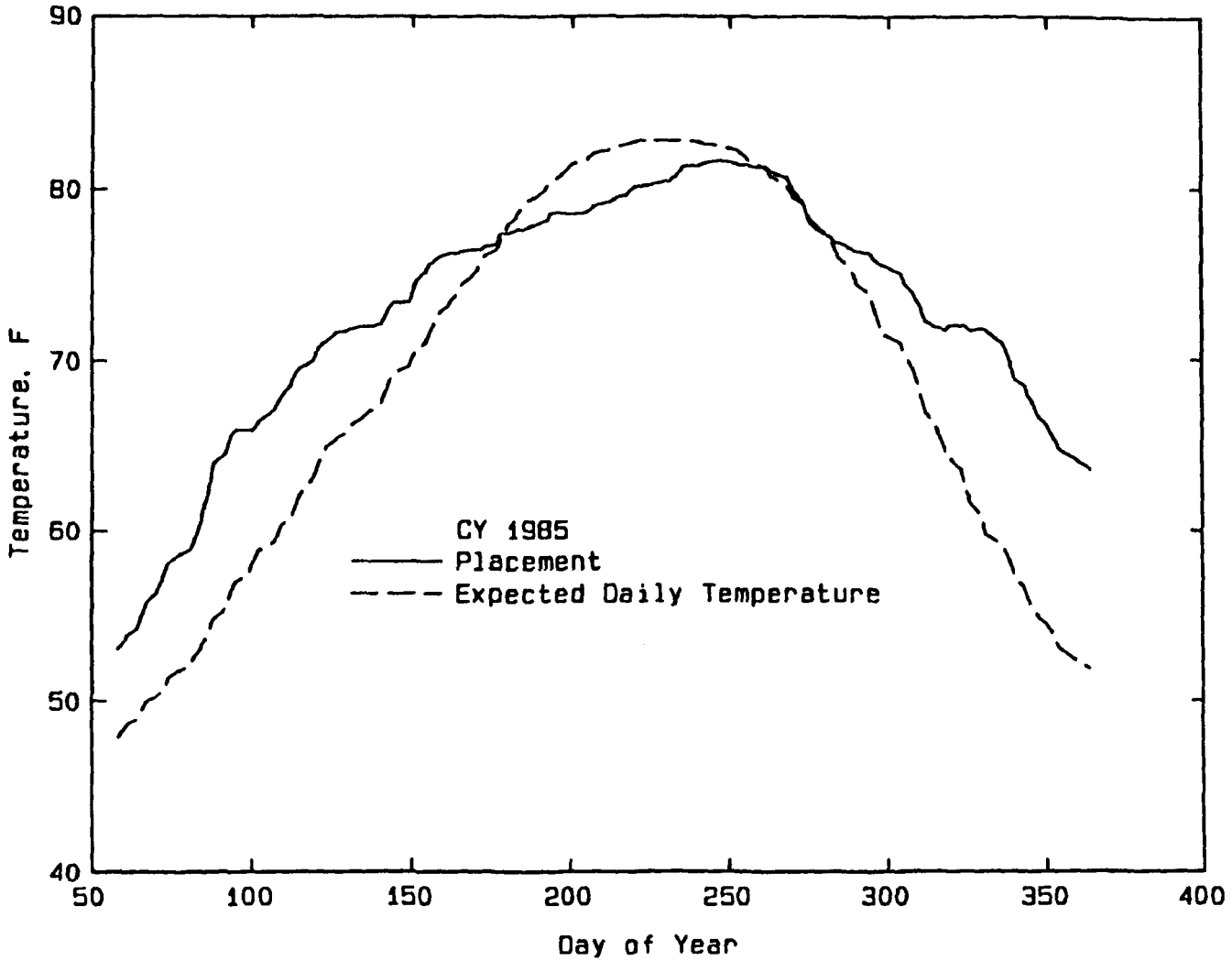

Figure 16. 28-Day moving average concrete placement and mean daily expected air temperatures

58. Because construction could begin at any time after midsummer, two possible construction starting dates were considered in the analyses. It was assumed that insulation would be required between 1 November and 1 April (as specified in the Lock and Dam 3 Concrete Specifications): therefore, an early summer start should result in the highest temperature differentials and thermal stresses for a given concrete mixture. Based on this assumption, a summer starting date of 1 July was selected for the initial analyses. However, two different mixtures were proposed for these structures: A13 for warm weather placement and A8 for cold weather placement. Because the A8 mixture exhibited a higher modulus and less creep at a given time than A13, the possibility existed that the winter start might produce significantly high stresses, and a 1 November start-of-placement date was also selected.

Thermal boundary conditions

59. The lower boundary of the soil temperature in all models was fixed at 70 °F based upon measured temperatures of soil borings as described earlier. No horizontal heat flow was permitted through vertical model boundaries at the symmetric monolith centerlines of the chamber and upper gate monoliths or through vertical soil boundaries.

60. All other heat flow from the surface is a function of the surface heat-transfer film coefficients which control heat exchange between the structure and the ambient air. A film coefficient is composed of a convection or surface conductance coefficient that defines heat exchange with surrounding air as a function of air velocity and a conduction heat-transfer coefficient which defines the heat flow through formwork or surface insulation, or both. The following general equation is used to compute the composite film coefficient

$$h = \frac{1}{1/h_{air} + 1/C_{formwork} + 1/C_{insulation}} \quad (Btu/ft^2\text{-}hr\text{-}^\circ F)$$

where

h_{air} = convection coefficient or surface conductance

$C_{formwork}$ = conductance of formwork (when in use)

$C_{insulation}$ = conductance of insulation (when in use).

61. The surface conductance was computed by the following equation (Jurges 1924) for a wind velocity less than or equal to 16.5 ft/s and a rough surface texture

$$h_{air} = 1.087 + 0.225V \qquad (Btu/ft^2\text{-}hr\text{-}^\circ F)$$

where V is air velocity in ft/s.

62. Wind velocity data were not available from the National Oceanic and Atmospheric Administration (NOAA) for Natchitoches, Louisiana, which is located near the construction site. Historical wind velocity data were available for each month in the year for Shreveport and Alexandria. Since the construction site is approximately midway between Shreveport and Alexandria, an average of the wind velocities from these cities was computed (V = 6.5 mph or 9.5 ft/s) to be representative of average wind velocity at the construction site for the months of July through March.

63. Formwork was assumed to be 0.75-in. plywood with a conductance of 1.07 $Btu/ft^2\text{-}h\text{-}^\circ F$. In temperature calculations when insulation was simulated, a conductance of 0.25 $Btu/ft^2\text{-}h\text{-}^\circ F$ (R value = 4) was used. Vertical formwork was assumed to be removed two days after placement of a lift. Horizontal formwork as used in the ceilings of culverts was assumed to be removed 5 days after concrete placement. The effect of insulation was simulated during the period of 1 November through 30 March as required in the specifications for Lock and Dam 3 for concrete freezing protection. The surfaces of culverts were assumed to be exposed to the same wind velocity as other exterior surfaces, although guide specifications require that the culverts be closed during construction. Table 5 shows the values used for the surface-film coefficients.

Kinematic boundary conditions

64. For the stress analysis, soil was not modeled. The FE grids were supported at the base and axes of symmetry with rollers. The dam weir section, which had no axis of symmetry, was fixed in both the x- and y-directions at the lower left-hand node for stability.

Table 5

Surface-Film Coefficients Used in Thermal Simulations

Surface Condition or Exposure	Film Coefficient (BTU/in^2-day-^oF)
wind only	0.53867
wind + forms	0.16549
wind + insulation	0.03868

PART V: TWO-DIMENSIONAL THERMAL STRESS ANALYSES

Heat-Transfer Analyses

65. A summary of all two-dimensional heat-transfer analyses is given in Table 6. The Mixture A13 adiabatic curve was used for all lifts with placement dates of 1 July - 31 October. Placement temperatures in the summer analyses (with a start-of-placement date of 1 July) varied from 85 °F to 73 °F except in the fourth upper-gate-bay run, where a 75 °F-maximum placement temperature was used in the floor section. The Mixture A8 curve was used in all lifts with placement dates between 1 November and 31 March. Placement temperatures for concrete in these lifts varied from approximately 68 °F to 53 °F. Placement temperatures for all analyses are presented in Tables 7-9. The time interval between successive lifts was chosen as 10 days. This interval was selected after careful study of construction records from Lock and Dam 2, Red River Waterway.

Table 6

Summary of Two-Dimensional Heat Transfer Analyses

Name	Start-of-Placement	Mixture	Notes
CMT1	July 1	A13	5-ft lifts
CMT2	July 1	A13	10-ft lifts in walls
CMT3	November 1	A8	5-ft lifts
UGBT1	July 1	A13	5-ft lifts
UGBT2	July 1	A13	10-ft lifts in walls
UGBT3	November 1	A8	5-ft lifts
UGBT4	July 1	A13	75 °F placement, lifts 1-7
UGBT5	July 1	A13	15 days between lifts, lifts 1-7
DWT1	July 1	A13	5-ft lifts

Table 7

Placement Temperatures, Chamber Monolith Analyses

	Temperatures, °F		
Lift	CMT1	CMT2	CMT3
1	85.0	85.0	67.6
2	85.0	85.0	64.6
3	85.0	85.0	61.5
4	85.0	85.0	59.4
5	85.0	85.0	58.3
6	85.0	85.0	57.2
7	85.0	85.0	56.1
8	85.0	85.0	55.1
9	85.0	85.0	54.0
10	82.0		53.7
11	80.0		53.5
12	78.0		53.3
13	77.0		53.3
14	73.0		53.3

Table 8

Placement Temperatures, Upper-Gate-Bay Monolith Analyses

	Temperatures, °F				
Lift	UGBT1	UGBT2	UGBT3	UGBT4	UGBT5
1	85.0	85.0	67.6	75.0	85.0
2	85.0	85.0	64.6	75.0	85.0
3	85.0	85.0	61.5	75.0	85.0
4	85.0	85.0	59.4	75.0	85.0
5	85.0	85.0	57.2	75.0	85.0
6	85.0	85.0	55.0	75.0	83.4
7	85.0	85.0	53.7	75.0	78.6
8	85.0	85.0	53.3	85.0	73.5
9	85.0	85.0	53.3	85.0	71.8
10	82.0	82.0	53.3	82.0	70.2
11	80.0	80.0	53.4	80.0	68.6
12	78.0		53.6	78.0	66.9
13	77.0		54.0	77.0	65.3
14	75.0		55.3	75.0	63.7
15	73.0		56.6	73.0	62.2

Table 9

Placement Temperatures, Dam Weir Section Analysis

Lift	Temperatures °F DWT1
1	85.0
2	85.0
3	85.0
4	85.0
5	85.0
6	85.0
7	85.0

66. Results of the various analyses are discussed below in terms of maximum temperatures and temperature differentials across a section. Although temperature differentials are a convenient way of quantifying the results of the heat-transfer analyses, they should not be considered the determining factor for the development of cracking. Monolith geometry, boundary conditions, concrete shrinkage, and linear coefficient of thermal expansion also affect cracking. The temperature differential that will result in cracking must be individually determined for each monolith, concrete mixture, and set of construction conditions.

Chamber monolith Run 1 (CMT1)

67. The location of nodes for which temperature-time history plots are presented is shown in Figure 17. For CMT1 the nominal lift height was 5 ft for all 14 lifts with a start of placement date of 1 July. Maximum temperatures in the floor and wall were approximately 101 °F, and temperature differentials between the center and top of the floor were less than 15 °F. Heat flow throughout the majority of the floor section was one-dimensional, i.e., the heat flow was through the top of the slab, and temperatures in this area were uniform for a given elevation. This can be seen in plots of nodal temperatures at elevation 65.0 ft, elevation 69.0 ft, and elevation 73.0 ft in Figures 18-20. At elevation 65 ft, temperatures were relatively uniform throughout most of the section. At higher elevations, heat flow became two-dimensional around the wall and culvert. Small inconsistencies in temperature

attributable to element size can be seen in Figure 18, where slight variations in temperatures (less than 1 °F) existed between nodes 1502 and 1562. Because of the relative thinness of the structure, internal temperatures dropped to close to ambient during the construction period. Temperatures at various nodes throughout the structure are plotted against ambient temperature in Figures 21-23. No contour plots were generated in this analysis.

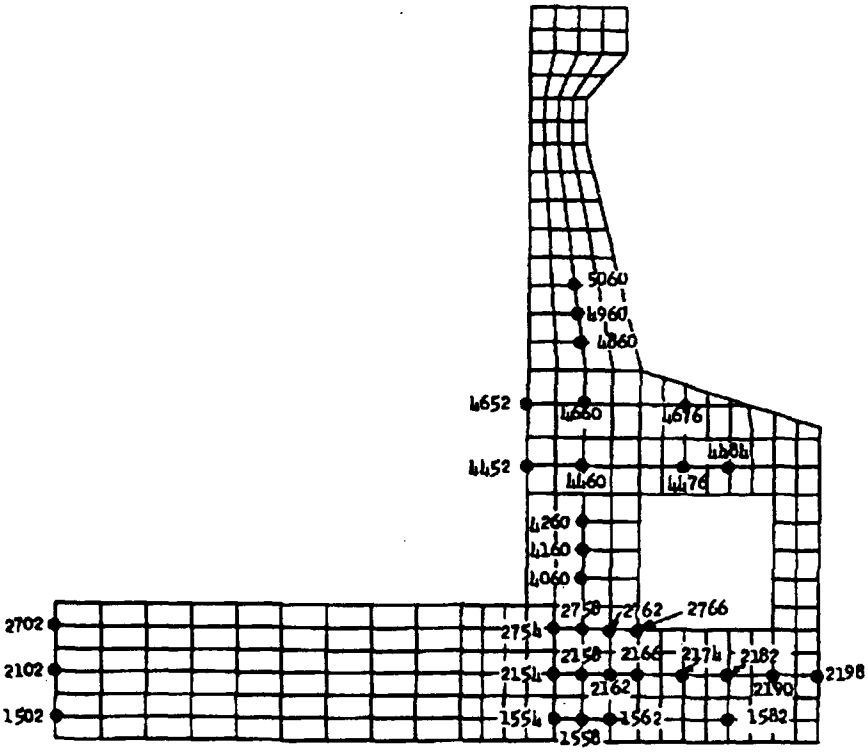

Figure 17. Location of selected nodes, chamber monolith thermal calculations

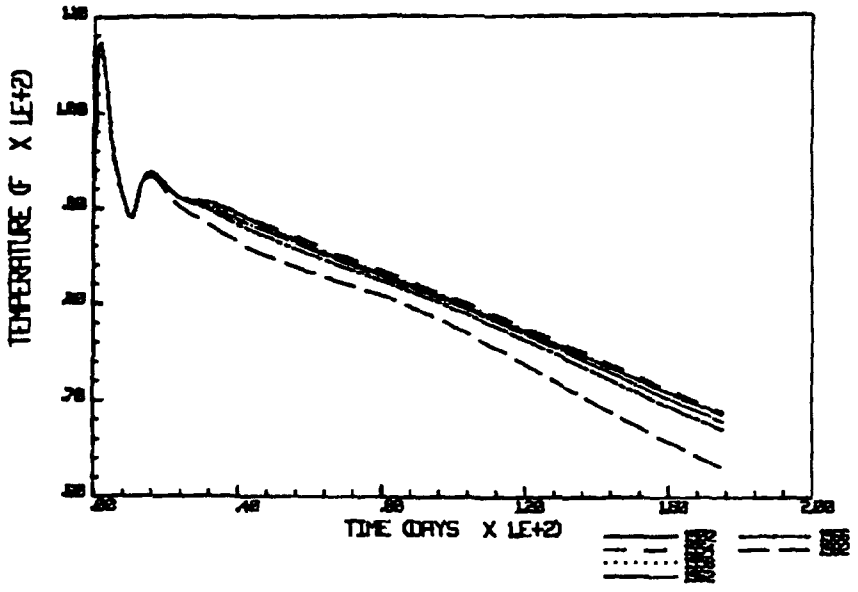

Figure 18. Temperatures at selected nodes, elevation 65 ft, CMT1

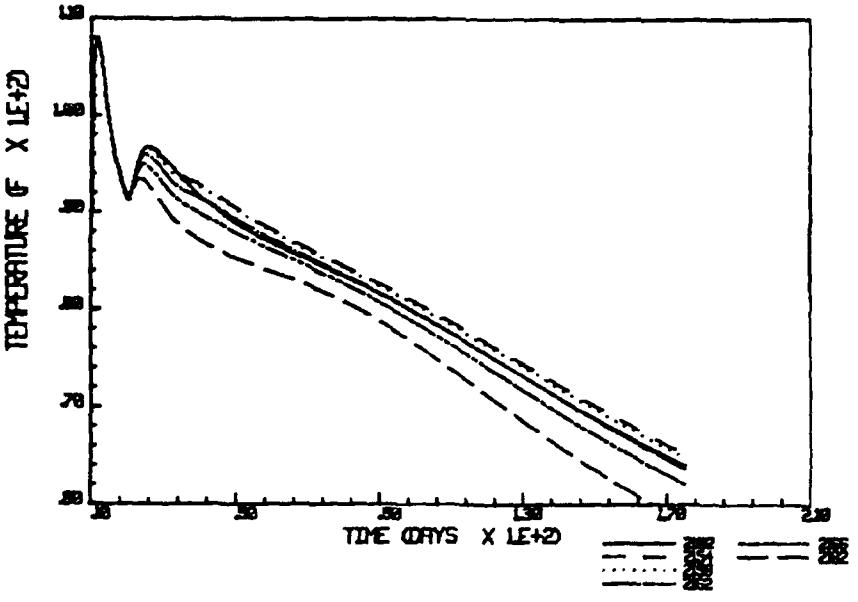

Figure 19. Temperatures at selected nodes, elevation 69 ft, CMT1

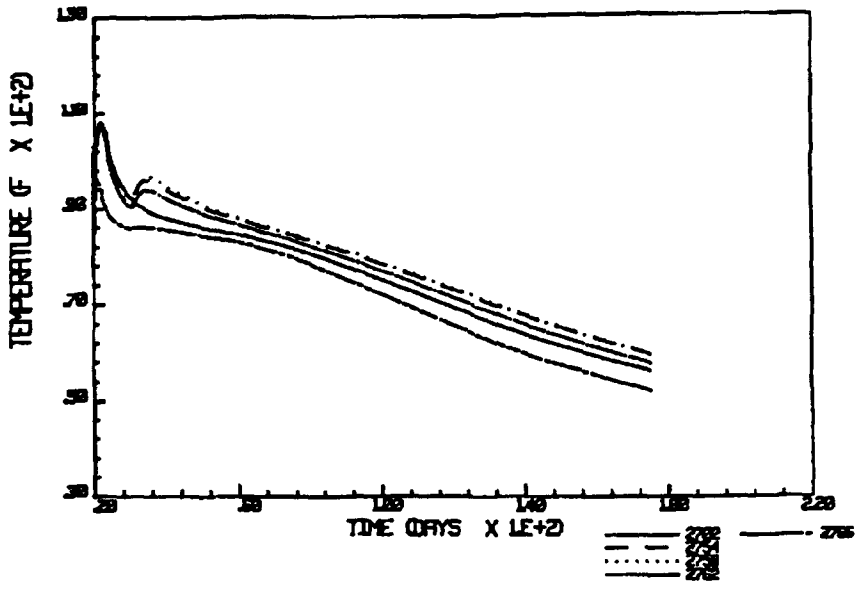

Figure 20. Temperatures at selected nodes, elevation 73 ft, CMT1

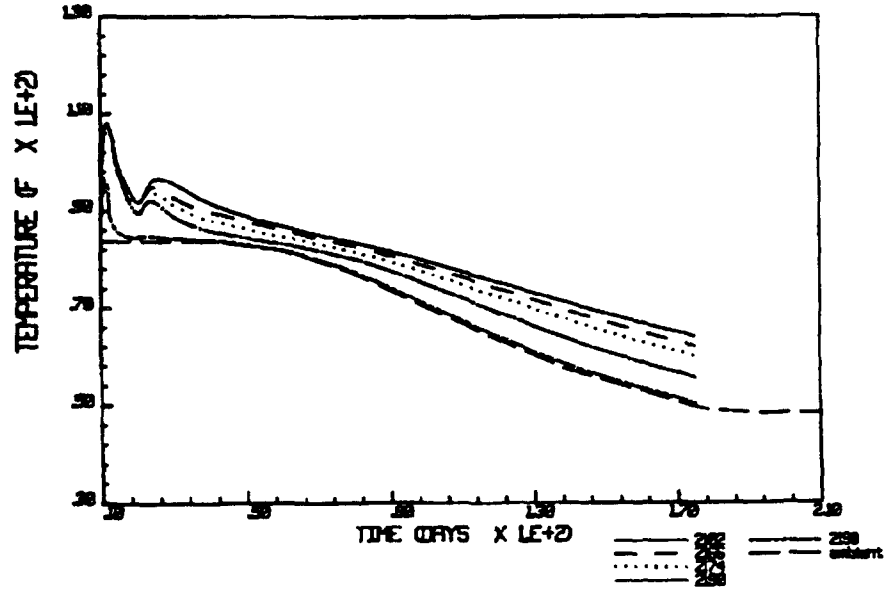

Figure 21. Temperatures at elevation 69 ft versus ambient temperature, CMT1

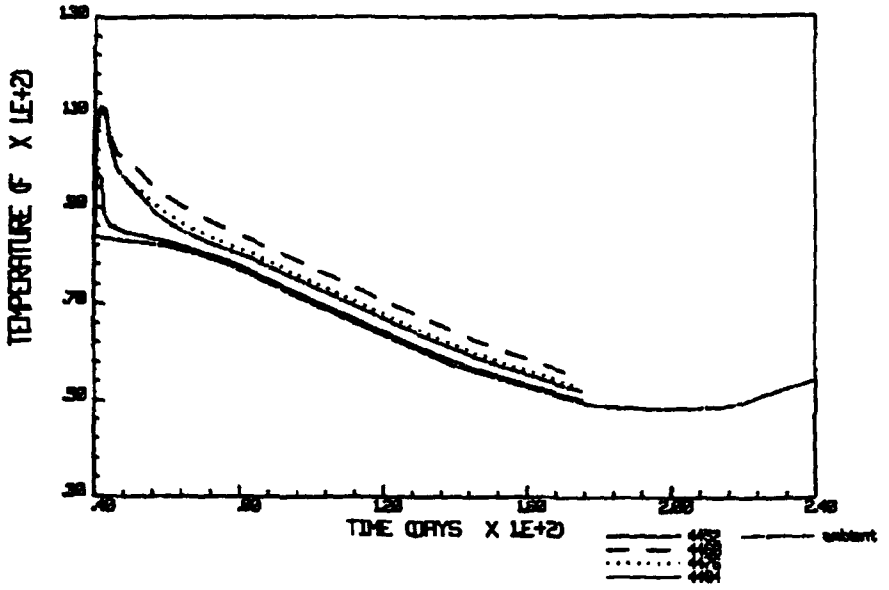

Figure 22. Temperatures in Lift 6 versus ambient temperature, CMT1

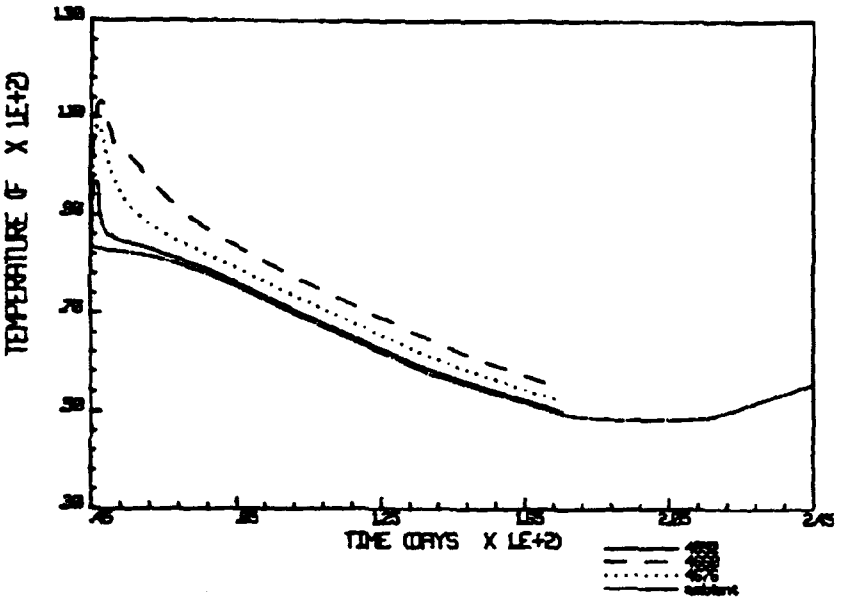

Figure 23. Temperatures in Lift 7 versus ambient temperature, CMT1

Chamber monolith Run 2 (CMT2)

68. Lift heights in the wall (lifts 4-10) were a maximum of 10 ft for this analysis. All other parameters remained the same as in CMT1. Because of the two-dimensional nature of heat flow in the walls, temperatures were only slightly higher than those in the previous analysis at 10 days after placement. Temperatures at various nodes in the first two analyses are compared in Figures 24 and 25. No contour plots were generated in this analysis.

Chamber monolith Run 3 (CMT3)

69. The starting date for concrete placement was 1 November. Nominal lift height for all 14 lifts was 5 ft. All exposed surfaces were insulated for 150 days.

70. Maximum temperatures in the first seven lifts were approximately 90 °F to 95 °F. Maximum temperatures in later lifts were lower as ambient temperature decreased and thinner lifts were placed. Temperatures in this relatively thin structure were very close to ambient by the time the insulation was removed. Maximum temperature differentials varied from about 10 to 15 °F degrees except in the area of the culvert. The lowest temperatures were at the outer edge of the culvert, where heat loss into the soil and the relative thinness of the section allowed temperatures to drop to close to ambient much sooner than in the rest of the structure.

Upper-gate-bay Run 1 (UGBT1)

72. The maximum lift height for all 15 lifts in the first upper-gate-bay run was 5 ft. The starting date for placement was 1 July. Maximum temperatures of approximately 110 °F in the floor and 104 °F in the walls were observed in the center of each lift within the first 2 days after placement. Just prior to the placement of the first wall lift (at 70 days), the maximum temperature in the floor was 98 °F, with a 16 °F difference in temperatures at the center and top of the section. By the end of the construction period (110 days after start of placement), maximum temperature in the center of the floor slab was still in excess of 90 °F, and a 20 °F differential existed between the center and top. Even though the concrete was less than 6 months old on 1 November, the run was continued without insulation, and temperature

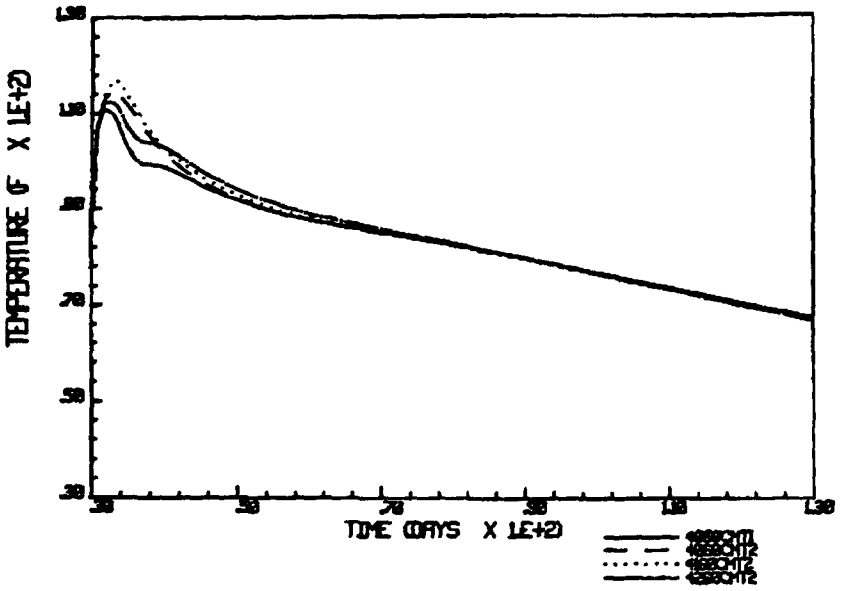

Figure 24. Comparison of temperatures in lift 4 for 5-ft lifts (CMT1) and 10-ft lifts (CMT2)

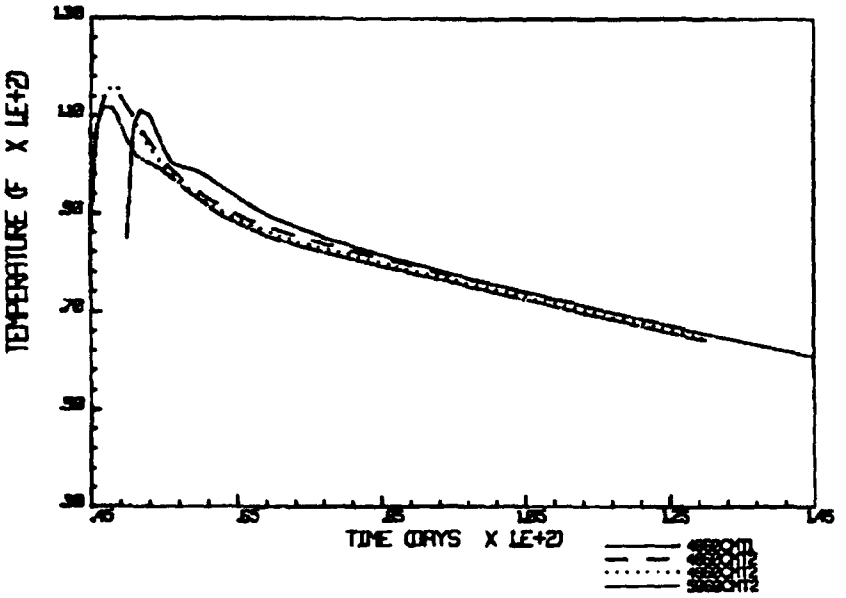

Figure 25. Comparison of temperatures in lift 8 of CMT1 and lift 7 of CMT2

differentials in the floor exceeded 30 °F during this period. This is an unacceptable temperature differential and is another indicator of the necessity of insulating thick sections (greater than approximately 15 ft) during cool months until the interior temperature has dropped significantly.

Upper-gate-bay Run 2 (UGBT2)

72. In Run 2, nominal lift height for the walls (lifts 8-11) was 10 ft. All other parameters remained the same as for Run 1. Maximum temperature in the walls was approximately 112 °F in Lift 8. Temperature differentials in Lifts 8 and 11 exceeded 25 °F at relatively early times (2 to 3 days after placement). Floor temperatures were similar to those in Run 1.

Upper-gate-bay Run 3 (UGBT3)

73. The starting date for placement in Run 3 was 1 November. All exposed surfaces were insulated for a period of 150 days, and a maximum lift height of 5 ft was used for all 15 lifts.

74. Maximum temperature in the floor was approximately 92 °F. Maximum temperatures in the walls (due to the lower placement temperatures at later times) were less than 82 °F. At the end of the construction period, the maximum temperature at the center of the floor had fallen to approximately 82 °F. Because of the insulation, temperature differentials were much lower than in previous upper-gate-bay runs, with a maximum differential between the center and top of the floor slab of about 16 °F. However, the outer edge of the culvert was considerably cooler than the rest of the structure due to heat loss into the soil at the base and the relatively thin section. The resulting temperature differentials across the base of the culvert exceeded 20 °F. The maximum temperature differentials in the wall were less than 10 °F.

Upper-gate-bay Run 4 (UGBT4)

75. In an effort to eliminate cracking problems discovered in the stress analysis (discussed in a subsequent section), Run 1 was resubmitted with a 75 °F placement temperature in the first seven lifts. Maximum temperature in the floor was approximately 101 °F. The maximum temperature in the floor at the end of the construction period was less than 90 °F. Temperature differentials between the center and top of the floor were less than 12 °F during the construction of the floor section, although they approached 20 °F at the end of the construction period after average ambient

temperatures dropped below 70 °F. As in previous runs, the floor section was left uninsulated after 1 November, and temperature differentials exceeded 30 °F during this period. Maximum wall temperatures and temperature differentials in the wall were similar to those in Run 1.

Upper-gate-bay Run 5 (UGBT5)

76. At the request of the Vicksburg District, an alternate method was attempted for reducing temperatures in the floor. Run 1 was resubmitted with lift placement intervals of 15 days rather than 10 days. This reduced maximum temperatures in the floor just prior to placement of the next lift by 2 °F to 4 °F. Because of the longer construction period, average ambient temperatures fell approximately 16 °F during the placement of the floor section. Prior to placement of the first wall lift (at 105 days after the start of construction) the maximum temperature at the center of the floor section was 92 °F, but the ambient temperature had dropped to 68 °F, resulting in a thermal differential exceeding 20 °F. Even though maximum temperatures were slightly reduced, thermal differentials were increased by the delayed construction schedule.

Dam weir section Run 1 (DWT1)

77. Because of batch-plant limitations, 10-ft lifts were not considered for the dam weir section. The start-of-placement date for Run DWT1 was 1 July. The higher-strength elements were located at the surface of the structure where they would cool rapidly. Therefore, the temperature rise of these elements would not greatly affect the temperatures or stresses in the structure; thus, the Mixture A13 curve was used throughout. Maximum temperatures were less than 112 °F. The maximum temperature prior to the placement of each lift was approximately 100 °F. Temperature differentials were generally less than 16 °F during the construction period. However, the analysis was continued well into the fall without insulation. As ambient temperatures decreased, temperature differentials reached 30 °F.

Stress Analyses

78. All two-dimensional stress analyses are listed in Table 10. Analyses were made using eight-node plane-strain elements with reduced integration unless otherwise noted. Mechanical properties for Mixture A13

were used in all lifts placed between 1 July and 31 October. Mixture A8 mechanical properties were used in all lifts placed between 1 November and 31 March. The first three chamber monolith analyses were made prior to completion of testing for linear coefficient of thermal expansion (α), and assumed lower and upper bound values of 4.5 and 7.0 millionths/°F were used in the calculations. The final test value for coefficient of linear thermal expansion for all mixtures (5.5 millionths/°F) was used in later analyses.

79. Stress contour and displacement plots were the primary choice for output of results. Although contour plots were made at the end of each step for horizontal, vertical, out-of-plane, and maximum principal stresses, only the plots appropriate to the problem have been included in this report. In plane strain problems, maximum principal stress as calculated by ABAQUS was often dominated by out-of-plane stresses and could not be used to determine areas of high in-plane stress. Generally, vertical stresses were negligible except at exterior vertical faces, supports and corners of openings. Unless noted otherwise, for the plane-strain analyses horizontal and occasionally vertical stress contour plots have been presented. For the plane-stress analyses maximum principle stress plots have been added. Only plots for the step prior to the placement of each new lift have been presented. Elapsed time is given on each plot for reference.

Chamber monolith Runs 1 and 2 (CMS1 and CMS2)

80. In the first chamber monolith analysis (CMS1), nominal lift height was 5 ft for all 14 lifts, start-of-placement date was 1 July and coefficient of linear thermal expansion was 4.5 millionths/°F. No cracking occurred. The highest tensile stresses occurred in the top center of the slab and in the area of the culvert. The magnitudes were less than 300 psi. In the second analysis (CMS2), a coefficient of linear thermal expansion of 7.0 millionths was used. All other parameters remained the same. Extensive cracking resulted due to out-of-plane stresses at the top of the floor and near the lower left-hand corner of the culvert. Horizontal tensile stresses the top center of the floor were less than 350 psi. Horizontal stresses at the lower left-hand corner of the culvert approached 400 psi, although no in-plane cracking occurred.

Table 10

Summary of Two-Dimensional Thermal Stress Analyses

Name	Start of Placement	Heat Transfer Analyses For loading	Mixture	Lift Ht (ft)	Notes
CMS1	1 July	CMT1	A13	5	α = 4.5 millionths/°F; plane strain
CMS2	1 July	CMT1	A13	5	α = 7.0 millionths/°F; plane strain
CMS3	1 July	CMT2	A13	5(floor) 10(walls)	α = 7.0 millionths/°F; plane stress
CMS4	1 July	CMT1	A13	5	α = 5.5 millionths/°F; plane strain
CMS5	1 November	CMT3	A8	5	Plane strain
UGBS1	1 July	UGBT1	A13	5	Rollers at base and centerline; plane strain
UGBS2	1 July	UGBT1	A13	5	No tensile forces at vertical supports; plane strain
UGBS3	1 July	UGBT1	A13	5	Springs at vertical supports; plane strain
UGBS4	1 July	UGBT1	A13	5(floor) 10(walls)	Rollers at supports; no cracking; plane strain
UGBS5	1 July	UGBT3	A13	5	75 °F placement; lifts 1-7; plain strain
UGBS6	1 July	UGBT3	A13	5	75 °F placement; lifts 1-7; plane stress
UGBS7	1 November	UGBT4	A8	5	Lifts 1-7; plane strain
DWS1	1 July	DWT1	A13,A11	5	Plane strain
DWS2	1 July	DWT1	A13,A11	5	Plane stress

81. Figure 26 gives the location of the elements for which stresses have been plotted. The effects of incremental construction on horizontal tensile stresses can be seen in Figures 27-29. When the first lift was placed, the concrete was not restrained along the base in the horizontal direction and was free to expand and contract as internal temperatures changed and shrinkage occurred. Initially the concrete expanded as the temperature rose. After approximately 2 days, the maximum temperature was reached. As the concrete began to contract due to cooling and shrinkage, low tensile stresses occurred at the center of the lift. Horizontal stresses along a section at the centerline of lift 1 (elements 113 and 137, integration points 1 and 3) are shown in Figure 27. When the next lift was placed at 10 days, it behaved similarly, except that its expansion and contraction was restrained by the concrete below. The restraint of expansion in the new lift resulted in low compressive stresses in the new lift and in higher tensile stresses in the lift below for the first 2 days after placement. Between 12 and 20 days, the restraint of contraction in the new lift resulted in tension in that lift and compression in the lift below. Horizontal stresses along a vertical section at the centerline of lift 2 are shown in Figure 28. When lift 3 was placed at 20 days, tensile stresses in lift 2 increased for the first 2 days and then decreased due to the restraint of lift 3 contractions. Since no additional floor lifts were placed, tensile stresses increased throughout the construction in lift 3. The slight drop that can be observed in horizontal stresses along the centerline of lift 3 in Figure 29 was due to the Poisson's effect and occurred when cracking reduced out-of-plane stresses to zero.

82. Although horizontal tensile stresses were not high enough to cause cracking, higher stresses would be undesirable. This may indicate that three lifts (or 12 to 15 ft) is a practical upper limit to the thickness of floor section that can be placed without taking steps to reduce temperature differentials. This observation applies only to floor sections constructed using mixture A13 and should not be applied as an upper limit for other structures or mixtures.

83. Throughout the area of one-dimensional heat flow (shown in Figure 26) horizontal and out-of-plane stresses at a given elevation were constant. Vertical and shear stresses were negligible except at supports, and

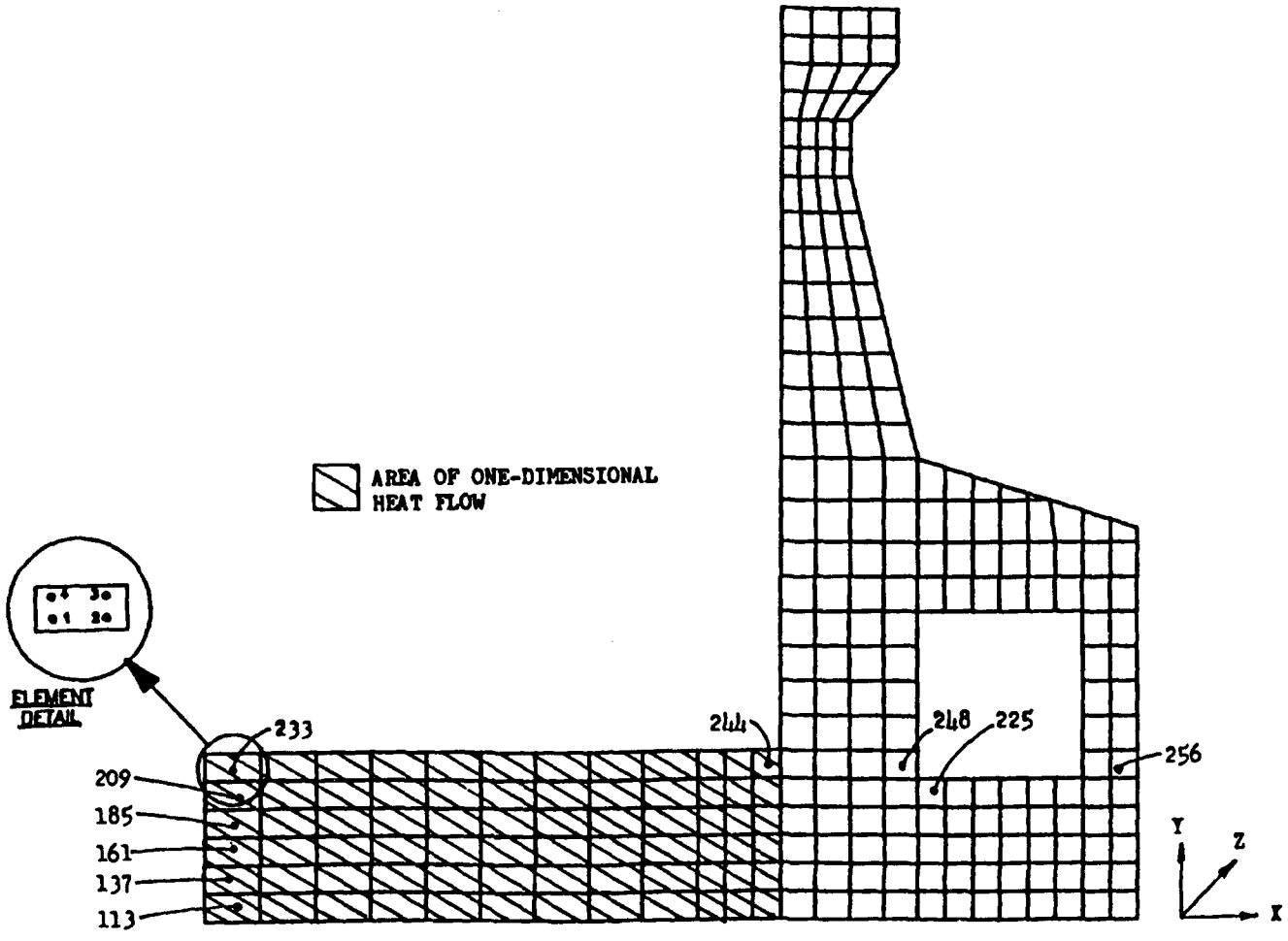

Figure 26. Location of selected elements, chamber monolith stress analyses

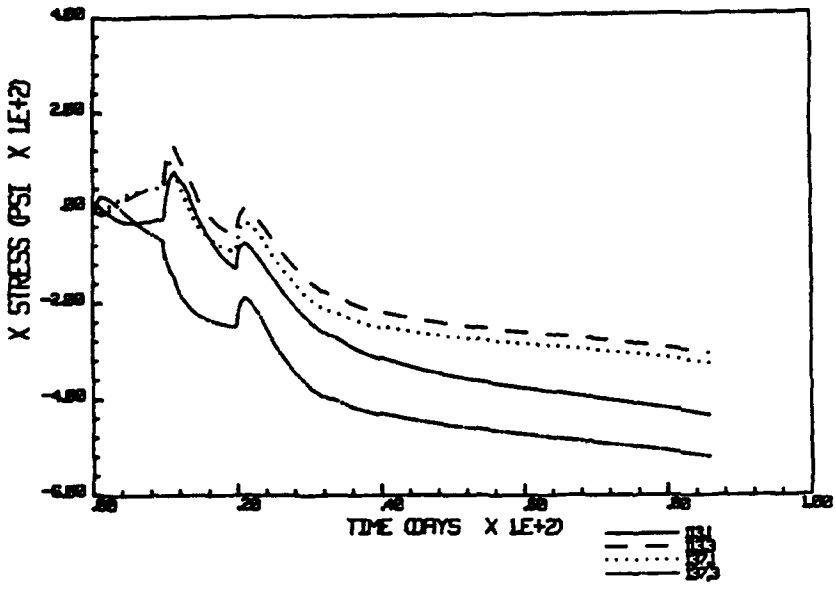

Figure 27. Horizontal stresses along a vertical section through the center line of Lift 1, CMS2

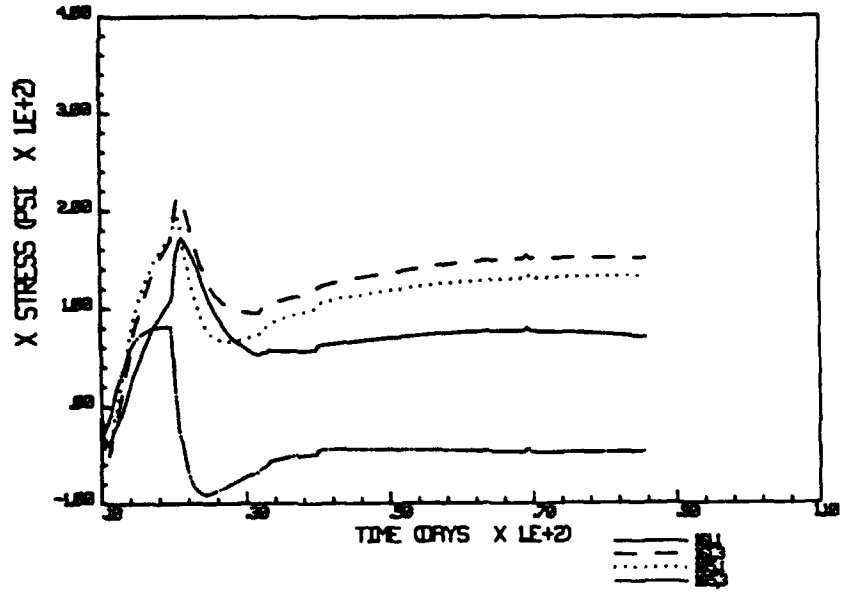

Figure 28. Horizontal stresses along a vertical section through the center line of Lift 2, CMS2

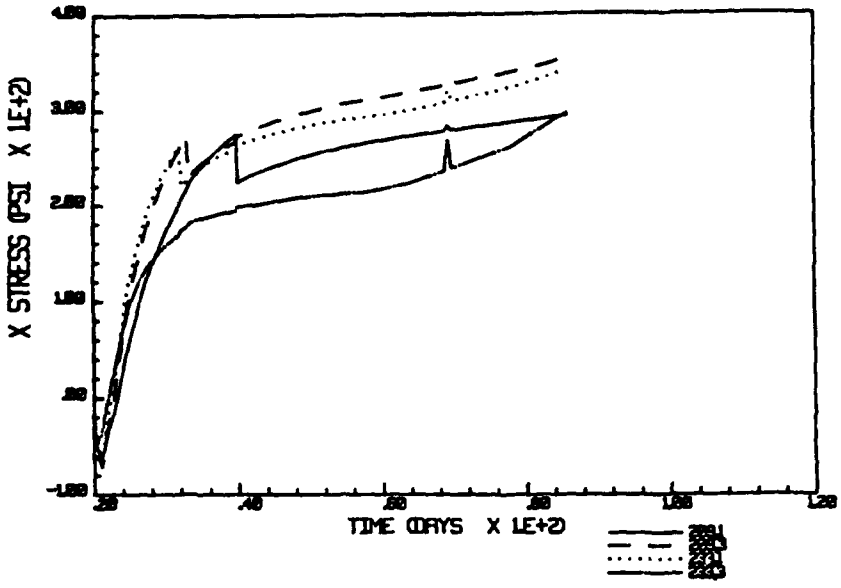

Figure 29. Horizontal stresses along a vertical section through the center line of Lift 3, CMS2

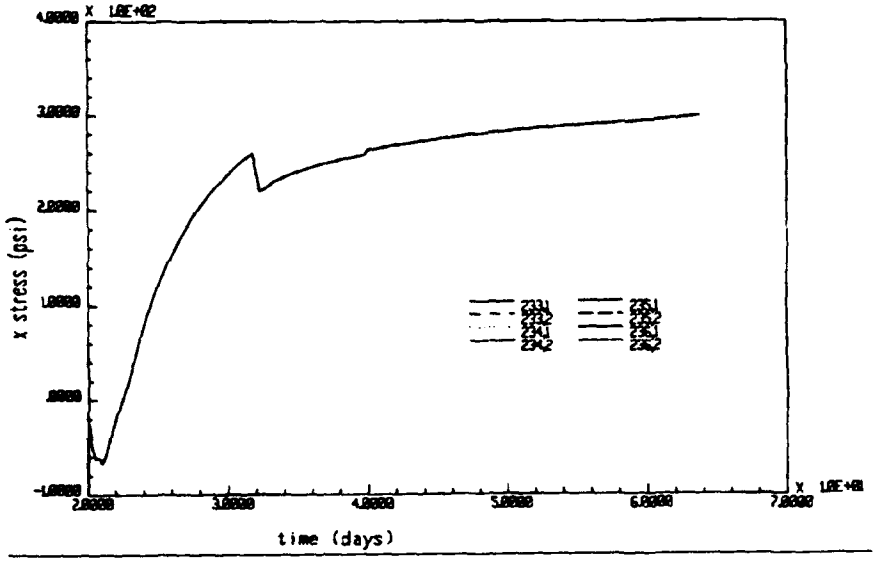

Figure 30. Horizontal stresses at integration points 1 & 2, Elements 233-236, CMS2

maximum principal stresses corresponded to either out-of-plane or horizontal stress. This is illustrated in plots of horizontal, vertical, and out-of-plane stresses in integration points 1 and 2 of elements 233 through 236 (Figures 30-32). Horizontal and out-of-plane stresses in elements 233, 240, 242, 244, and 246 through 248 along the horizontal centerline of Lift 3 are plotted in Figures 33 and 34. Stresses in these plots are relatively constant between elements 233 and 242. In elements 245 through 248, located directly under the wall, stresses are much less uniform. Out-of-plane cracking is indicated when out-of-plane stress suddenly drops to zero (see Figure 34). Plots of stresses in element 225 at the lower left-hand corner of the culvert are shown in Figures 35-38. No stress contour plots were generated for these two analyses.

84. Two significant problems were encountered in the plane-strain analyses: (1) after cracking was initiated, several iterations were necessary in each increment to reach a convergent solution, adding to the expense and time required to do the calculations and (2) horizontal stresses may have been somewhat higher than was realistic due to the Poisson's effect of the out-of-plane stresses.

Chamber monolith Run 3 (CMS3)

85. The CMS2 analysis was then repeated with a maximum lift height of 10 ft in the walls (lifts 4 through 10) and using plane stress elements. Lift spacings for this analysis are shown in Figure 39. The bounding nature of plane-strain and plane-stress analyses is apparent when the stresses in the floor in CMS2 and CMS3 are compared. Even though the floor lift heights and material parameters were identical in both analyses, maximum stresses predicted in the floor in CMS3 (including areas around the culvert) were less than 250 psi during the construction period. Horizontal stresses in elements 225 and 233 for the plane-strain and plane-stress analyses are plotted for comparison in Figures 40 and 41. In each of these plots the first two curves are for CMS2, and the last two are for CMS3. A dramatic increase in horizontal tensile stresses occurred in the plane-stress analysis after about 85 days when the analysis was continued into October and ambient temperature began to drop. Stresses in the wall were relatively low (generally under 100 psi) in all of the first three analyses.

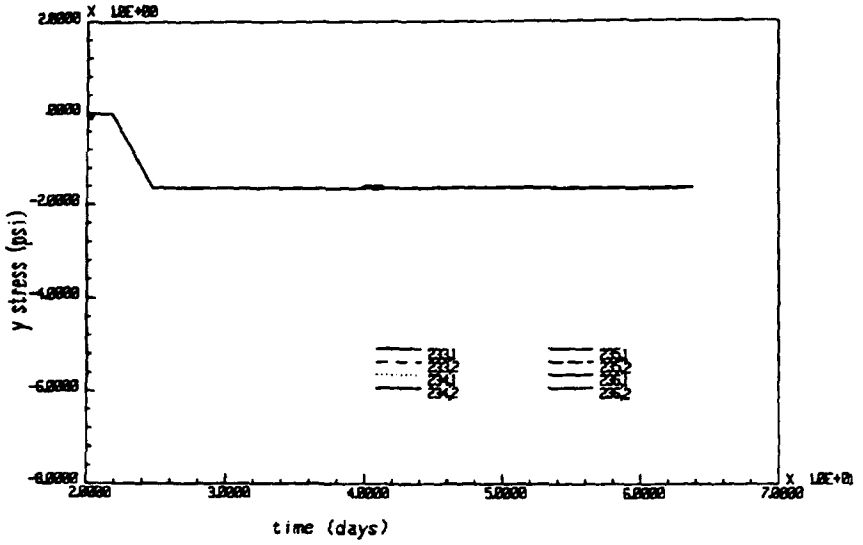

Figure 31. Vertical stresses at the center of Lift 3, Elements 233-236, CMS2

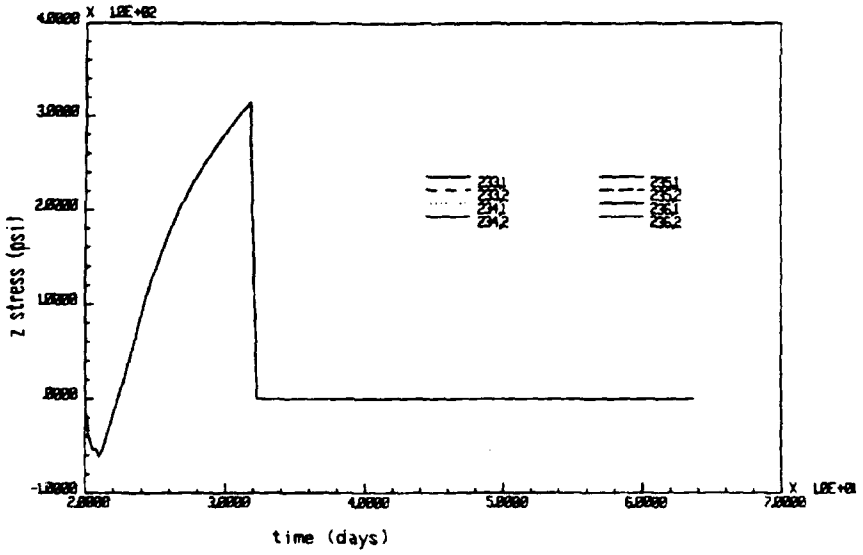

Figure 32. Out-of-plane stresses at the center of Lift 3, Elements 233-236, CMS2

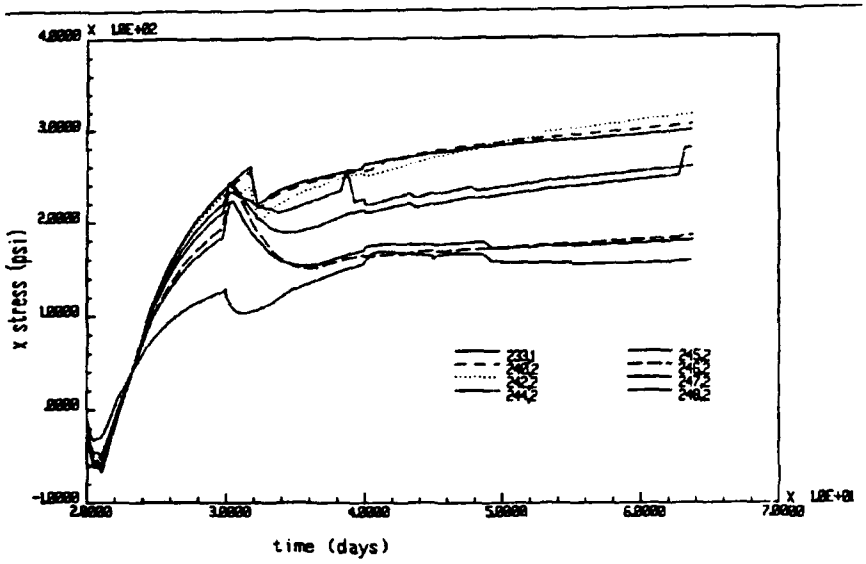

Figure 33. Horizontal stresses along center of Lift 3, CMS2

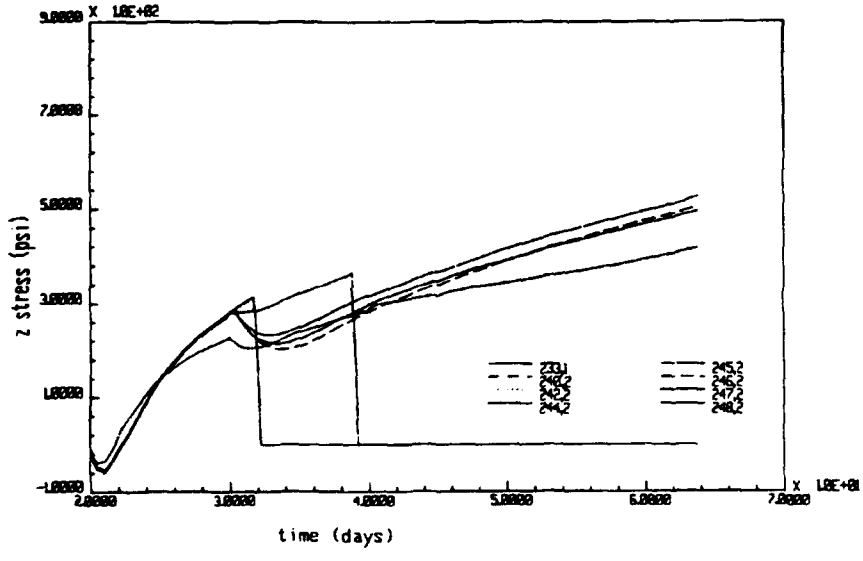

Figure 34. Out-of-plane stresses at center of Lift 3, CMS2

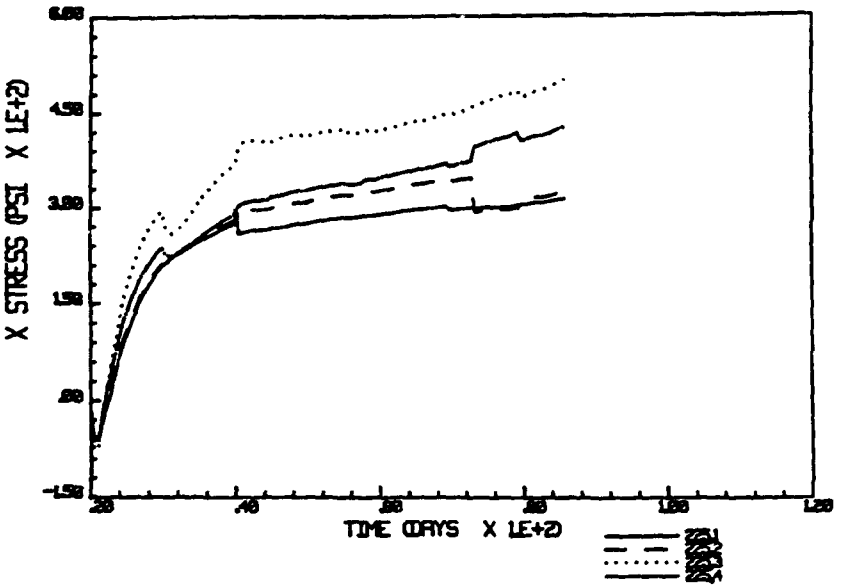

Figure 35. Horizontal stresses in Element 225, CMS2

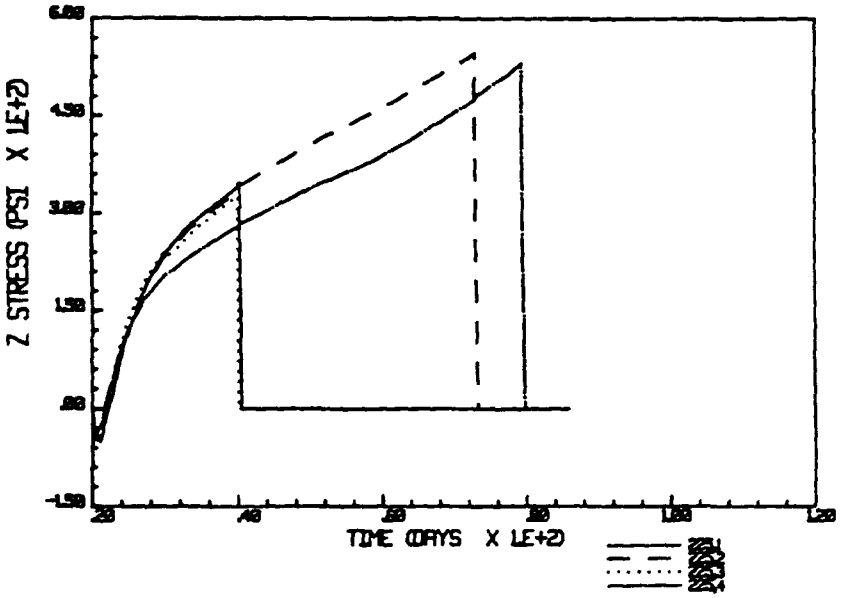

Figure 36. Out-of-plane stresses in Element 225, CMS2

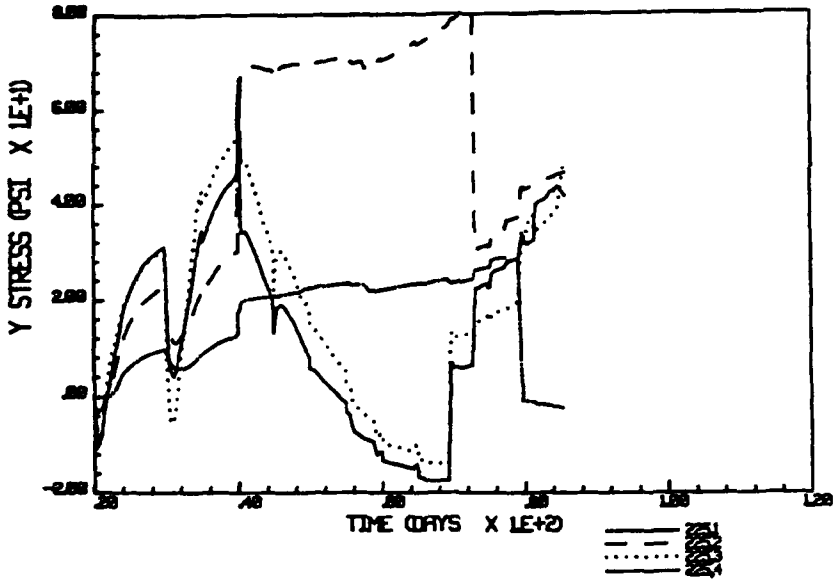

Figure 37. Vertical stresses in Element 225, CMS2

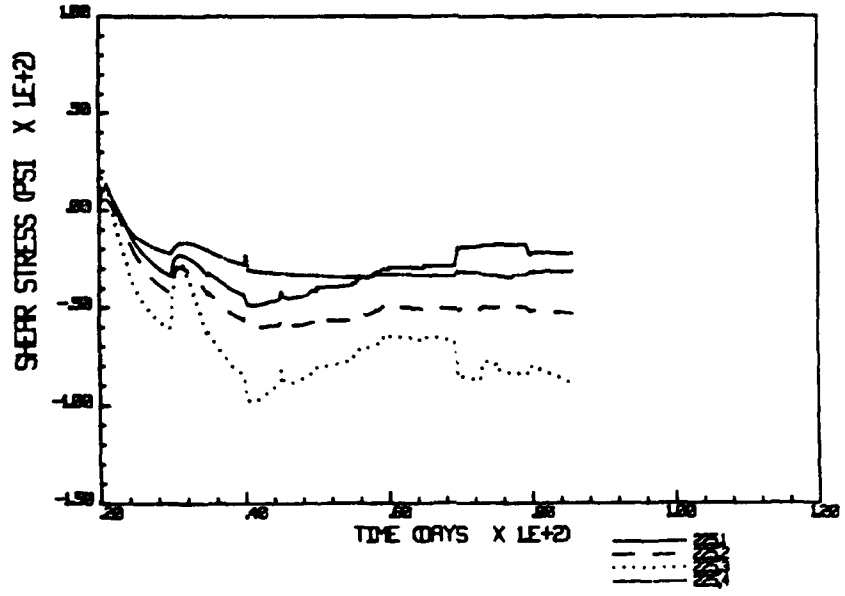

Figure 38. Shear stresses in Elements 225, CMS2

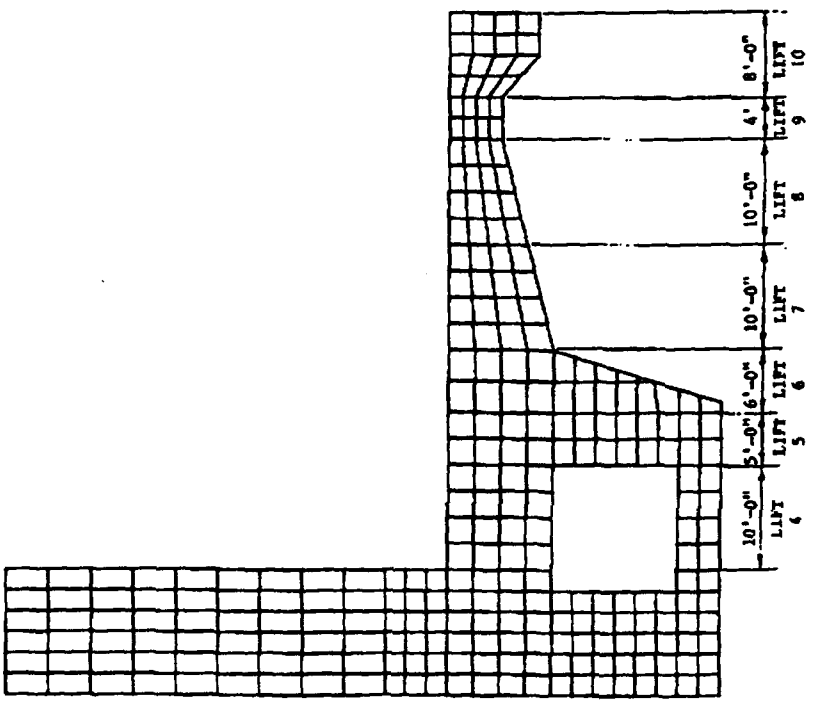

Figure 39. Lift spacing in wall section, analysis CMS3

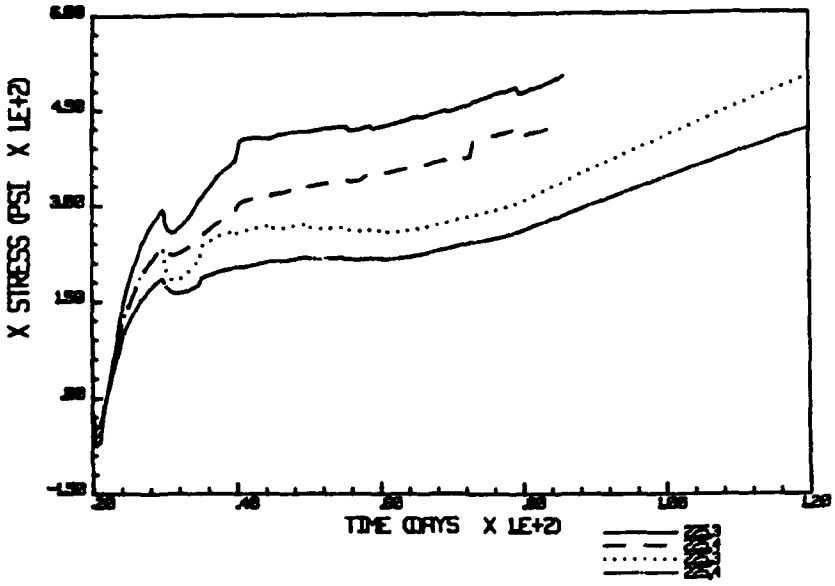

Figure 40. Comparison of horizontal stresses in Element 225, Runs CMS2 and CMS3

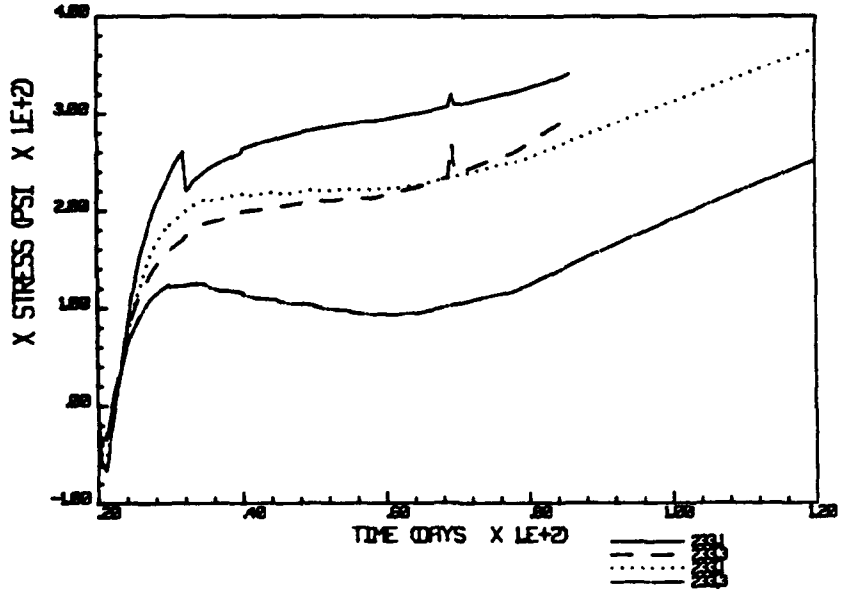

Figure 41. Comparison of horizontal stresses in Element 233, Runs CMS2 and CMS3

Chamber monolith Run 4 (CMS4)

86. This analysis was a repeat of the CMS1 analysis using the correct coefficient of thermal expansion (5.5 millionths/°F). The analysis resulted in extensive cracking due to out-of-plane stresses, but no cracking due to horizontal or vertical stresses. Horizontal tensile stresses in the center of Lift 3 exceeded 400 psi at late times (120 days after the start of concrete placement). In-plane wall stresses were relatively low. Horizontal and out-of-plane stresses in Lift 3 are shown in Figures 42 and 43. Horizontal, vertical and out-of-plane stresses at the lower left-hand corner of the culvert are shown in Figures 44-46.

Chamber monolith Run 5 (CMS5)

87. Start-of-placement date for this analysis was November 1, nominal lift height was 5 ft throughout and plane-strain elements were used. Mixture A8 mechanical properties were used in all lifts. Although no cracking was predicted, out-of-plane tensile stresses across the top of the floor and around the outside of the culvert were in excess of 600 psi at late times. In-plane vertical stress were compressive except at the outer base of the floor, where vertical tensile stresses approached 200 psi due to support conditions. Maximum horizontal tensile stresses were less than 200 psi at the top center of the floor and the lower left-hand corner of the culvert. This run was stopped in Lift 13 due to lack of computer storage (disc) space.

88. Displacements and horizontal stress contours from the CMS3 and CMS5 analyses just prior to placing the first wall lift are presented in Figures 47 through 50. The advantage of the slow heat loss that occurs in an insulated structure can be observed from these plots. In the uninsulated structure, contraction due to cooling occurs fairly quickly. Because temperature in the concrete is higher than ambient at time of setting and shrinkage is also occurring, each lift contracts until it occupies a smaller volume than when placed (Figure 47). This provides some restraint to the expansion of the next lift. However, the concrete in the next lift does not set until much of its initial expansion has occurred, and only low compressive stresses are induced

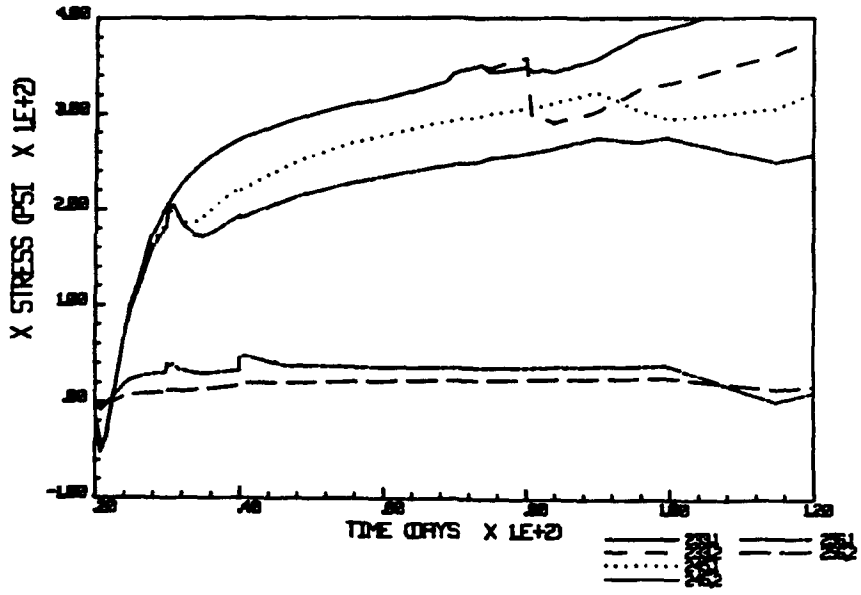

Figure 42. Horizontal stresses along center of Lift 3, CMS4

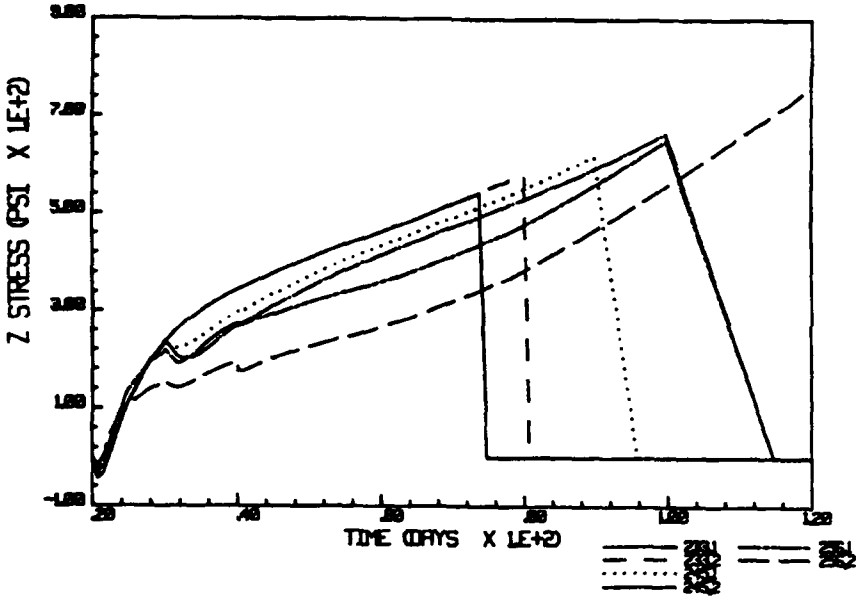

Figure 43. Out-of-plane stresses along center of Lift 3, CMS4

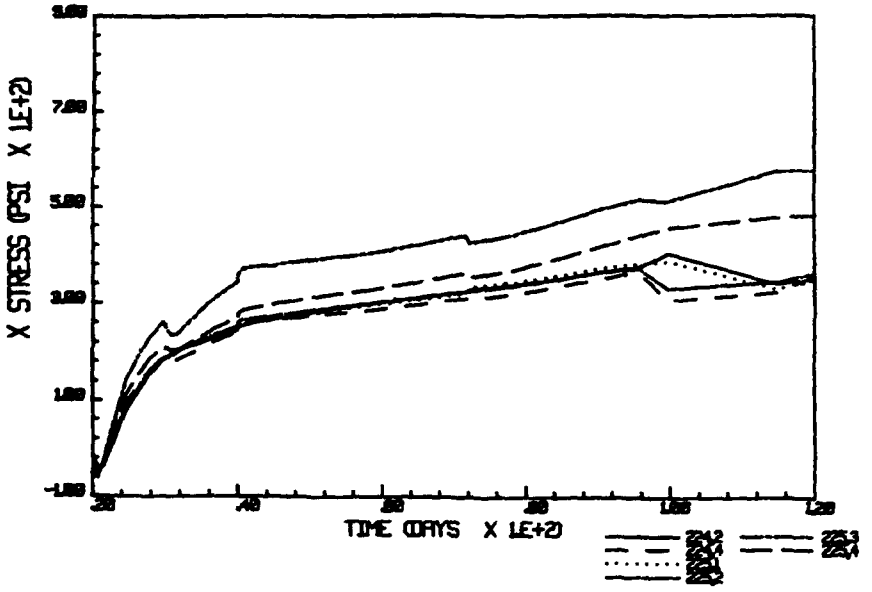

Figure 44. Horizontal stresses at the lower left-hand corner of the culvert, CMS4

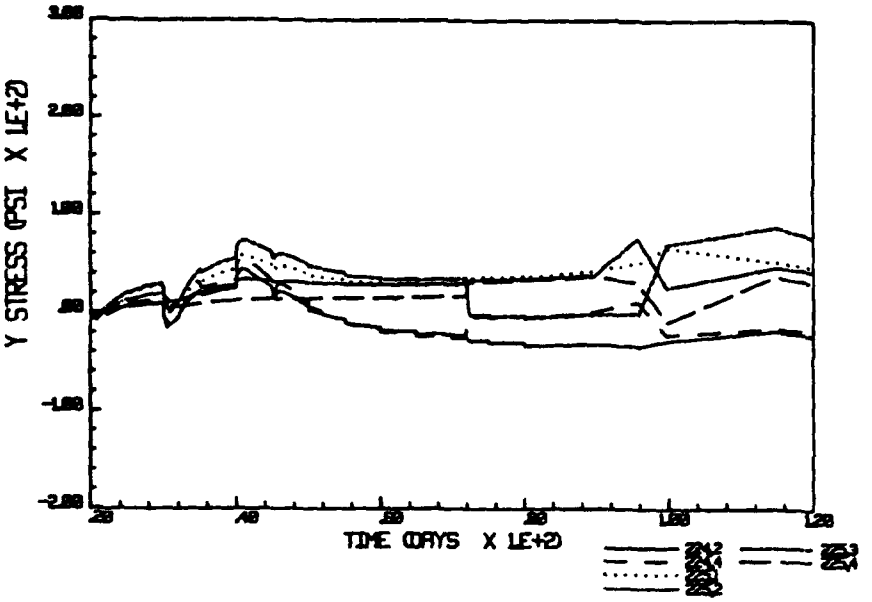

Figure 45. Vertical stresses at the lower left-hand corner of the culvert, CMS4

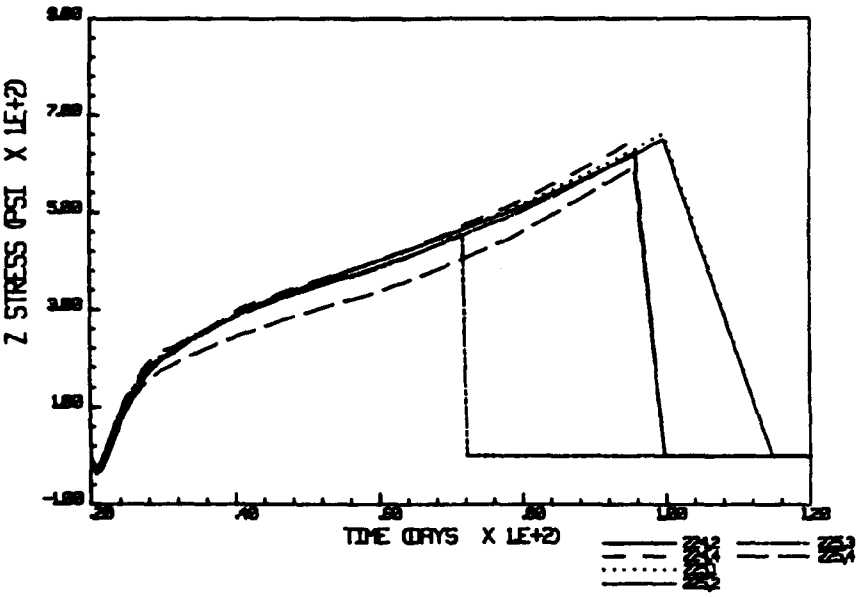

Figure 46. Out-of-plane stresses at the lower left-hand corner of the culvert, CMS4

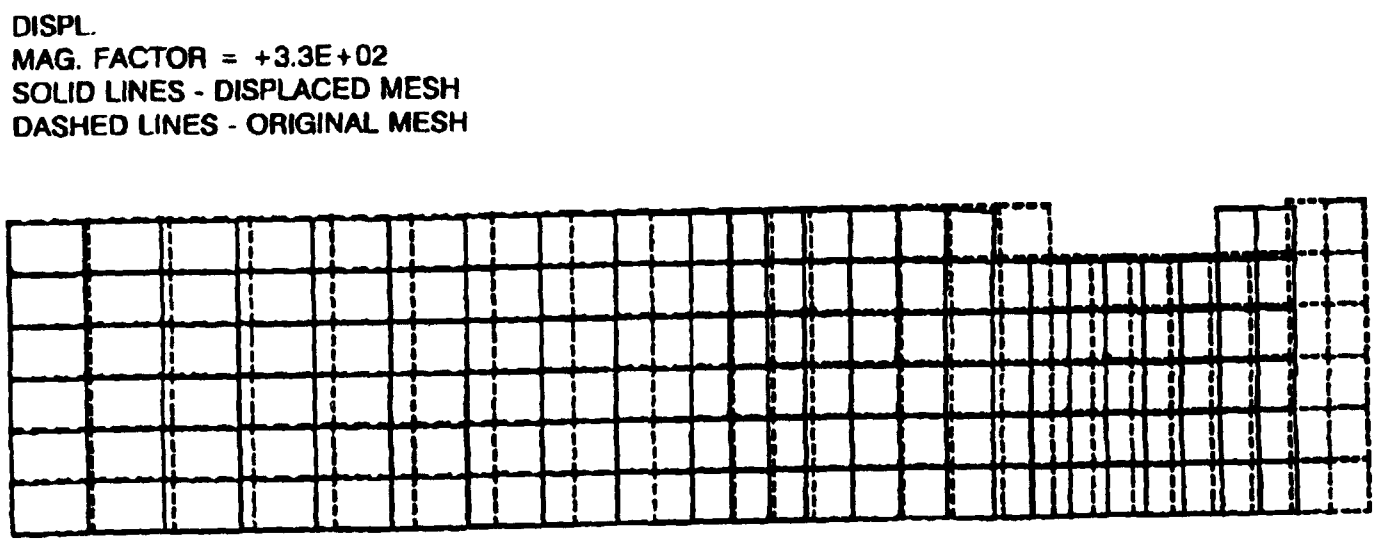

Figure 47. Displacements in an uninsulated structure (CMS3) at t = 30 days

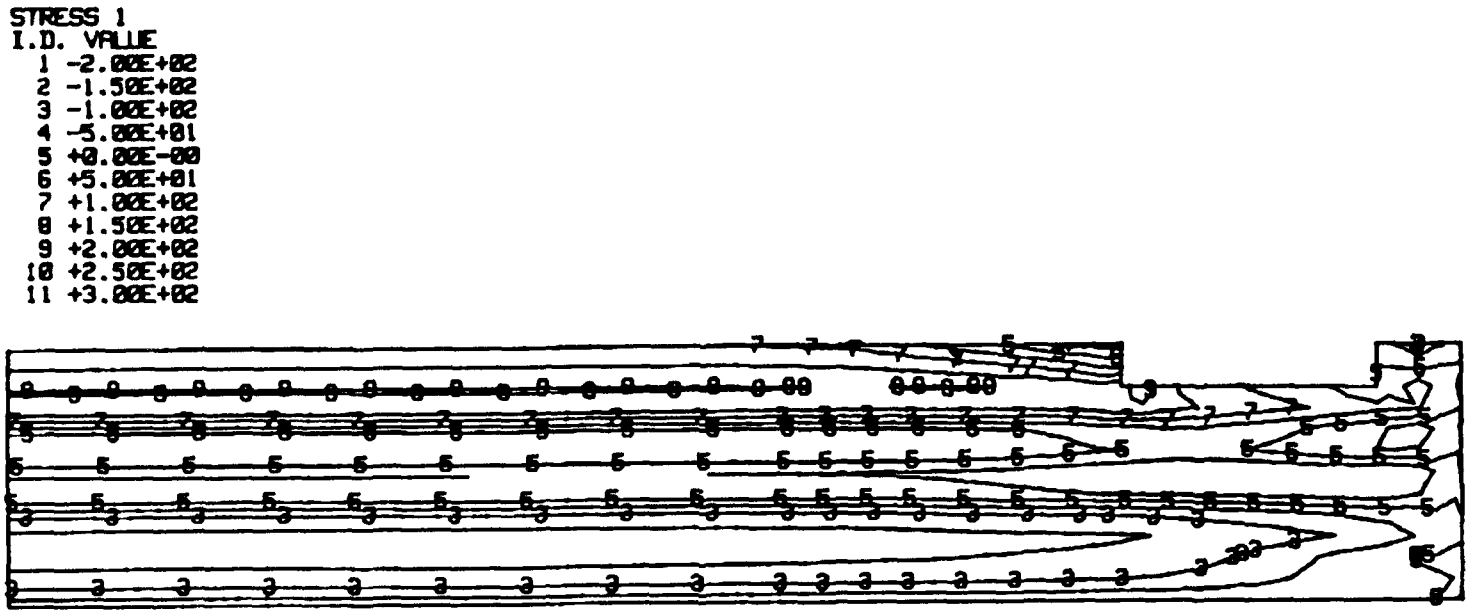

Figure 48. Horizontal stress contours in an uninsulated structure (CMS3) at t = 30 days

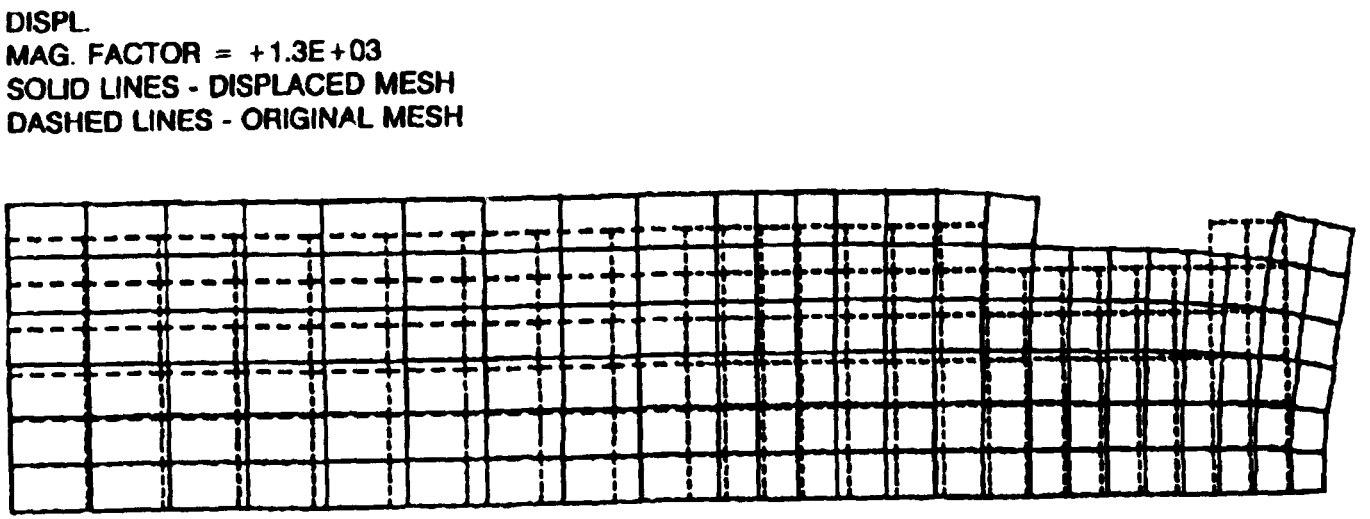

Figure 49. Displacements in an insulated structure (CMS5) at t = 30 days

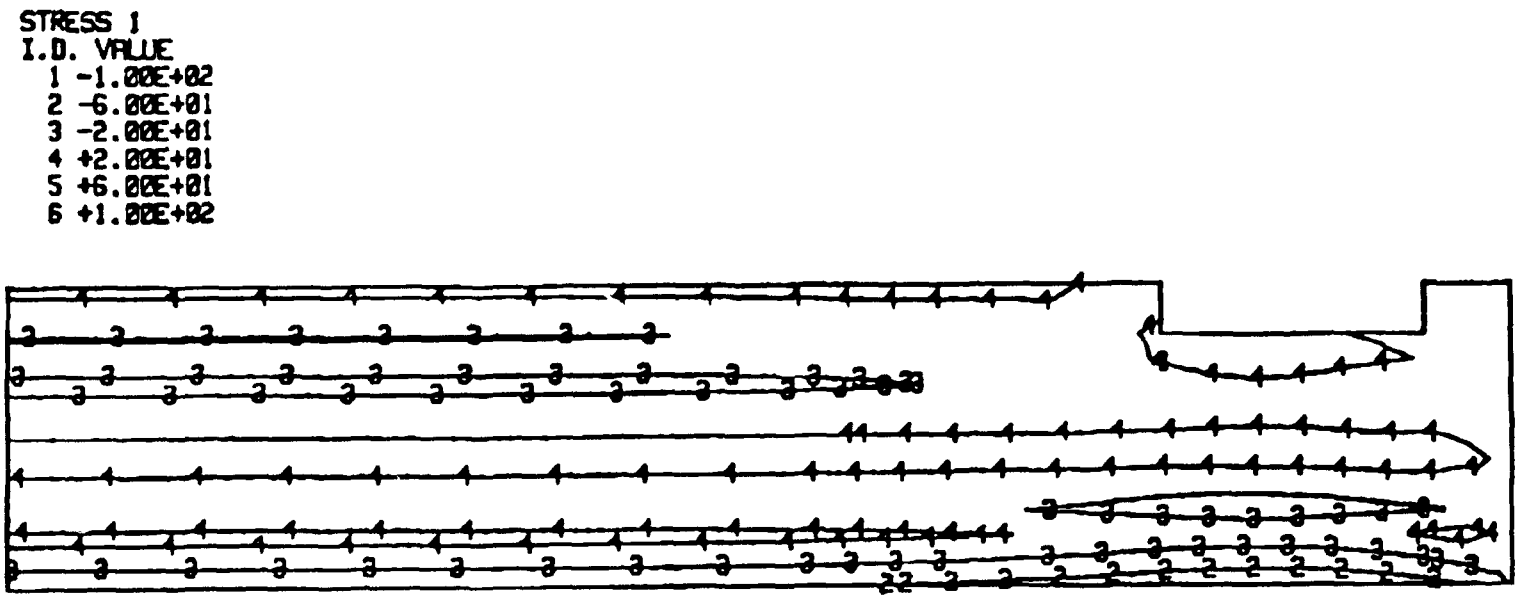

Figure 50. Horizontal stress contours in an insulated structure (CMS5) at t = 30 days

by the restraint of expansion. Upon cooling, the concrete attempts to contract as though it were unrestrained, but is restrained by the bond to the underlying concrete and its own stiffness, inducing high horizontal tensile stresses. Figure 48 illustrates the high horizontal stresses in the center of Lift 3. In the insulated structure, cooling and contraction due to cooling occur at a much slower rate, and less restraint is provided by existing concrete. At the same time, cooling and contraction in each new lift occur very slowly. In Figure 49 very little contraction has occurred, and the concrete occupies a larger volume than when placed. The resulting horizontal stresses throughout the new lift are close to zero, as shown in Figure 50.

Upper-gate-bay monolith Runs 1-3 (UGBS1, UGBS2, UGBS3)

89. Starting date for placement in Runs 1 through 3 was 1 July. All runs were conducted using plane strain elements and mixture A13 mechanical properties. Analyses of the upper-gate-bay floor section were made using several methods of support at boundaries, but all resulted in severe cracking and convergence problems. In the first upper-gate-bay analysis (UGBS1) the structure was supported at the base and centerline by rollers. Severe in-plane cracking initiated at the base and lower left-hand corner of the culvert during Lift 4. The cracking at the culvert occurred as the section to the left of the culvert became cooler at the top and began to curl upward away from the lower section of floor. Crack propagation made numerical convergence unlikely by Lift 5, and the run was stopped. In the next analysis (UGBS2) interface elements at the base prevented tensile support. This resulted in the structure curling upward as it cooled and cracking at the base and around the culvert. In UGBS3 the structure was supported on springs with similar results.

Upper-gate-bay monolith Run 4 (UGBS4)

90. In Run 4 cracking was prevented by using artificially high values for 3-day compressive strength (6,000 psi) and tensile strain capacity (1000 millionths). Start-of-placement date was 1 July, and plane-strain elements were used. This analysis yielded horizontal tensile stresses at the top center of the floor and lower left-hand corner of the culvert in excess of 600 psi at relatively early times after placement. Stresses in these areas approached 1,000 psi at the end of the analysis. As expected, tensile

stresses in the walls were relatively low. Vertical tensile-stress concentrations were predicted at the base (due to the boundary conditions) and at the corners of the culvert. Horizontal stresses were excessive at the top of the floor, along the base, and at corners of the culvert.

Upper-gate-bay monolith Run 5 (UGBS5)

91. Although the thermal differentials predicted in UGBT1 were within the 20 degrees normally considered acceptable, stresses calculated in the first four upper gate bay analyses (with the UGBT1 thermal loading) were high enough to cause serious cracking problems. This is probably due to the combined effects of cooling and shrinkage in each new lift and to the restraint to new lifts provided by the very thick section. Even though 20 °F may be an acceptable gradient for thinner sections, lower gradients appear to be required for very thick floor sections.

92. In an effort to prevent cracking in the floor, placement temperatures in the first seven lifts were reduced to 75 °F in the next analysis. Plane-strain elements were used, and the run was continued through Lift 7 only. Although some in-plane cracking occurred near the lower left hand corner of the opening, in-plane tensile stresses in the floor were generally less than 200 psi.

93. The effects of cracking at the corner can be seen in the contour plots of vertical stress just prior to the placement of Lift 7 and at the end of the analyses (Figures 51 and 52). Stresses in the lower left-hand corner were approaching 300 psi at the beginning of the step. In Figure 52 cracking in elements 225 through 228 has shifted the region of high stress to elements to the left of element 225. Stresses in elements 225 through 228 near the bottom of the culvert are shown in Figures 53-57. The locations of these elements are shown in Figure 58. Prior to cracking, high tensile stresses existed only near the opening in element 228. As cracking occurred, vertical and out-of-plane stresses dropped to zero, and stresses in the next elements became high enough to cause cracking.

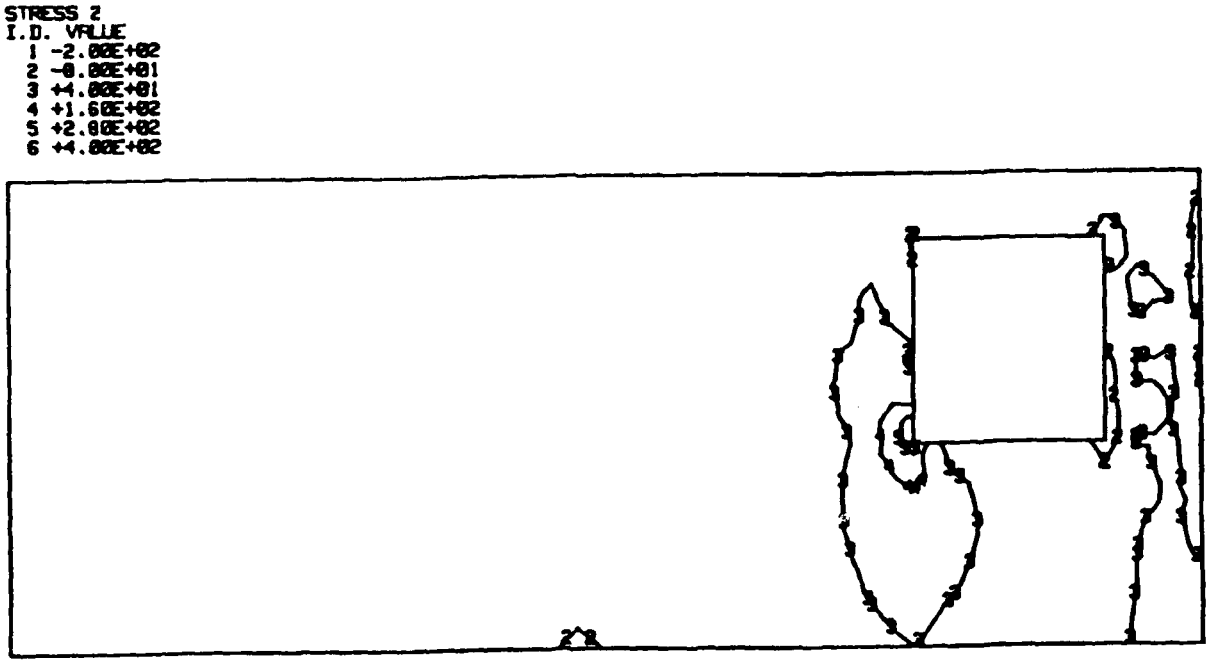

Figure 51. Vertical stress contours from UGBS5 analysis at t = 60 days

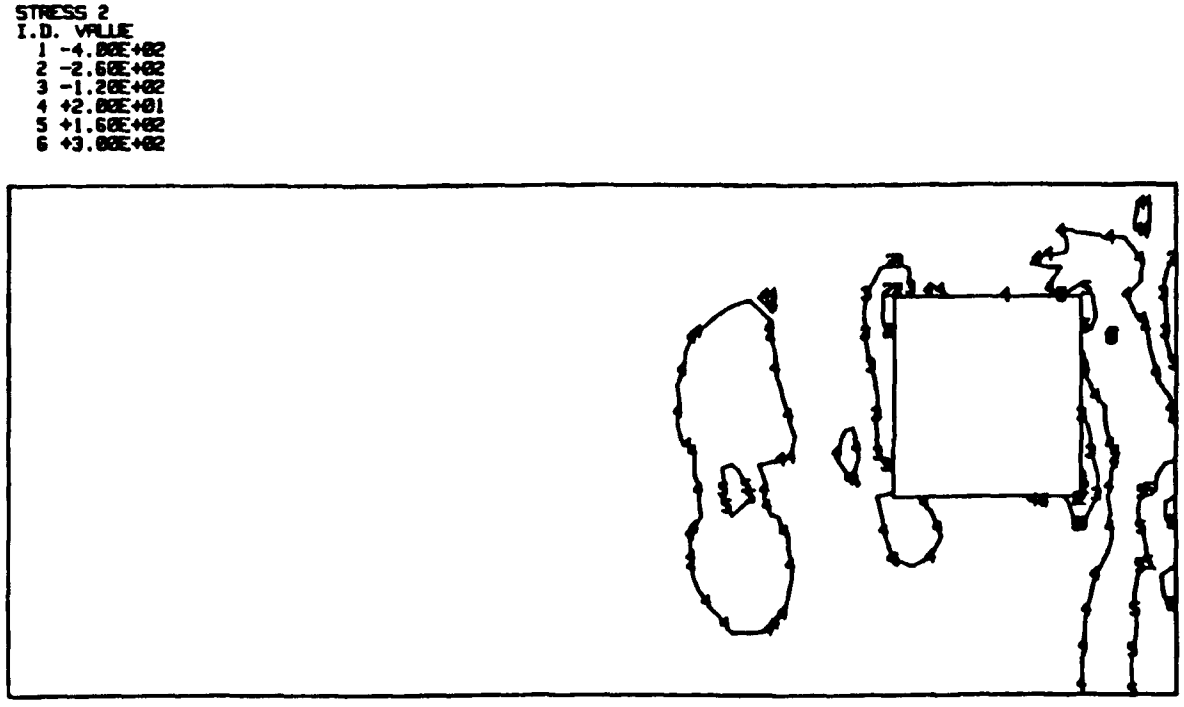

Figure 52. Vertical stress contours from UGBS5 analysis at t = 70 days

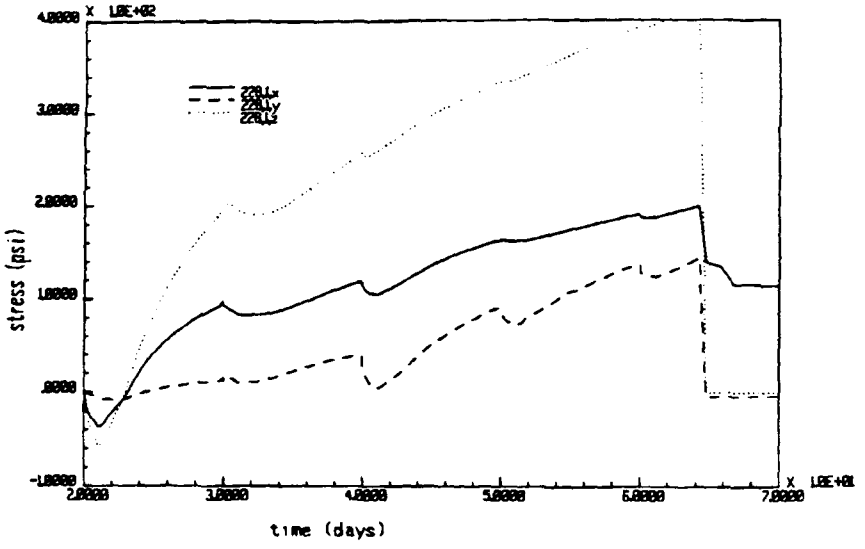

Figure 53. Stresses at integration point 1, Element 228, UGBS5

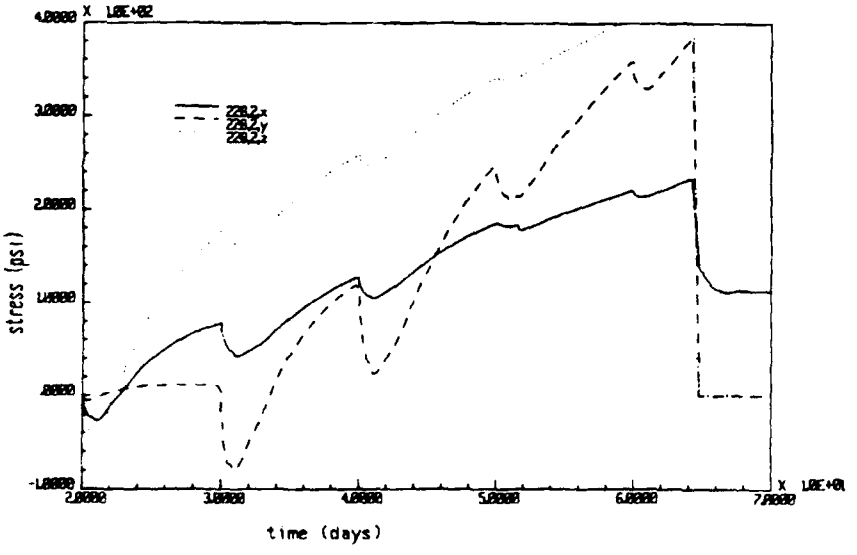

Figure 54. Stresses at integration point 2, Element 228, UGBS5

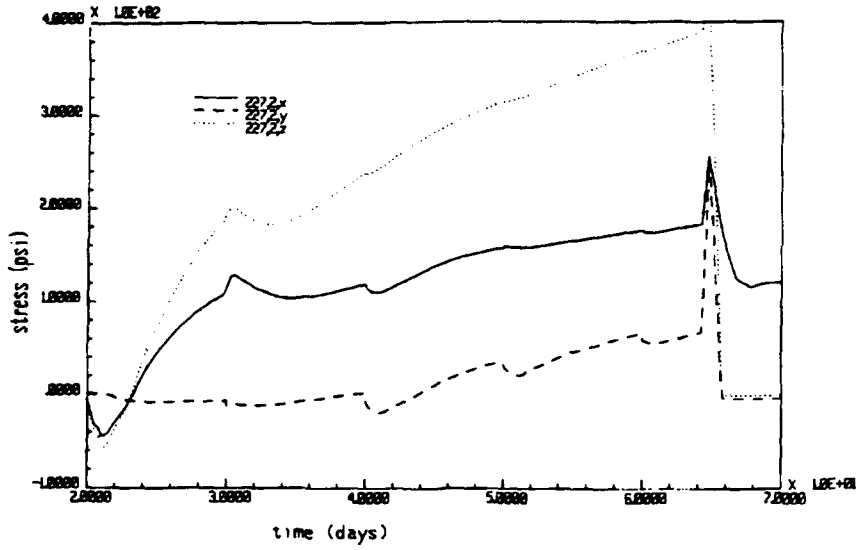

Figure 55. Stresses at integration point 2, Element 227, UGBS5

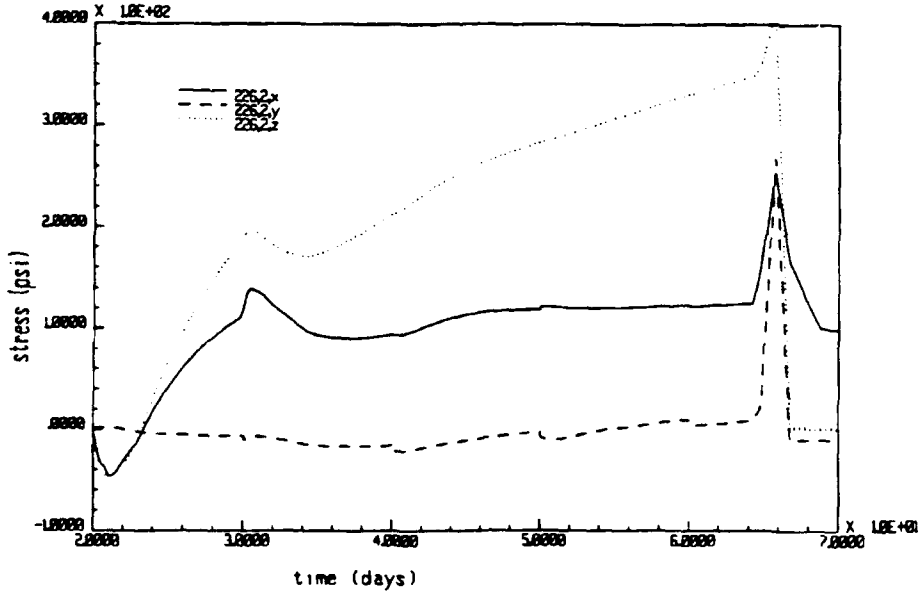

Figure 56. Stresses at integration point 2, Element 226, UGBS5

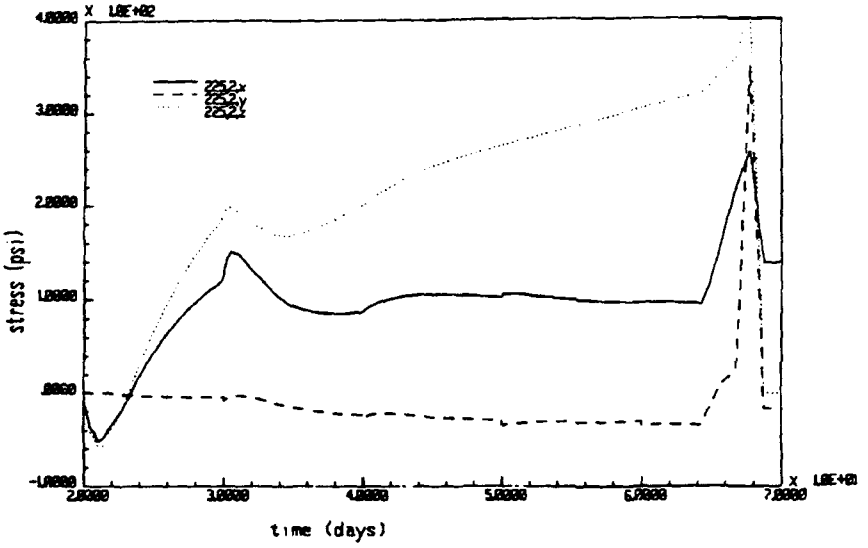

Figure 57. Stresses at integration point 2, Element 225, UGBS5

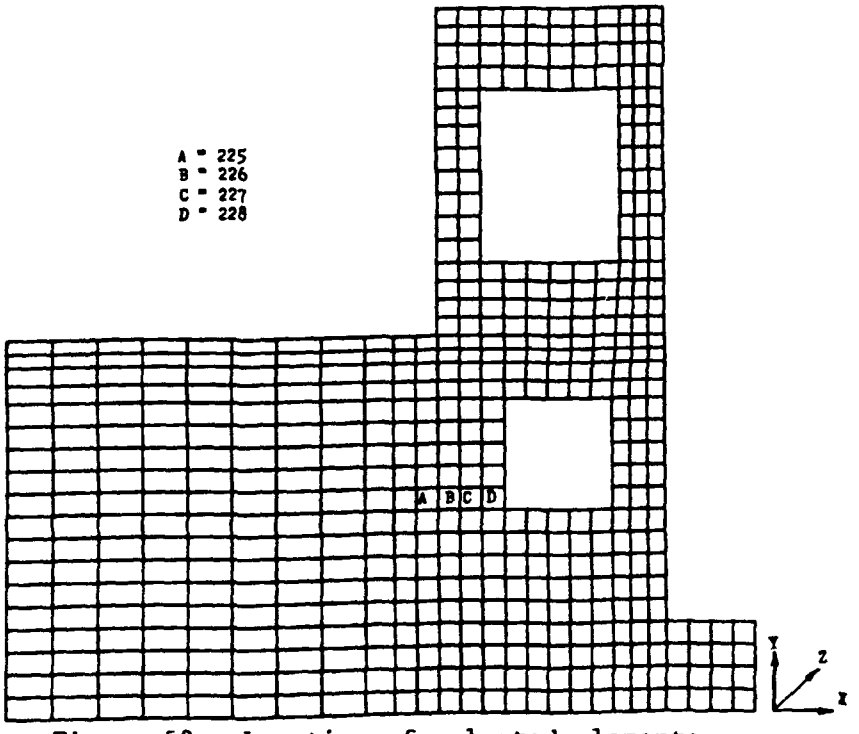

Figure 58. Location of selected elements, upper-gate-bay monolith

Upper-gate-bay Run 6 (UGBS6)

94. The next analysis was made using a 75 °F placement temperature and a plane-stress element. For this section, the plane-stress element may be more realistic than a plane-strain element, since the floor thickness varies across the monolith and is large when compared with the overall length of the monolith. No cracking occurred, and maximum horizontal tensile stresses in the top center of the floor were less than 200 psi. However, maximum principal stress approached 500 psi by the end of the analysis in the lower left-hand corner of the culvert.

Upper-gate-bay Run 7 (UGBS7)

95. Start-of-placement date for this analysis was November 1. Mixture A8 mechanical properties, plane-strain elements, and 5-ft lifts were used throughout. Only the first seven lifts were used in this analysis, and all exposed surfaces were insulated throughout the analysis. Vertical tensile stresses were negligible except at the lower right-hand corner of the base. Horizontal tensile stresses were less than 40 psi except at the lower left-hand corner of the culvert, where they reached approximately 100 psi. Out-of-plane tensile stresses were also relatively low (less than 300 psi) except around the base and outer edge of the culvert. In this area, stresses exceeded 600 psi. Temperatures in the outer edge of the culvert were lower than those in the rest of the structure, and the high stresses were due to the restraint of contraction due to cooling. Although it is unlikely that the magnitude of stresses induced in a plane-strain analysis could occur in a real structure, a three-dimensional analysis of the floor section would give a more realistic picture of stresses in the third direction.

Dam weir section Run 1 (DWS1)

96. Mixture A13 mechanical properties were used in this analysis except in the top layer of elements. In this layer, mixture A11 properties were used to model the high-strength concrete at the surface of the structure. Start-of-placement date was July 1, and all concrete was placed at 85°F. Cracking due to vertical stresses occurred at the change in section between Lifts 2 and 3. This cracking is similar to the cracking observed in the Upper Gate Bay section at the lower left-hand corner of the culvert. As in the previous structure, the upper layers tended to curl up from the lower layers at the

interface that occurs at the change in section. Cracking due out-of-plane stresses occurred throughout the high-strength layer, starting at the interface with the lower strength concrete. Stresses at integration point 2 of elements 369 and 371 are shown in Figures 59 and 60. In element 369 cracking due to out-of-plane stresses occurred at 25 days, while in-plane cracking was initiated at a much later time (55 days). Out-of-plane stresses at integration points 1 and 3 of elements 464 and 581 are shown in Figures 61 and 62. Locations of elements 369, 371, 464 and 581 are indicated in Figure 63.

Dam weir section Run 2 (DWS2)

97. The analysis was redone using plane stress rather than plane strain elements. No cracking occurred in this analysis, and maximum horizontal tensile stresses were less than 200 psi. Maximum principal stresses of up to 300 psi occurred along the sloped face and in the curve providing the transition from the sloping face to the horizontal face. This run was stopped at Lift 6 due to failure of the power to the computer system.

98. No fall run was performed on this section, since the problems encountered (change in section and a relatively thick section) were adequately described in the upper-gate-bay analysis.

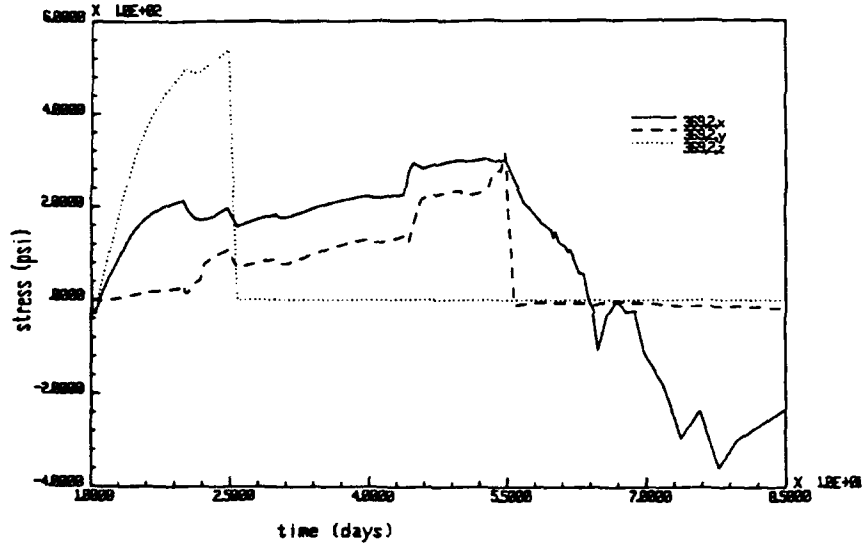

Figure 59. Stresses at integration point 2, Element 369, DWS1

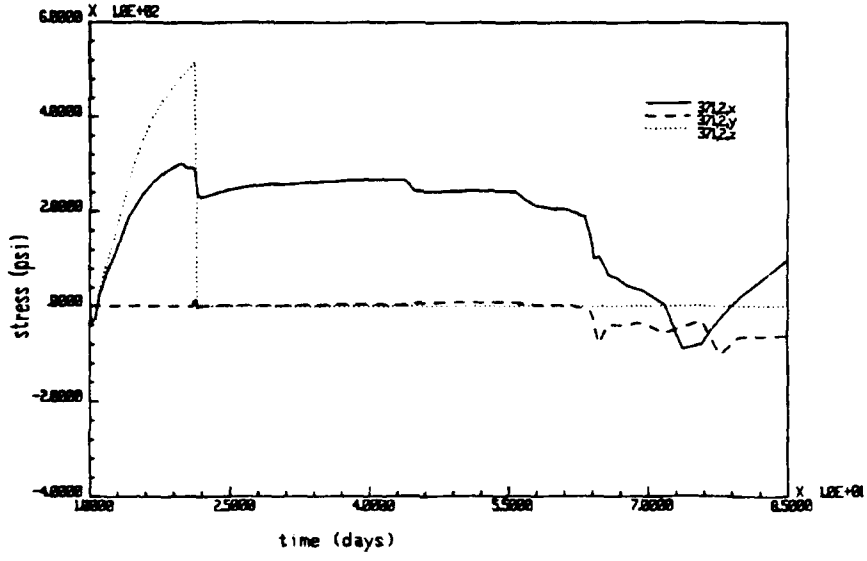

Figure 60. Stresses at integration point 2, Element 371, DWS1

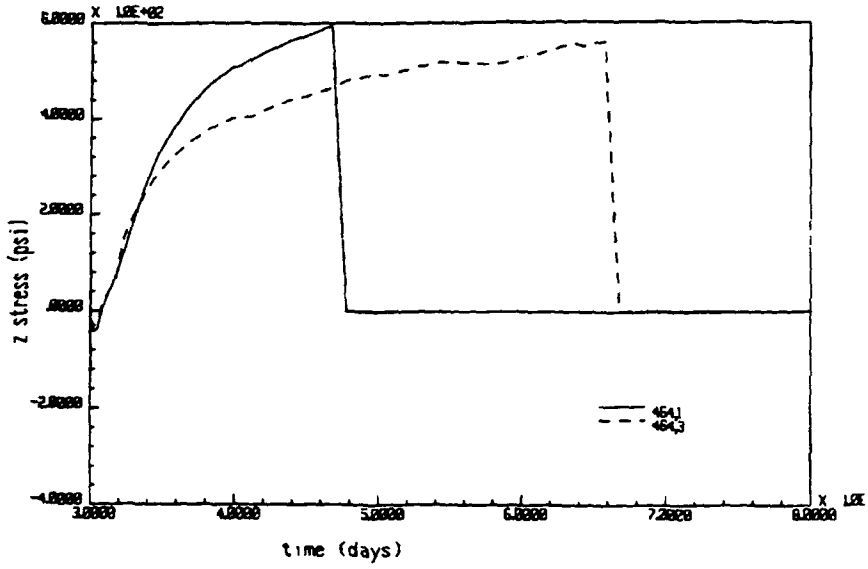

Figure 61. Out-of-plane stresses at integration points 1 & 3, Element 464, DWS1

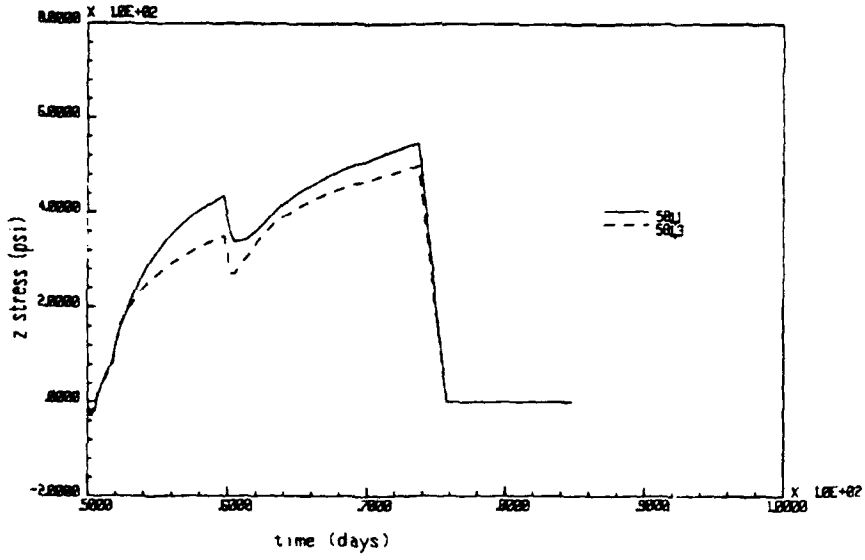

Figure 62. Out-of-plane stresses at integration point 1 & 3, Element 581, DWS1

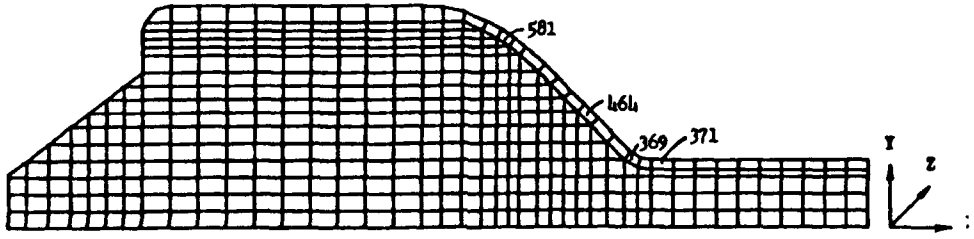

Figure 63. Location of selected elements, dam wier monolith

PART VI: THREE-DIMENSIONAL THERMAL STRESS ANALYSES

Grid Selection

99. Critical features for three-dimensional analyses were chosen based on the results of two-dimensional analyses. Although a great deal of information was provided by the two-dimensional analyses, at least two important questions remained unanswered:

a. What are the effects of doubling chamber monolith length (from 43 to 86 ft)?

b. Will out-of-plane cracking occur in the higher-strength, lower water-cement ratio layer of the dam-weir section?

100. To answer these questions two sections were chosen for three-dimensional analyses: (1) the chamber monolith and (2) the dam-weir monolith. Due to time and disk-space limitations, the finite-element grids were simplified based on the results of the two-dimensional analyses.

101. In the two-dimensional chamber-monolith runs reported in Part V of this report, in-plane stresses in the wall were low compared to those in the floor. The highest stresses in walls should be in the out-of-plane direction. However, maximum temperature rises were lower in the walls than in the floor. This should result in smaller changes in temperature during cooling, less contraction due to cooling, and lower stresses due to the restraint of that contraction. Because of the lower stresses expected in the walls, only the floor section was modeled in the three-dimensional chamber monolith analyses.

102. Because of the large number of elements required, modeling the entire dam-weir section in three dimensions was not practical. The effect of placing a thin, higher-strength layer on a lower strength base was simulated by a thick, rectangular floor section with a thin, higher-strength upper layer. The rectangular section was modeled in three lifts, with the top lift consisting of 4 ft of mass concrete and 1-1/2 ft of higher-strength concrete.

103. No contour or displacement plots were generated for the three-dimensional analyses.

Heat Transfer Analyses

104. Twenty-node brick elements with standard 3 × 3 × 3 integration were used in all heat-transfer analyses. The start-of-placement date for all analyses was 1 July. Placement temperatures were 85 °F throughout except in Analysis 3DDWT2. The Mixture A13 adiabatic curve and the average thermal properties used in the two-dimensional analyses were used in all analyses for mass concrete properties. A summary of heat transfer analyses is given in Table 11.

Table 11

Summary of Three-Dimensional Heat Transfer Analyses

Name	Notes
3DCMT1	Chamber monolith floor, 43 ft length
3DCMT2	Chamber monolith floor, 86 ft length
3DDWT1	Floor section with higher-strength layer, 85 °F placement temperature
3DDWT2	Floor section with higher-strength layer, 75 °F placement temperature

Chamber monolith Runs 1 and 2, 3DCMT1 and 3DCMT2

105. The finite-element grid used in Run 3DCMT1 (length = 43 ft) is shown in Figure 64. This grid represents a quarter symmetric section of the floor slab. To save computing time, only half as many elements were used in the x-y plane as in the two-dimensional analyses. The grid consisted of two rows of 12 elements in each lift in the x-y plane, and five elements in the z-y plane.

106. In Run 3DCMT2, the number of elements in the z-direction was doubled to model a total length of 86 ft. Temperatures along the center

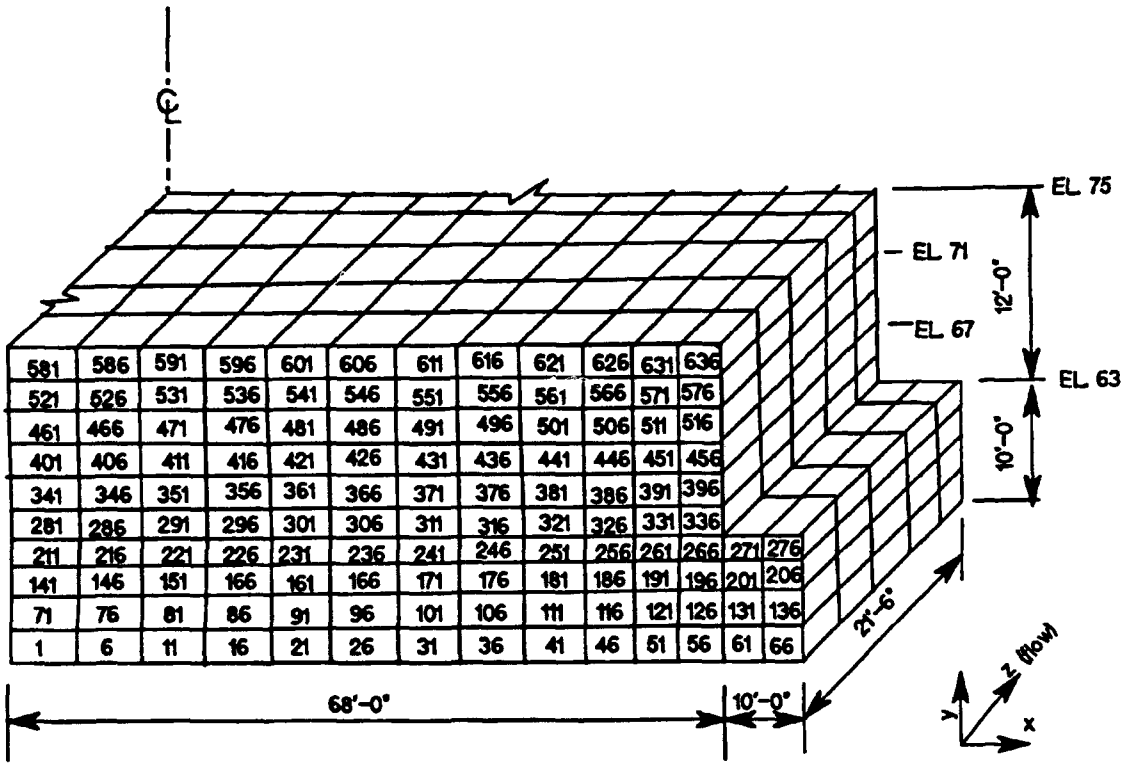

Figure 64. Grid used in 3DCMT1 analyses

planes of each lift parallel to the axis of flow are shown in Figures 65 through 67. Temperatures along the center planes transverse to the axis of flow are shown in Figures 68 through 70. Locations of referenced nodes are shown in Figures 71 and 72. Temperatures at corresponding nodes (i.e., 1502, 17502, 41502, etc) in Run 1 were approximately equal to those in Run 2 and have not been plotted.

107. As expected, temperatures at the center of each lift were the same in Runs 3DCMT1, 3DCMT2 and CMT1. This indicates that heat flow is one-dimensional at the center of the floor section. A two-dimensional heat transfer analysis represents a worst case, since no heat loss can occur in the out-of-plane direction. This condition is reached at approximately the quarter point (in the z direction) in the 43 ft monolith and at the eighth point in the 86 ft monolith. Plots of temperatures at the center nodes of each lift for each of the 3 runs are shown in Figures 73 through 75.

Dam weir Run 1, 3DDWT1

108. The grid used in this analysis was similar to the grid used in Run 3DCMS2 except that a 1-1/2-ft higher-strength concrete layer was added to the top surface. For this model, the x-y plane located at the center of the monolith was parallel to the axis of flow. The length of the quarter symmetric section was adjusted to simulate 1/2 of the length of a dam weir monolith transverse to the axis of flow (34 ft 6 in.). The finite element grid is shown in Figure 76.

109. Because no adiabatic curve was available for the higher-strength concrete (Mixture A11), the Mixture A13 adiabatic curve was used to generate temperatures for all elements. Predicted temperatures were similar to those in Runs 3DCMS1 and 3DCMS2 and have not been plotted.

Dam weir monolith Run 2, 3DDWT2

110. In an attempt to lower stresses in the higher-strength layer (see 3DDWS1) Run 3DDWT2 was repeated with 75 °F placement temperatures in all three lifts. This lowered maximum temperatures at the center of each lift by approximately 6 °F at two days after placement, but had very little effect at later times. Temperatures at nodes along a vertical center line in Runs 3DDWS1 and 3DDWS2 are compared in Figures 77 through 79. Node locations are shown in Figure 80.

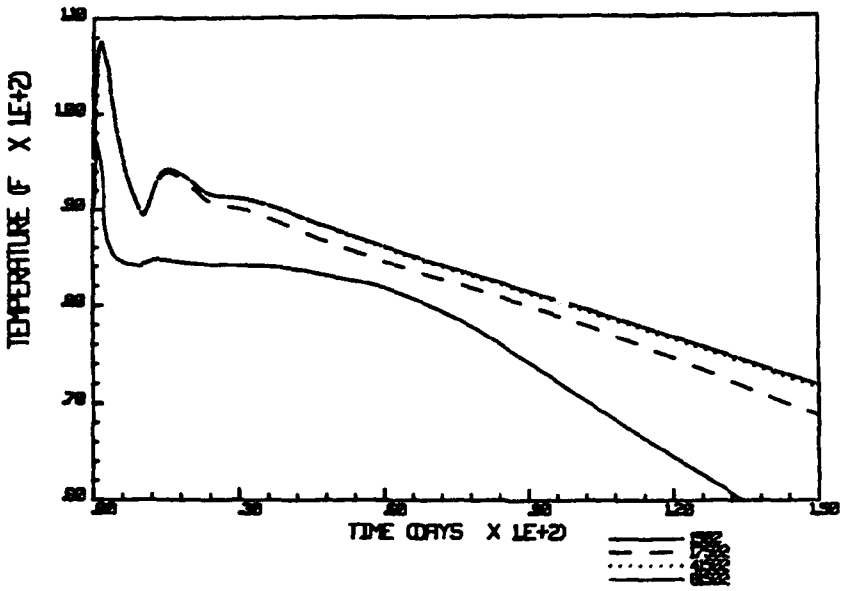

Figure 65. Temperature along a center line parallel to the axis of flow, Lift 1, 3DCMT2

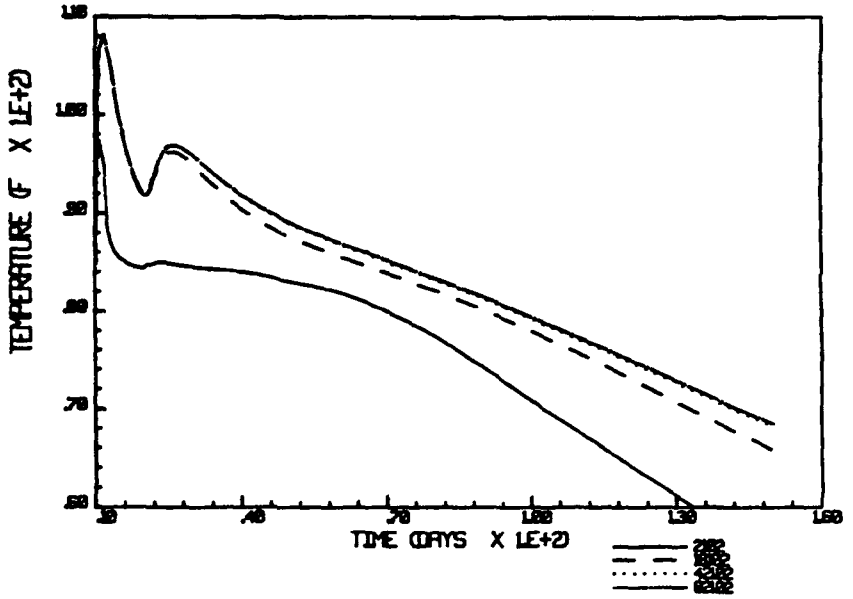

Figure 66. Temperature along a center line parallel to the axis of flow, Lift 2, 3DCMT2

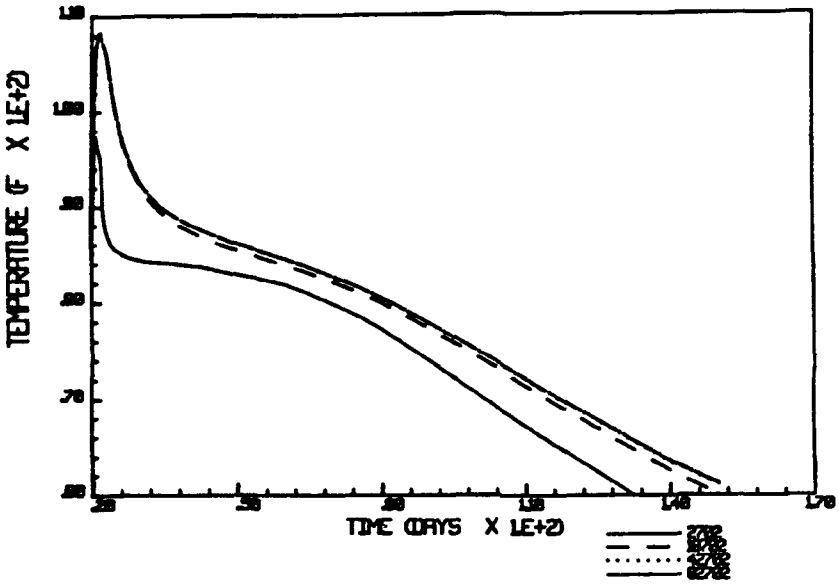

Figure 67. Temperature along a center line parallel to the axis of flow, Lift 3, 3DCMT2

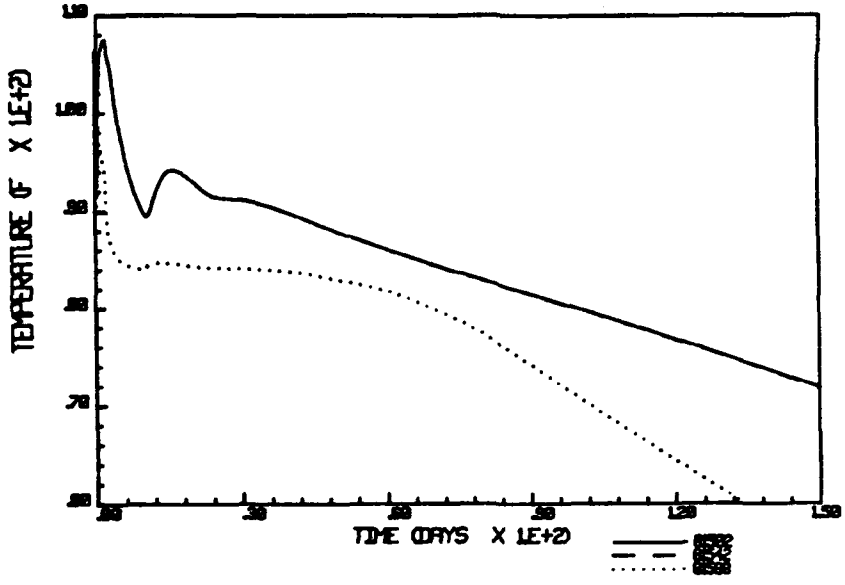

Figure 68. Temperature along a center line transverse to the axis of flow, Lift 1, 3DCMT2

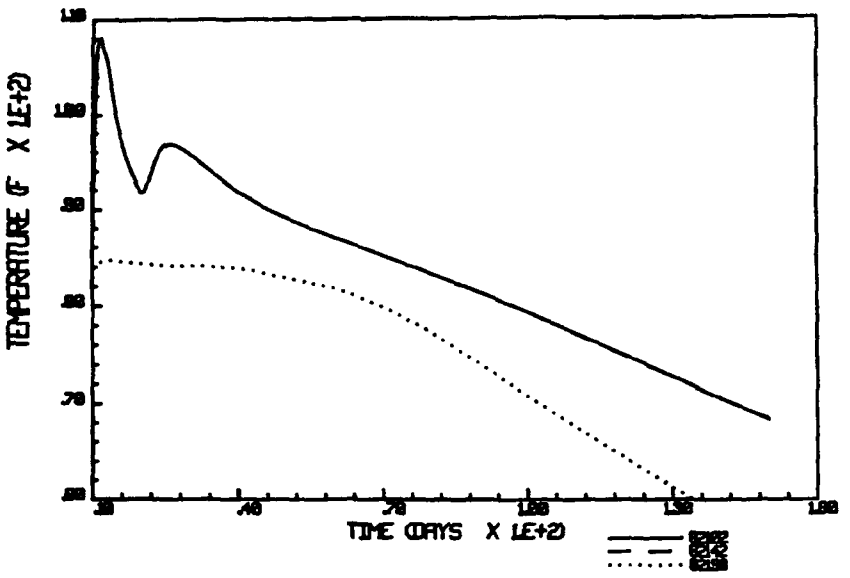

Figure 69. Temperature along a center line transverse to the axis of flow, Lift 2, 3DCMT2

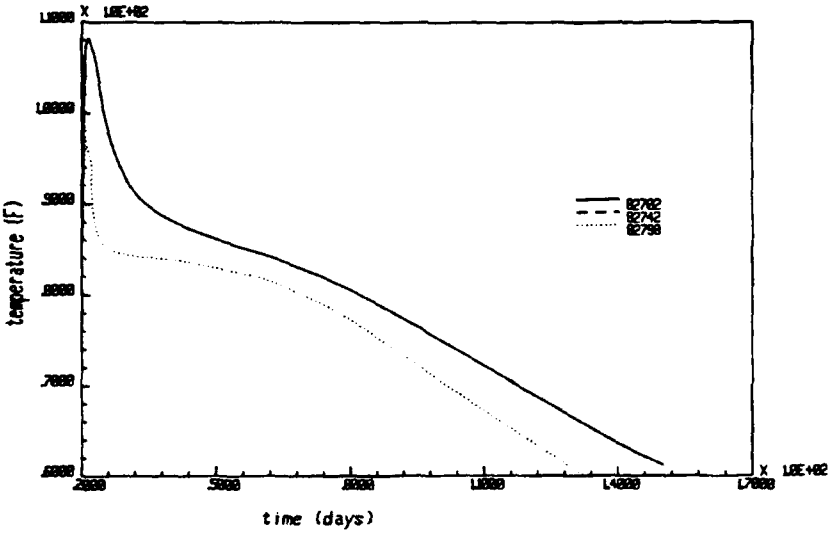

Figure 70. Temperature along a center line transverse to the axis of flow, Lift 3, 3DCMT2

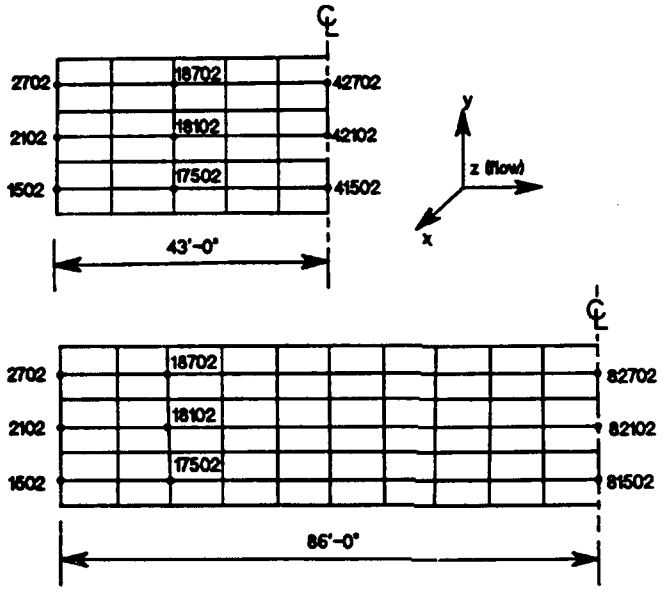

Figure 71. Location of nodes in center planes parallel to axis of flow, 3DCMT1 and 3DCMT2 grids

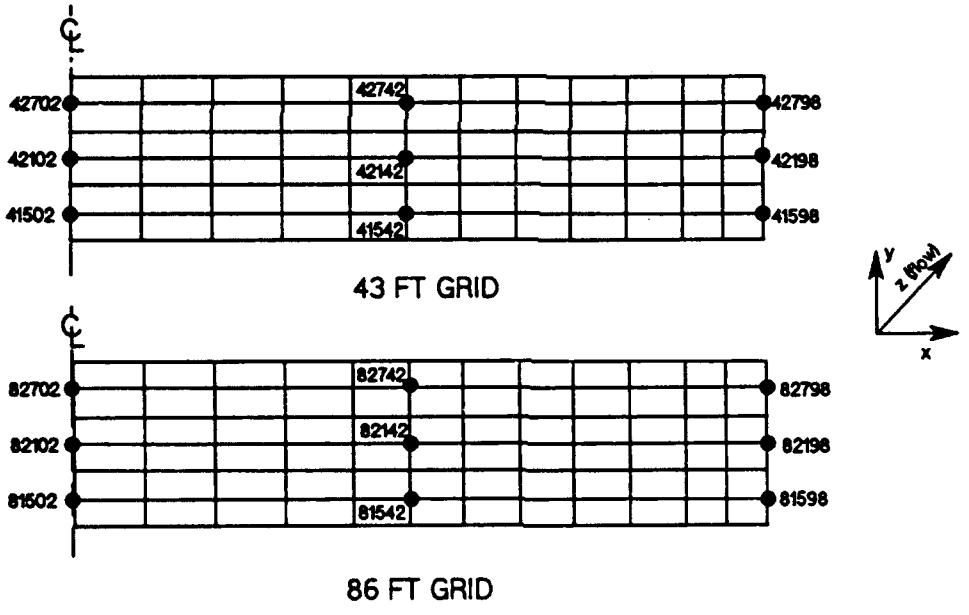

Figure 72. Location of nodes in center planes transverse to the axis of flow, 3DCMT1 and 3DCMT2 grids

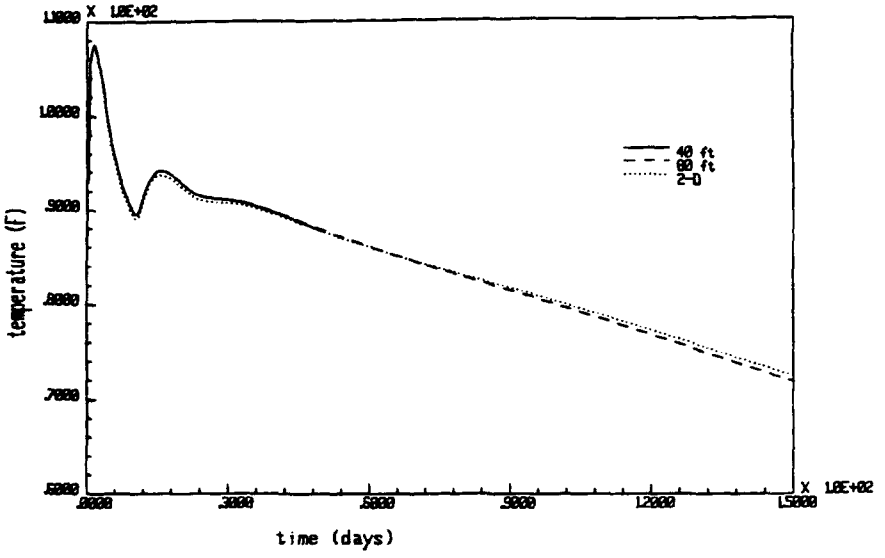

Figure 73. Temperature at the center line node of Lift 1 from 3DCMT1, 3DCMT2 and CMT1

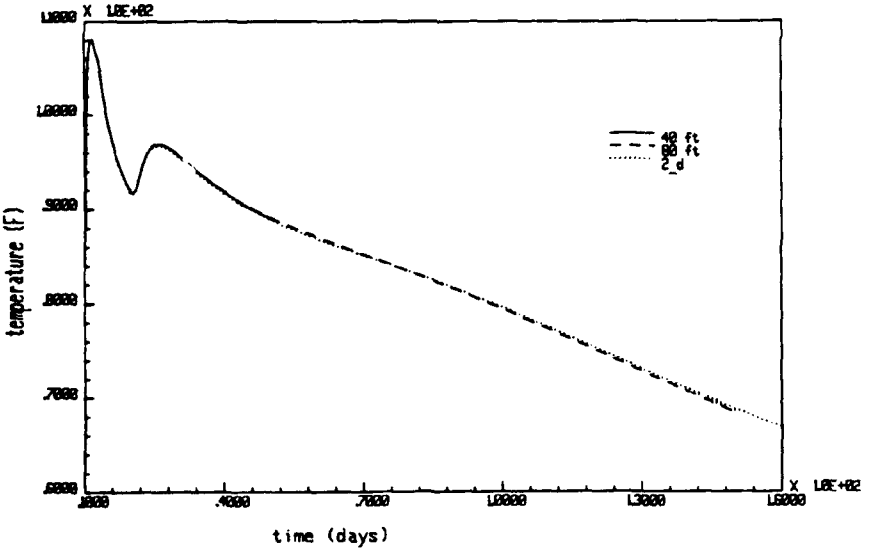

Figure 74. Temperature at the center line node of Lift 2 from 3DCMT1, 3DCMT2 and CMT1

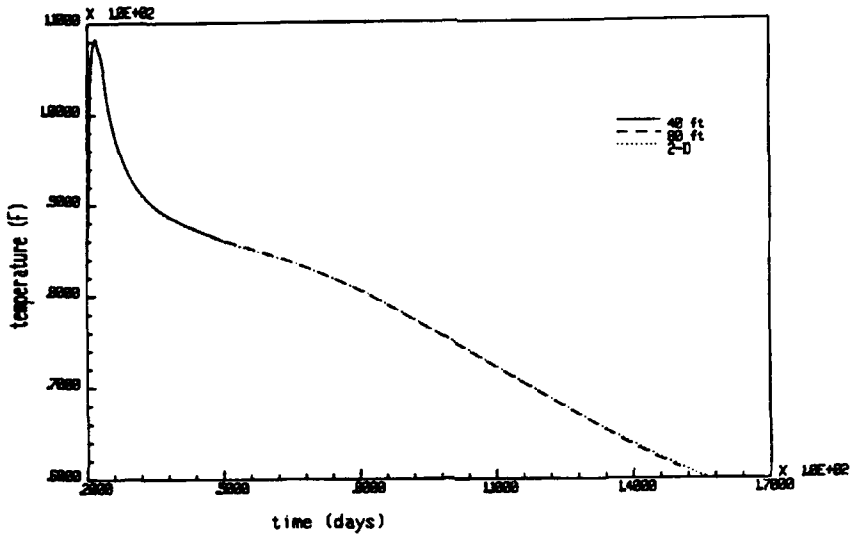

Figure 75. Temperature at the outer node of Lift 3 from 3DCMT1, 3DCMT2 and CMT1

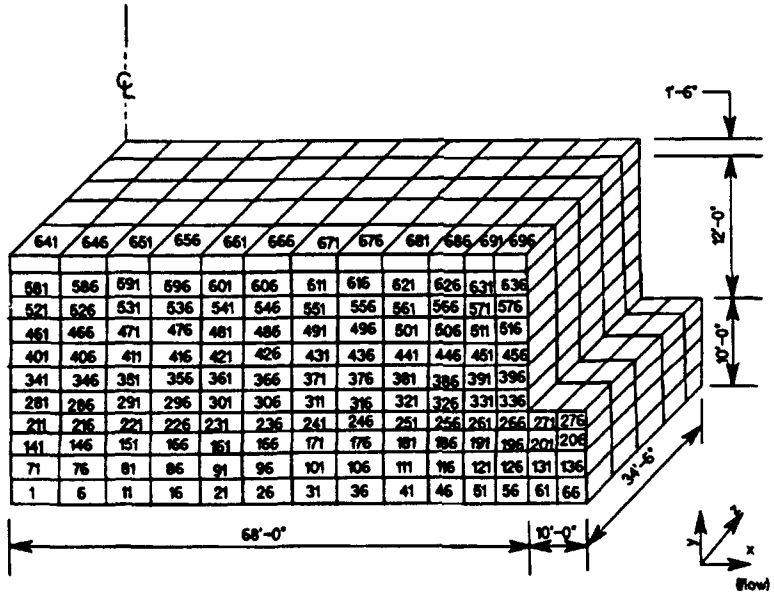

Figure 76. Grid used in 3DCMT1 and 3DCMT2 analyses

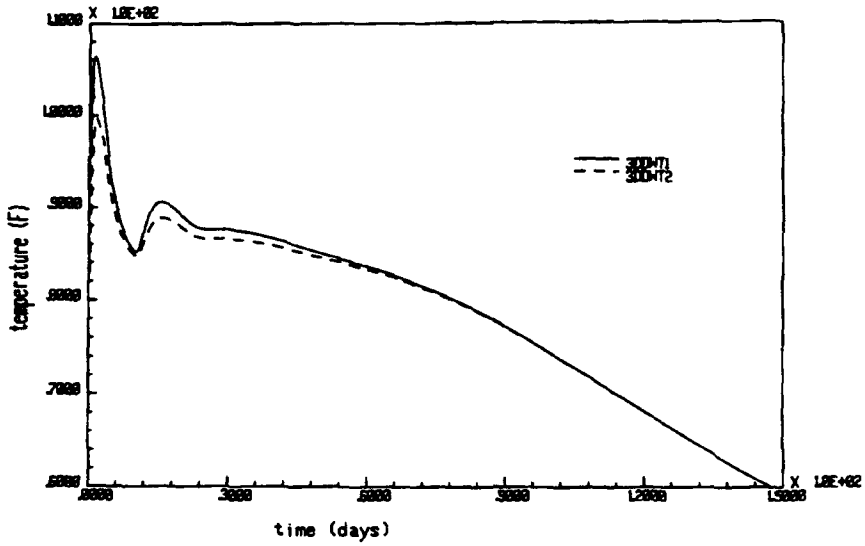

Figure 77. Temperature at Node 81502, Lift 1, 3DDWT1, 3DDWT2

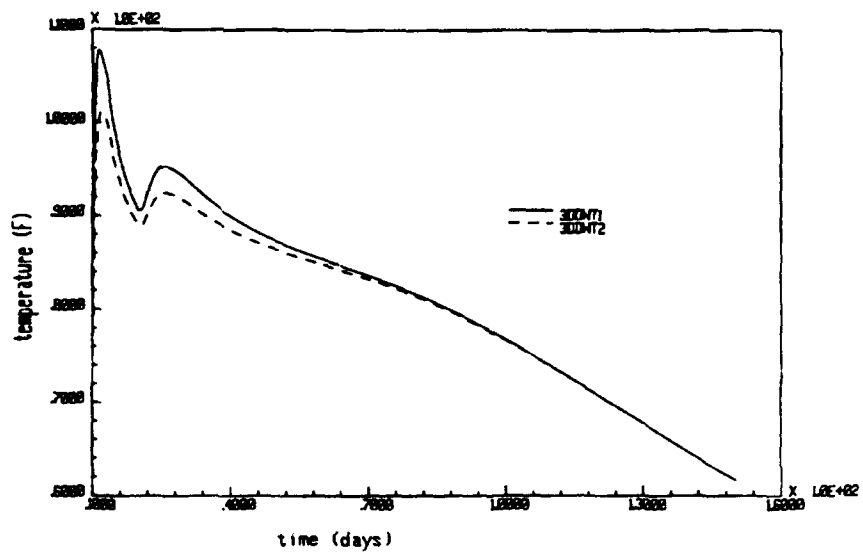

Figure 78. Temperature at Node 82102, Lift 2, 3DDWT1 and 3DDWT2

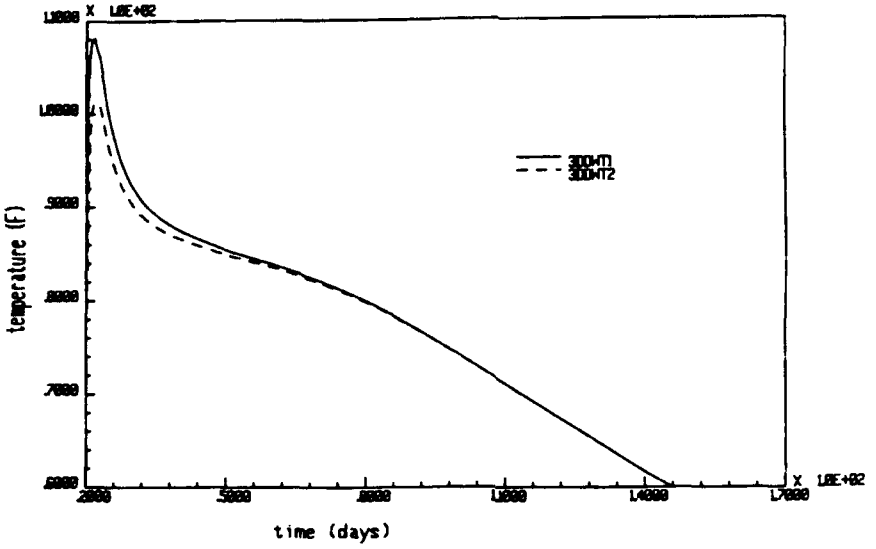

Figure 79. Temperature at Node 82852, Lift 3, 3DDWT1 and 3DDWT2

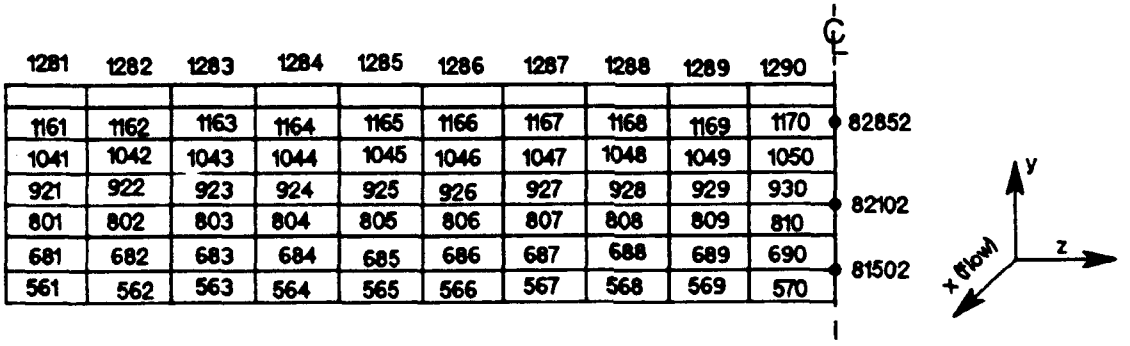

Figure 80. Location of Nodes and Elements Along Center Plane Parallel to Axis of Flow, 3D Dam Weir Analyses.

Stress Analyses

111. All three-dimensional stress analyses were made using 20-node brick elements with reduced integration. The orientation of elements and the location of integration points within an element is shown in Figure 81. Mixture A13 mechanical properties were used throughout except in the higher-strength layer of the dam weir analyses. For these elements, 3-day modulus and compressive strength were 3.12×10^6 psi and 1,100 psi, respectively. A summary of stress analyses is given in Table 12.

Table 12

Summary of Stress Analyses

Name	Corresponding Heat Transfer Analysis	Notes
3DCMS1	3DCMT1	43-ft monolith length, A13
3DCMS2	3DCMT2	86-ft monolith length, A13
3DDWC1	3DDWT1	dam-weir simulation, 85 °F placement temperature
3DDWC2	3DDWT2	dam-weir simulation, 75 °F placement temperature
3DDWC3	3DDWT1	dam-weir simulation, 85 °F placement temperature, ϵ_f=50 millionths

Chamber monolith Run 1, 3DCMS1

112. Stresses in the x and z directions at integration points along a vertical line near the center of Lift 3 are shown in Figures 82 and 83. As expected, the highest tensile stresses were at integration points near the center elevation (73 ft) of the lift. Stresses in the x and z direction at the centerline transverse to the axis of flow are shown in Figures 84 and 85. Stresses along the centerline parallel to the axis of flow are shown in Figures 86 and 87. Element locations are shown in Figures 88 and 89.

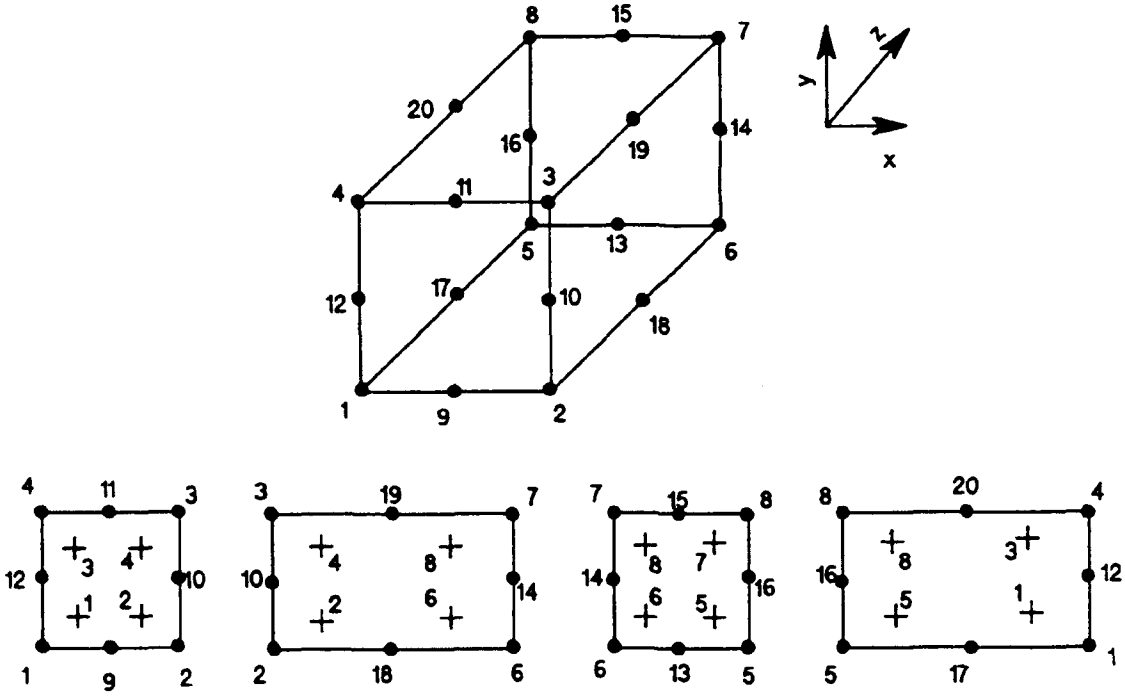

Figure 81. Location of integration points, 20-node reduction integration element

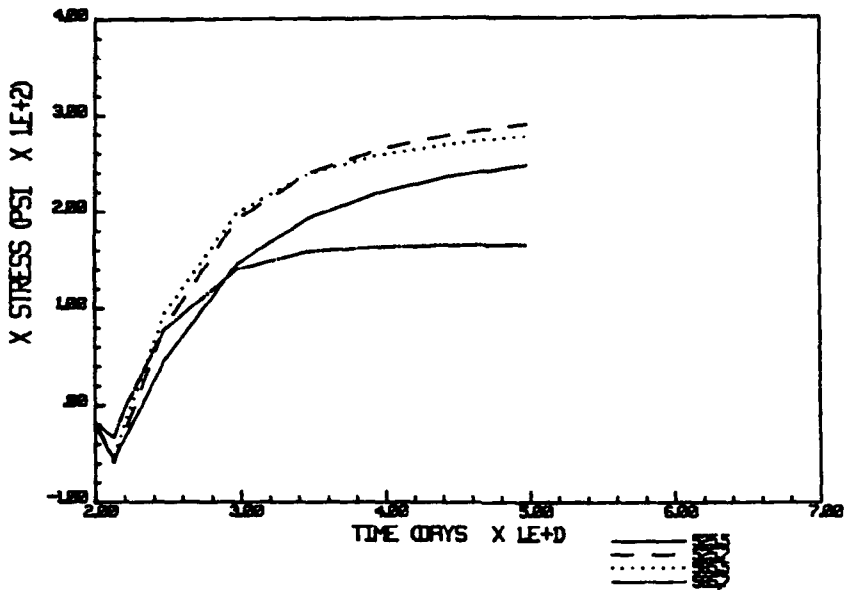

Figure 82. Stresses in the X-direction along the vertical center line of Lift 3, 3DCMS1

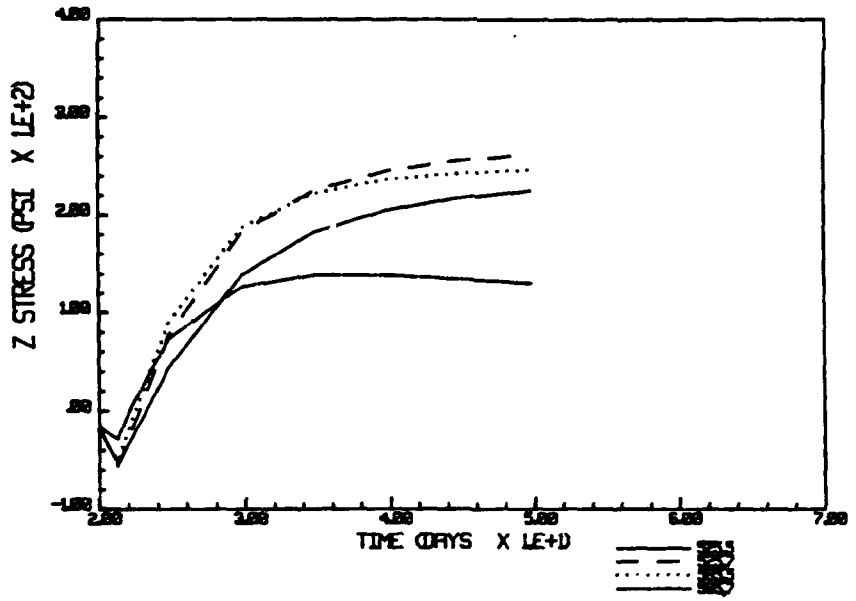

Figure 83. Stresses in the Z-direction along the vertical center line of Lift 3, 3DCMS1

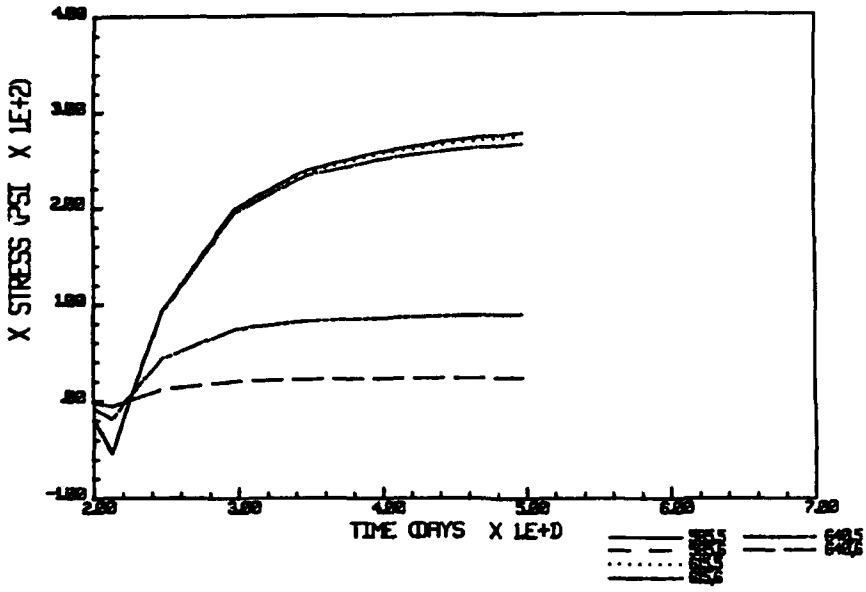

Figure 84. Stresses in the X-direction at the center line of Lift 3 transverse to the axis of flow, 3DCMS1

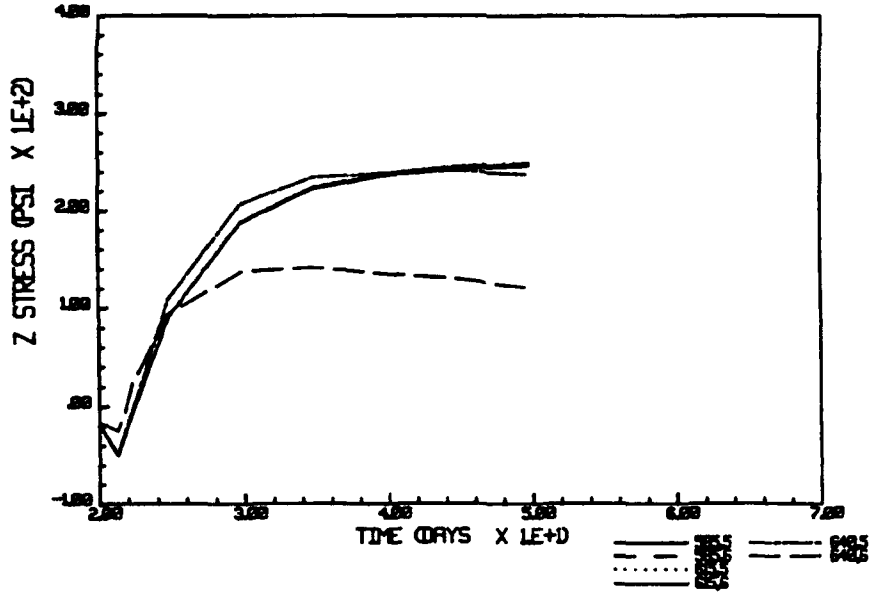

Figure 85. Stresses in the Z-direction at the center line of Lift 3 transverse to the axis of flow, 3DCMS1

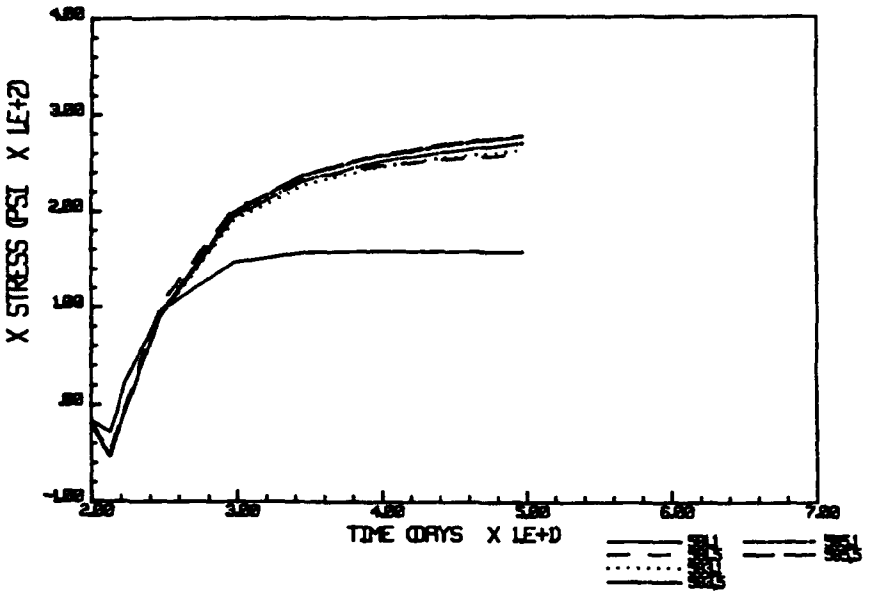

Figure 86. Stresses in the X-direction along the center line of Lift 3 parallel to the axis of flow, 3DCMS1

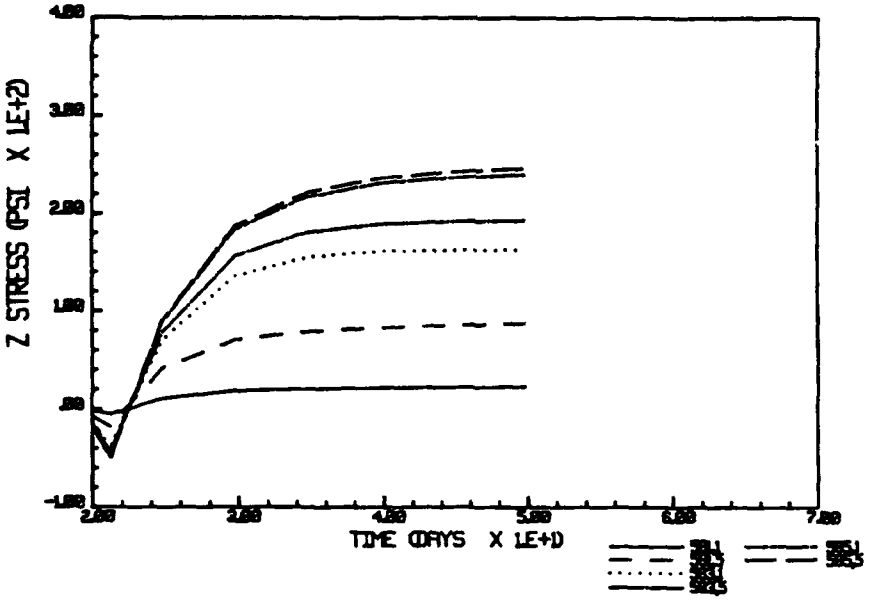

Figure 87. Stresses in the Z-direction along the center line of Lift 3 parallel to the axis of flow, 3DCMS1

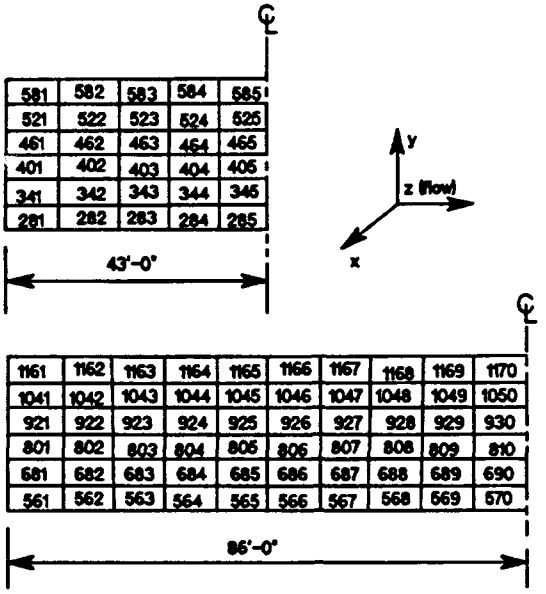

Figure 88. Location of elements in center planes parallel to axis of flow 3DCMS1 and 3DCMS2

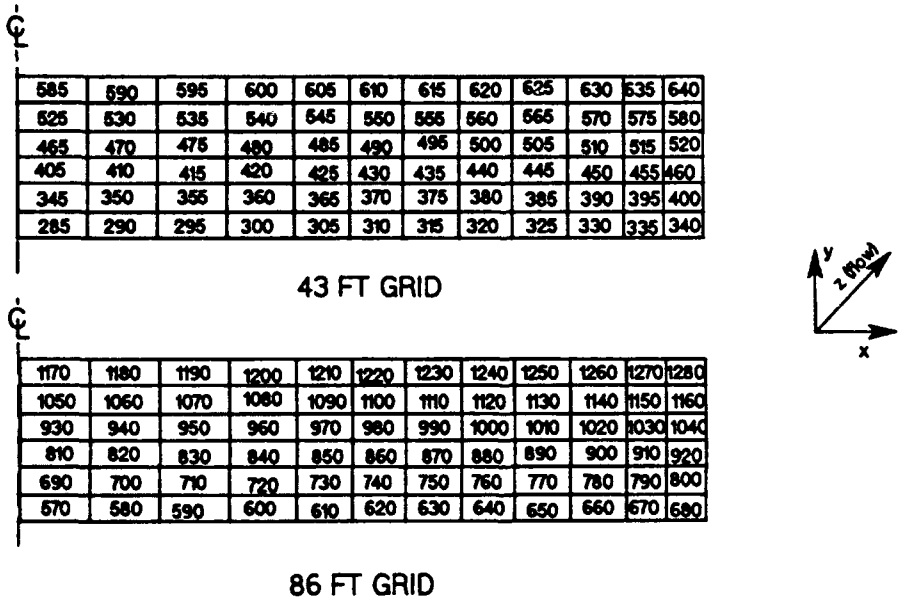

Figure 89. Location of elements in center planes transverse to axis of flow 3DCMS1 and 3DCMS2

113. As can be seen from Figures 82 and 83, stresses in the x direction were slightly higher than stresses in the z direction at the center of the monolith. Maximum stresses in the z direction at the end of the analysis period (50 days) were 250 psi, while horizontal stresses in the x-y plane approached 300 psi.

114. Some cracking occurred at the base due to support conditions, but no cracking was observed at any other location within the floor.

Chamber monolith Run 2, 3DCMS2

115. The analysis on the 86-ft chamber monolith floor was continued for a period of 150 days without insulation. In this longer model, stresses at the center of the third lift were approximately the same in the x and z directions. Stresses in the x and z directions along a vertical centerline are plotted in Figures 90 and 91. Stresses along a centerline transverse to the axis of flow are plotted in Figures 92 and 93. Stresses along a centerline parallel to the axis of flow are plotted in Figures 94 and 95. Element locations are shown in Figures 88 and 89.

116. In each plot, stresses at the center of Lift 3 approached 300 psi at approximately 70 days after the start of construction (roughly the middle of September). At this point the slope of the stress-time curve increased as ambient temperature began to drop, and final stresses (at approximately the start of December) exceeded 450 psi. Cracking occurred at the base only.

117. Stresses at the center of lift 3 in the two 3-dimensional analyses (3DCMS1 and 3DCMS2) and in the 2-dimensional analysis (CMS4) are plotted in Figures 96 and 97. Horizontal stresses were similar for all three runs. Stresses in the z direction were only slightly greater in 3DCMS2 (at element 1170, point 5) than in 3DCMS1 (at element 585, point 5) and never approached the plane strain condition of CMS4 (element 233, point 1).

Dam weir Run 1, 3DDWS1

118. Stresses in the x and z directions along the vertical center line of Lift 3 are shown in Figures 98 and 99. Element locations are shown in Figure 80.

119. Tensile stresses in the higher-strength layer were much greater than those in the underlying concrete, reaching approximately 1,100 psi at

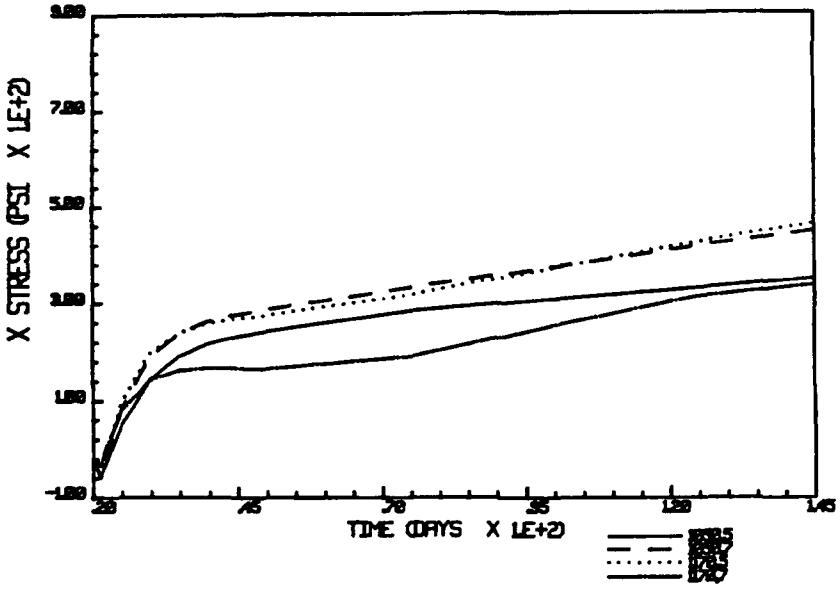

Figure 90. Stresses in the X-direction along the vertical center line of Lift 3, 3DCMS2

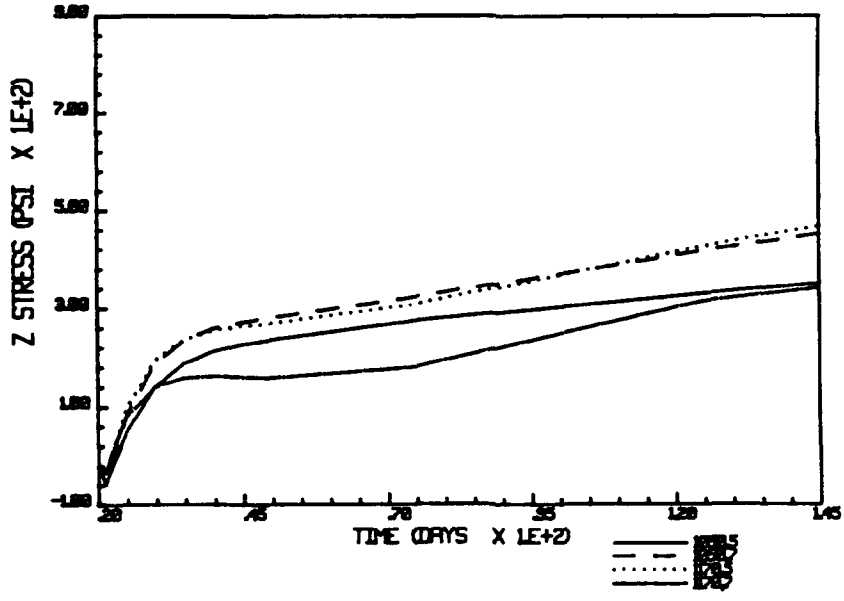

Figure 91. Stresses in the Z-direction along the vertical center line of Lift 3, 3DCMS2

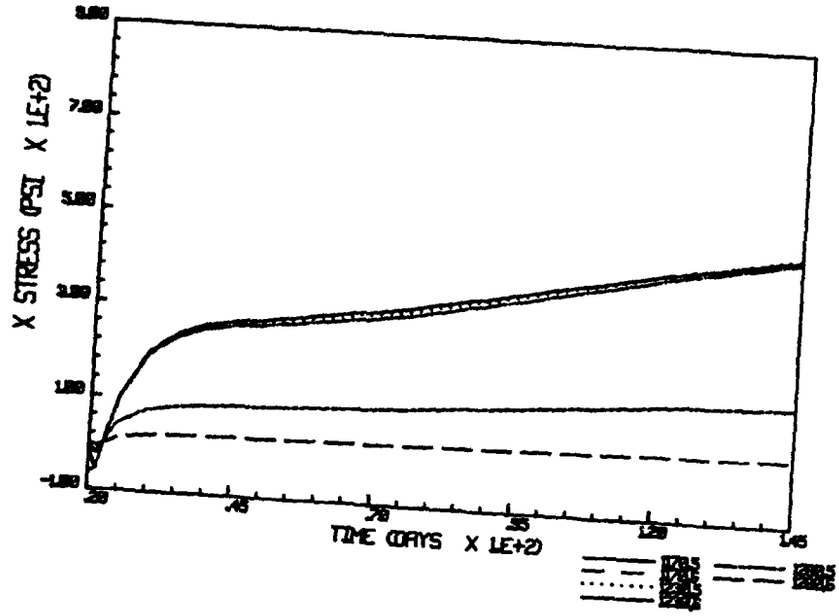

Figure 92. Stresses in the X-direction at the center line of Lift 3 transverse to the axis of flow, 3DCMS2

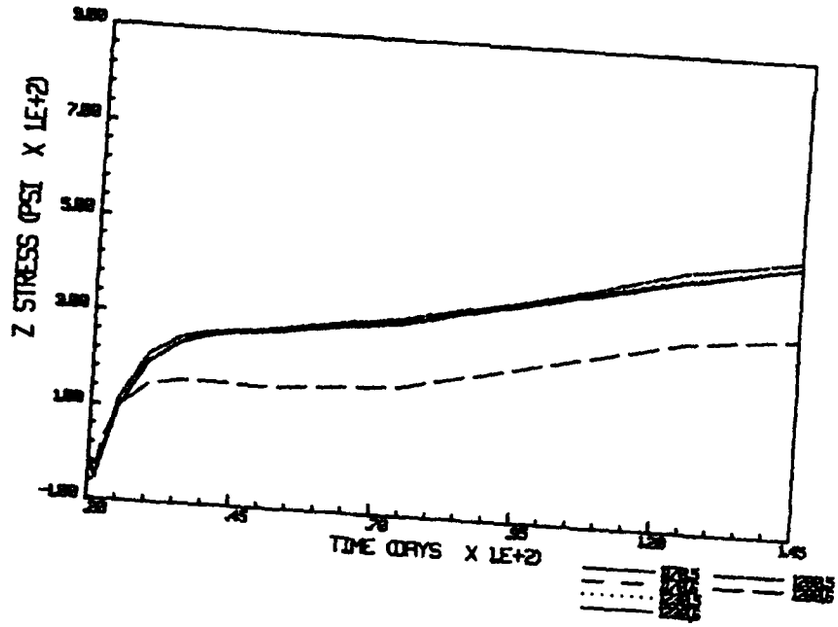

Figure 93. Stresses in the Z-direction at the center line of Lift 3 transverse to the axis of flow, 3DCMS2

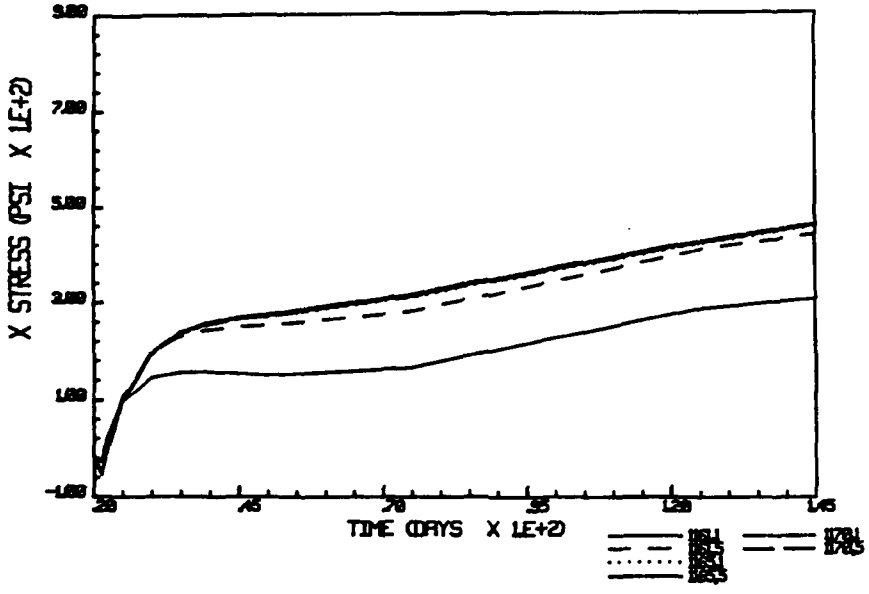

Figure 94. Stresses in the X-direction at the center line of Lift 3 parallel to the axis of flow, 3DCMS2

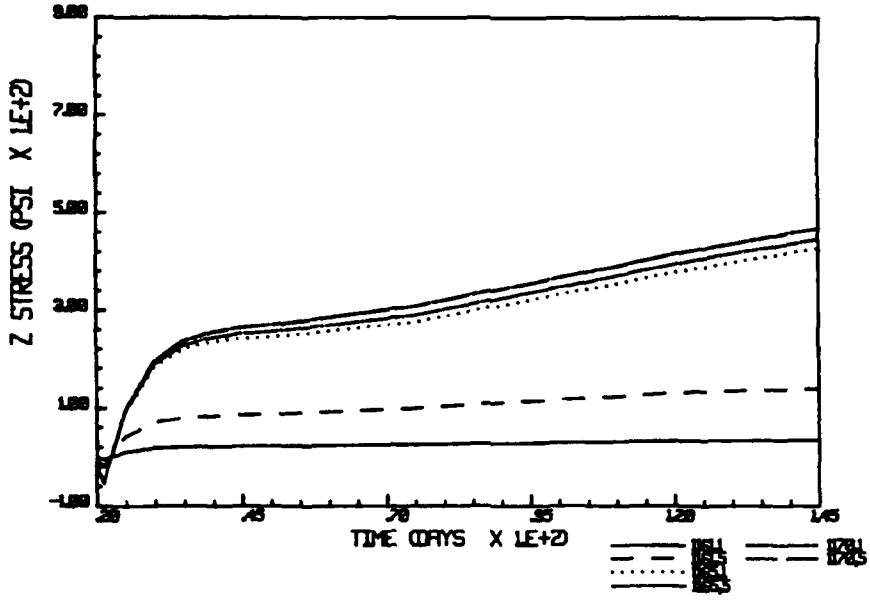

Figure 95. Stresses in the Z-direction at the center line of Lift 3 parallel to the axis of flow, 3DCMS2

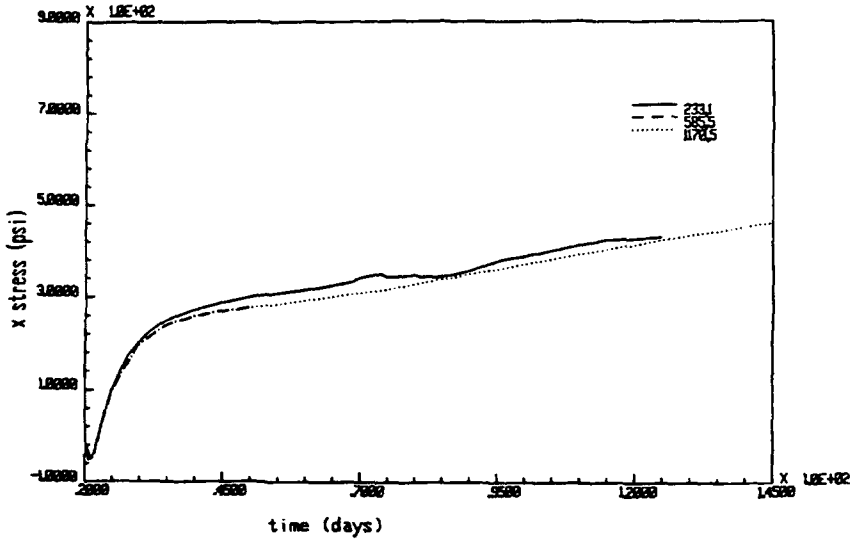

Figure 96. Stresses in the X-direction at the center of Lift 3, 3DCMS1, 3DCMS2 and CMS4

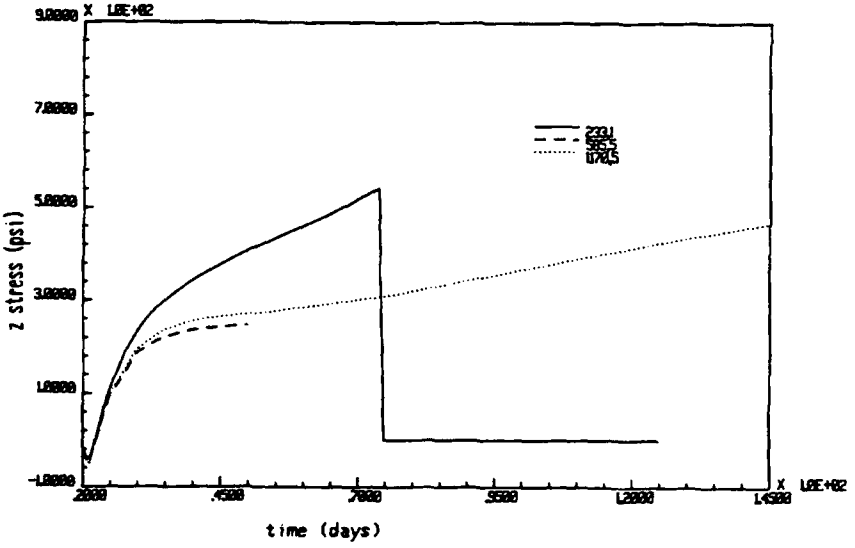

Figure 97. Stresses in the Z-direction at the center of Lift 3, 3DCMS1, 3DCMS2 and CMS4

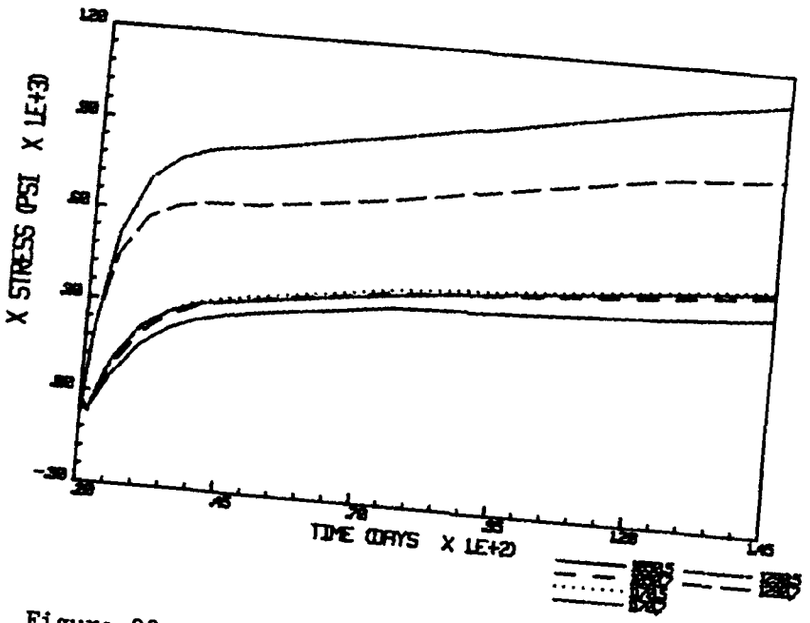

Figure 98. Stresses in the X-direction along the vertical center line of Lift 3, 3DDWT1

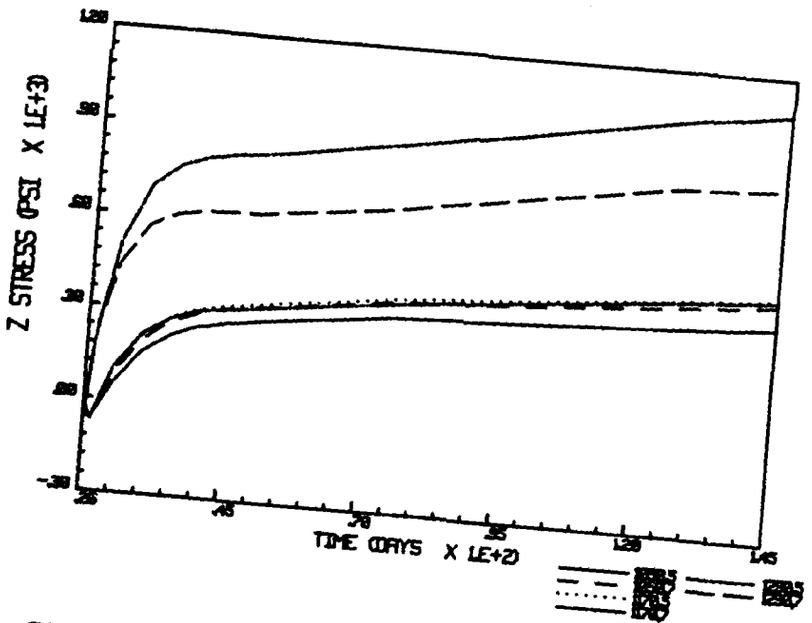

Figure 99. Stresses in the Z-direction along the center line of Lift 3, 3DDWS1

125 days after placement. Stresses at the top of the lower-strength layer of Lift 3 became tensile at approximately 3 days, while stresses in the higher-strength layer were tensile at less than one day after placement and exceeded 300 psi by 3 days after placement. Even though cracking was not predicted in Lift 3, stresses of this magnitude are not desirable.

120. A possible reason for excessive tensile capacity was discovered in a report by Holland, Liu, and Bombich (1982) on the properties of Lock and Dam 2 concretes. Ultimate strain capacity tests using 12- by 12- by 66-in. beams were run for two mixtures, one with a design compressive strength of 3,000 psi at 28 days and the other with a design compressive strength of 3,000 psi at 90 days. Loading rates of 40 psi/min and 25 psi/week were used. For the higher strength mixture under rapid loading, average tensile strain capacity varied little after 3 days, but average test capacity at 1 day was only 50 millionths as opposed to 80 millionths at 3 days. Tensile strain capacities for all specimens loaded at the slower rate were well over 100 millionths. This indicates that the constant tensile strain capacity used in the analyses (100 millionths) is probably adequate for Mixture A13 but may be too high for a mixture which undergoes rapid increase in tensile stresses and strains at very early ages.

Dam weir monolith Run 2, 3DDWS2

121. In an attempt to lower stresses in the higher-strength layer, a stress run was made using 3DDWT2 as the loading. Resulting stresses along a vertical centerline of Lift 3 are plotted in Figures 100 and 101. Maximum out-of-plane stresses in this analysis varied from approximately 50 percent at 1 day to 75 percent at 150 days of stresses in 3DDWS1. This is a significant decrease at early times, when cracking is most likely to occur. Predicted stresses in the z direction for the two runs are compared in Table 13.

Dam weir monolith Run 3, 3DDWS3

122. To determine the effect of lowering the tensile strain capacity on early-time cracking in the higher-strength layer, Run 3DDWS1 was repeated using a tensile strain capacity of 50 millionths in the higher-strength layer. The run was stopped after 67 days when no cracking had occurred in the higher-strength layer. Since predicted stresses were the same as in the 3DDWS1 analysis, no stress-time plots were made.

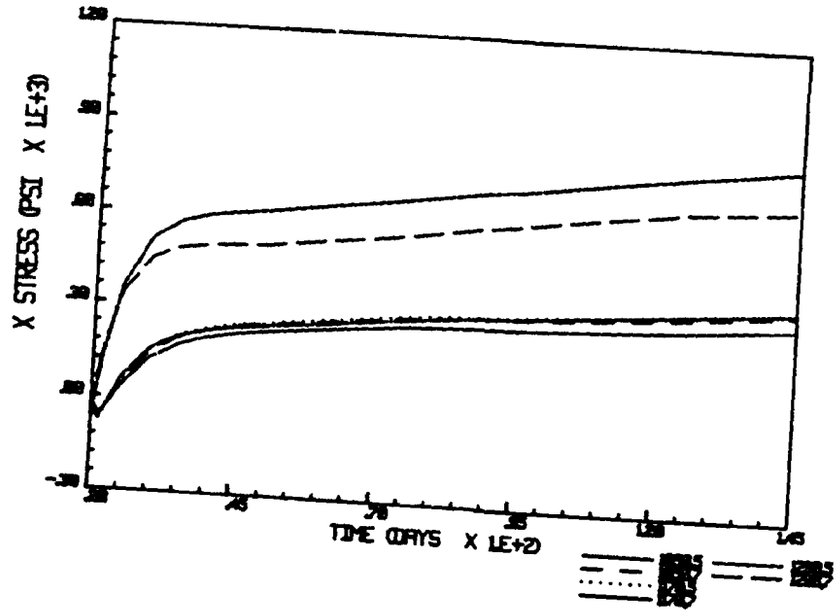

Figure 100. Stresses in the X-direction along the vertical center line of Lift 3, 3DDWS2

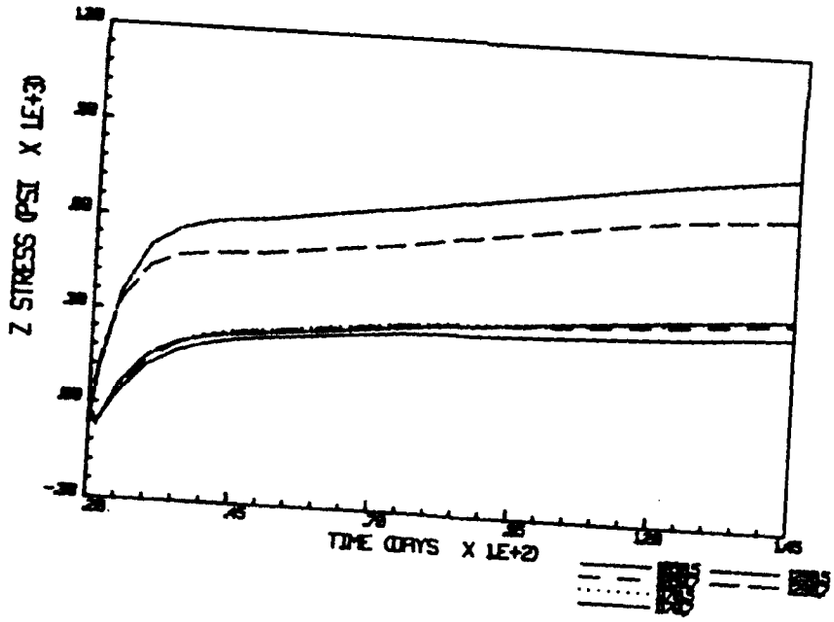

Figure 101. Stresses in the Z-direction along the center line of Lift 3, 3DDWS2

Table 13

Stresses at Element 1290, Integration Point 5

Time After Placement (days)	Out-of-Plane Stress (psi) 3DCMS1	3DCMS2	$\sigma_{CMS2}/\sigma_{CMS1}$
1.5	156	78	0.5
2.5	268	160	0.6
10.0	694	504	0.73
150.0	1,109	824	0.74

123. Although no cracking was predicted in any of the three-dimensional dam weir analyses, the high stresses predicted in 3DDWS1 left little margin to allow for variations in construction procedures, stress concentrations due to changes in section, and other circumstances that could increase tensile stress and result in cracking.

PART VII: CONCLUSIONS AND RECOMMENDATIONS

Conclusions

Two-dimensional analyses

124. In the two-dimensional thermal-stress analyses, two start-of-placement dates were considered: 1 July and 1 November. Concrete in the 1 July analyses was not insulated, and Mixture A13 properties were used throughout as the mass concrete mixture. Concrete in 1 November runs was insulated throughout the construction period, and Mixture A8 properties were used. Initial placement temperatures for all lifts were 5 °F above ambient with a maximum of 85 °F. As expected, the highest thermal differentials for a given monolith occurred in the 1 July analyses (CMT1, CMT2, UGBT1, UGBT2, and DWT1). In these analyses, temperatures in the center of the relatively thin chamber monolith floor section decreased at about the same rate as ambient temperature after the first 20 days, resulting in temperatures roughly 15 °F above ambient at the end of the construction period. For thicker sections, interior temperatures decreased at a slower rate than ambient temperatures, resulting in temperatures at the center of the upper-gate-bay floor in excess of 20 °F above ambient at the end of the construction period. For both the upper-gate-bay and lock-chamber monoliths, the analyses were continued beyond 1 November without insulation and temperature differentials of approximately 30 °F resulted in the floor sections. Temperature differentials were not a problem in wall sections less than 10 ft thick. Cooling occurred fairly rapidly, and wall temperatures in the summer analyses generally reached ambient temperature by 10 to 20 days after placement. In all cases temperatures were more uniform across the sections when insulation was used.

125. Horizontal stresses in floors were higher in the 1 July analyses than in the 1 November analyses. In the summer analyses, each new lift expanded during the first two days after placement when the concrete had very little stiffness and very little compressive stress resulted. Temperatures reached a maximum at approximately 2 days after placement and cooling began to occur. At this point, unrestrained concrete would have contracted due to cooling and shrinkage. Concrete in the first lift of each monolith was

unrestrained in the horizontal direction and expanded and contracted freely with very little stress. Following lifts were restrained by the concrete below, resulting in horizontal tensile stresses near the center of each new floor lift. These tensile stresses were generally decreased or eliminated as additional lifts were placed and restraint of strains due to cooling and shrinkage in upper lifts tended to force the existing concrete into compression. Horizontal tensile stresses in new lifts became higher as the number of lifts increased. Horizontal tensile stresses in the chamber monolith floor were within acceptable limits in all analyses. For the thicker upper-gate-bay monolith, horizontal stresses reached unacceptable levels in summer analyses if no precooling of the concrete was simulated. Cooling was slower and more uniform in insulated structures, resulting in less restraint from existing concrete and low horizontal stresses.

126. In areas of one-dimensional heat flow, vertical stresses were generally due to gravity rather than the restraint of thermal or shrinkage strains. Vertical tensile stress concentrations were predicted at supports in all summer analyses and at the corners of culverts in all analyses. As with horizontal stresses, vertical tensile stresses in these areas increased with thickness of the monolith, resulting in cracking in the upper-gate-bay monolith when precooling of the concrete was not assumed.

127. Limiting warm-weather placement temperatures to a 75 °F maximum in the upper-gate-bay floor section reduced thermal differentials to approximately 12 °F throughout most of the construction period. Stresses and cracking were significantly reduced.

128. Using a longer period between placement of lifts to allow cooling in thick floor sections reduced the sustained maximum temperature by several degrees. However, thermal differentials were increased since the extended construction period resulted in lower ambient temperatures.

129. In the past, 20 °F has been suggested as a safe upper limit in mass concrete for temperature differentials across a section. This limit was not adequate to protect against cracking in the upper-gate-bay monolith analyses. Other factors such as geometry of the section and shrinkage of the concrete must also be considered. For floor sections with no more than three 5-ft nominal lifts (15 ft total), 20 °F may be an acceptable level. Thicker

sections provide more restraint of shrinkage and thermal strains, result in higher stresses and require lower limits.

130. Analyses using plane-stress and plane-strain elements represented bounding conditions. Plane-stress elements exhibited lower stresses and less cracking in all cases. The appropriate type of analysis for a given structure depends on the ratio of thickness of the floor and wall sections to length of the monolith. For thin sections a plane-strain analysis may approximate field conditions, while very thick sections approach a plane-stress condition.

131. All analyses were made based on average ambient temperatures. No attempt was made to simulate short-term perturbations due to strong cold fronts. However, maximum predicted tensile stresses rose sharply due to temperature differentials in all runs continued without insulation beyond 1 November. In the chamber monolith, temperatures in the center of the floor were still about 15 °F above ambient in October. In the center of the upper-gate-bay monolith, predicted temperatures were over 20 °F above ambient by October. A 20 °F drop in mean daily temperature due to a cold front during this period could result in an additional 10 °F added to the temperature differential. Cold fronts resulting in a 20 °F drop in mean daily temperature are possible in October in central and northern Louisiana, and insulating the structures beginning 1 October rather than 1 November would provide additional protection against thermal cracking.

132. These results apply only to the concretes and geometries used in the analysis. In general, the high fly-ash content concretes exhibited relatively little shrinkage, low early-time stiffness, and high creep when compared with conventional mixtures. Conclusions from these analyses should not be applied to other mixtures and structures in lieu of thermal-stress analyses.

Three-dimensional analyses

133. The start-of-placement date for all three-dimensional analyses was 1 July. The Mixture A13 adiabatic curve and average thermal properties for all mixtures were used in the heat-transfer analyses. Mixture A13 mechanical properties were used in the stress analyses except for the higher-strength layer on the ogee section in analyses 3DDWS1, 3DDWS2 and 3DDWS3, where

Mixture All properties were used. Initially, placement temperatures of 85 °F were used in all lifts.

134. Temperatures in the chamber monolith floor analyses were the same as those in the worst case two-dimensional analysis throughout most of the model for both the 43-ft long and 86-ft long models. This indicates that heat flow is one-dimensional throughout much of the actual structure. Temperatures in the first dam weir heat-transfer analysis were similar to those in the chamber monolith analyses. Lowering the placement temperatures to 75 °F in the next analysis resulted a 6 °F drop in maximum temperatures.

135. In-plane stresses (x-y plane) at the center of the chamber monolith floor were similar to those in the two-dimensional analysis for both the 43-ft and 86-ft models. However, the plane-strain analysis greatly overpredicted stresses in the out-of-plane direction (z-direction). Although stresses in the z-direction increased with monolith length, predicted stresses were much lower for both three-dimensional analyses than for the corresponding plane strain analysis, and no cracking was predicted except at the external constraints.

136. In the simulated dam weir analyses, stresses in the center of the monolith in the higher-strength layer were over twice those in the lower-strength layer immediately below. Tensile stresses occurred at earlier times in the high-strength layer and were as high as 300 psi at 3 days in the first analysis. Stresses in both the x- and z-directions were reduced by 50 percent at early times when placement temperatures were lowered to 75 °F. Even though stresses seemed excessive, no cracking was predicted in the third layer for either analysis. Changing the tensile strain capacity in the high-strength layer from 100 to 50 millionths in the third analysis did not cause cracking to occur.

Recommendations

137. For purposes of making specific recommendations, monoliths were placed in one of four groups based on thickness of floor and wall sections. Recommendations for each group follow.

Group I monoliths

138. Group I monoliths have floors less than 15 ft thick and relatively thin wall sections. Monoliths in this category are L-4 through L-15. These monoliths require no special provisions to reduce temperatures during warm weather construction other than limiting the maximum placement temperature to 85 °F. The maximum recommended lift height for floor slabs is 5 ft. Maximum recommended lift height for walls is 10 ft, except in the transition area directly over the culvert, which should be placed in two lifts. All concrete in floor slabs placed less than 3 months prior to 1 October and all concrete in walls placed less than 1 month prior to that date should be insulated from 1 October until 1 April.

139. Doubling the length of these monoliths (from 43 to 86 ft) is acceptable and should result in an increase in maximum tensile stress in the out-of-plane direction of about 20 percent.

Group II monoliths

140. Group II monoliths have floors less than 15 ft thick and wall thicknesses of over 10 ft. Monoliths in this category are L-1, L-3, L-16 and L-18. All recommendations for Group I apply to these monoliths except that the maximum recommended lift height for walls is 5 ft throughout for all concrete placed without insulation. If wall lifts greater than 5 ft are allowed in these monoliths, insulation must be applied from the start of wall placement.

Group III monoliths

141. Group III monoliths have floor sections thicker than 15 ft and relatively thick walls. Monoliths in this category are L-2 and L-17. In the floor sections of these monoliths, thermal differentials must be reduced during warm-weather placement. The following alternative methods are recommended:

a. In floor lifts placed between 1 May and 1 October concrete can be precooled to insure that the maximum placement temperature of the concrete is at or below 75 °F.

b. Insulation can be applied to all exposed surfaces in the floor sections from the start of construction through 1 April.

142. The maximum recommended lift height is 5 ft in both floors and walls. However, lifts of up to 10 ft may be allowed in the walls if all

exposed wall surfaces (including the inside of culverts) are insulated from the start of construction through 1 April. All concrete in floor slabs placed less than 6 months prior to the earliest date specified for insulation and all concrete in walls placed less than one month prior to that date should be insulated from that date until 1 April. The 6-month requirement is necessary because of the slow rate at which temperatures are dissipated in the center of thick sections.

Group IV monoliths

143. Group IV monoliths are the dam weir monoliths. These monoliths are comparatively thick throughout, but have a gradually changing section and a higher-strength layer intended to resist erosion of the concrete due to cavitation. Maximum recommended lift height for these monoliths is 5 ft. In lifts placed between 1 May and 1 October concrete should be precooled to ensure that the maximum placement temperature of the concrete is at or below 75 °F. This should significantly reduce cracking in the higher-strength upper layer. An alternative to cooling the concrete is to place the dam weir monoliths during the winter when the concrete must be insulated. Higher-strength concrete should be placed at the same time as the lower-strength concrete in a given lift. All concrete placed less than 6 months prior to the earliest date specified for insulation should be insulated from that date until 1 April.

General recommendations

144. We recommend that the time between placement of sequential lifts not exceed approximately 1 month for all floor slabs or walls for thickness greater than approximately 10 ft.

145. The two concrete mixtures used in these analyses for mass concrete applications are substantially different in terms of their thermal and mechanical properties. Mixture A8 develops more heat and is significantly stiffer at early ages than Mixture A13. The analyses show that Mixture A8 is an appropriate mixture for insulated lifts, but should not be used if insulation is not employed. Mixture A13 should be used for all mass concrete placed between 1 April and 1 October. It was assumed in all analyses that the thermal and mechanical properties determined in the laboratory would be representative of those of the concrete used in the field. Therefore, the

recommended concrete mixtures should not be changed substantially by varying the cementitious materials content or ratio of fly ash to total cementitious materials without careful consideration as to how these changes might affect the performance of the concrete and its influence on cracking. Should adjustments to the concrete mixtures be desired to increase workability, we recommend that the fly ash content of the mixtures be adjusted no more than 5 percent.

146. The importance of insulation should be stressed, and construction should be carefully monitored to ensure that specification requirements regarding insulation are followed. Insulation will not only provide protection from sudden drops in temperature during cooler months, it will also help to prevent unacceptable thermal differentials that occur when mean ambient temperature drops more quickly than the interior temperatures in existing thick sections. In all analyses with insulation, insulation was assumed to be in contact with all exposed concrete surfaces at all times. If air gaps are allowed to develop between insulation and the concrete surface, the effectiveness of the insulation will be compromised and cracking may result.

REFERENCES

ABAQUS Users Manual, Version 4.7. 1988. Hibbit, Karlsson & Sorensen, Inc., Providence, RI.

ACI Committee 209. 1989. "Prediction of Creep, Shrinkage, and Temperature Effects in Concrete Structures," Report 209R-82, Manual of Concrete Practice, American Concrete Institute, Detroit, Michigan.

Bombich, A. A., Norman, C. D., and Jones, H. W. 1987. "Thermal Stress Analyses of Mississippi River Lock and Dam 26(R)", Technical Report SL-87-21, USAE Waterways Experiment Station, Vicksburg, MS.

Bombich, A. A., Garner, Sharon, and Norman, C. D. 1991. "Evaluation of Parameters Affecting Thermal Stresses in Mass Concrete", Technical Report SL-91-2, USAE Waterways Experiment Station, Vicksburg, MS.

Chen, W. F. 1982. Plasticity in Reinforced Concrete, McGraw-Hill, New York.

Garner, S. B., and Hammons, M. I. 1991. "Development and Implementation of Time-Dependent Cracking Material Model for Concrete," Technical Report SL-91-7, USAE Waterways Experiment Station, Vicksburg, MS.

Hammons, M. I., Smith, D. M., and Neeley, B. D. 1990. "Red River Waterway Thermal Studies, Report 1, Concrete Mixture Selection and Characterization," Technical Report SL-90-8, USAE Waterways Experiment Station, Vicksburg, MS.

Hammons, M. I., Garner, S. B., and Smith, D. M. 1989. "Thermal Stress Analyses of Lock Wall, Dashields Locks, Ohio River," Technical Report SL-89-6, USAE Waterways Experiment Station, Vicksburg, MS.

Holland, T. C., Liu, T. C., and Bombich, A. A. 1982. "Determination of Properties of Concrete Used in Thermal Studies for Lock and Dam No. 2, Red River Waterway," Miscellaneous Paper SL-82-5, USAE Waterways Experiment Station, Vicksburg, MS.

Jurges, W. 1924. "Der Warm Eubergang an einer ibenen Wand" (Heat Transfer to a Plane Wall), Beih. z. Ges. Ing. 1, No. 19.

Kirsten, M. S. 1949. "Thermal Properties of Soils," Technical Report 23, U.S. Arny Corps of Engineers, St. Paul District, St. Paul, MN.

Norman, C. D., and Anderson, F. A. 1985. "Reanalysis of Cracking in Large Concrete Dams in the US Army Corps of Engineers," Commission Internationale Des Grande Barrages, Quinzieme Congres Des Grande Barrages, Lausanne, Switzerland.

Norman, C. D., Campbell, R. L., Sr., and Garner, Sharon. 1988. "Analysis of Concrete Cracking in Lock Wall Resurfacing," Technical Report REMR-CS-15. USAE Waterways Experiment Station, Vicksburg, MS.

Truman, K., Petruska, D., and Ferhi, A. 1989. "Evaluation of Thermal and Incremental Construction Effects for Monolith AL-3 and AL-5 of Melvin Price Locks and Dam," Structural Engineering Report No. 84, Washington University, St. Louis, MO.